QUANTITATIVE CHEMICAL IMAGING: A TOP-DOWN SYSTEMS PATHOLOGY APPROACH TO PREDICT COLON CANCER PATIENT SURVIVAL

BY

SAUMYA TIWARI

DISSERTATION

Submitted in partial fulfillment of the requirements
for the degree of Doctor of Philosophy in Bioengineering
in the Graduate College of the
University of Illinois at Urbana-Champaign, 2018

Urbana, Illinois

Doctoral Committee:

Professor Rohit Bhargava, Chair
Professor Andre Kajdaçsy-Balla
Associate Professor Dipanjan Pan
Professor Jonathan Sweedler

ABSTRACT

Colon cancer is the second deadliest cancer, affecting the quality of life in older patients. Prognosis is useful in developing an informed disease management strategy, which can improve mortality as well as patient comfort. The morphometric assessment provides diagnosis, grade, and stage information. However, it is subjective, requires multi-step sample processing, and annotations by pathologists. In addition, morphometric techniques offer minimal molecular information that can be crucial in determining prognosis.

The interaction of the tumor with its surrounding stroma, comprised of several biomolecular factors and cells is a critical determinant of the behavior of the disease. To evaluate this interaction objectively, we need biomolecular profiling in a spatially specific context. In this work, we achieved this by analyzing tissue microarrays using infrared spectroscopic imaging. We developed supervised classification algorithms that were used to reliably segment colon tissue into histological components, including differentiation of normal and desmoplastic stroma. Thus, infrared spectroscopic imaging enabled us to map the stromal changes around the tumor. This supervised classification achieved >0.90 area under the curve of the receiver operating characteristic curve for pixel level classification.

Using these maps, we sought to define evaluation criteria to assess the segmented colon images to determine prognosis. We measured the interaction of tumor with the surrounding stroma containing activated fibroblast in the form of mathematical functions that took into account the structure of tumor and the prevalence of reactive stroma. Using these functions, we found that the interaction effect of large tumor size in the presence of a high density of activated fibroblasts provided patients with worse outcome. The overall 6-year probability of survival in patient groups that were classified as “low-risk” was 0.73 whereas in patients that were “high-risk” was 0.54 at p-value <0.0003. Remarkably, the risk score defined in this work was independent of patient risk assessed by stage and grade of the tumor. Thus, objective evaluation of prognosis, which adds to the current clinical regimen, was achieved by a completely automated analysis of unstained patient tissue to determine the risk of 6-year death.

In this work, we demonstrate that quantitative chemical imaging using infrared spectroscopic imaging is an effective method to measure tumor-tumor microenvironment interactions. As a top-down systems pathology approach, our work integrated morphometry based spatial constraints and biochemistry based stromal changes to identify markers that gave us mechanistic insights

into the tumor behavior. Our work shows that while the tumor microenvironment changes are prognostic, an interaction model that takes into account both the extent of microenvironment modifications, as well as the tumor morphology, is a better predictor of prognosis. Finally, we also developed automated tumor grade determination using deep learning based infrared image analysis. Thus, the computational models developed in this work provide an objective, processing-free and automated way to predict tumor behavior.

To my family

ACKNOWLEDGMENTS

I would like to thank my advisor, Professor Rohit Bhargava for his guidance during my doctoral study, for believing in me and for supporting me so strongly in all my endeavors. I have been very fortunate to have an advisor who greatly inspires me and motivates me to be the best version of myself. It was a great honor to work with Professor Bhargava, and I will always cherish my time in the Bhargava lab.

Thank you to Dr. Georgina Cheng for bringing the clinical perspective in my work and for critical reading of this manuscript. Her passion for this study and her kind words have been a constant source of motivation and encouragement to me.

I would like to acknowledge Dr. André Kajdacsy-Balla for his invaluable input and collaboration in this study. I am very thankful for his support in this work and my career development.

I want to extend my gratitude to my doctoral committee, for their guidance, critical comments, and thoughtful discussions, which have greatly benefited this work.

My warm regards to my fellow Bhargava lab members, for their comments and suggestions throughout this work. A special thank you Mark Gryka, for being a great colleague and friend and huge support at work. I also want to acknowledge Joshua J Whitley who has participated with great enthusiasm in the last stages of my work.

This work would not have been possible without the love and support from my family. I will be forever grateful to my parents for providing me with every opportunity that has brought me here. A special thank you to my fiancé Digvijay, for supporting me through this journey, for inspiring me with his work ethic and passion for science and for our continued collaboration in life. Living away from home, my friends have been a source of strength and motivation. Thank you to Amruta, Mark, Hailey, Nayab, and Sumbul for being my family. Last five years would not have been half as fun without their presence in my life. Finally, two non-humans that deserve mention are eternal puppies, Leo and Echo, whose antics have filled my life with joy and laughter.

TABLE OF CONTENTS

CHAPTER 1: INTRODUCTION 1

MOTIVATION AND IMPACT 1
COLORECTAL CANCER PREVALENCE AND CLINICAL ASSESSMENT 2
CHEMICAL IMAGING AS A TOOL FOR COLON CANCER ASSESSMENT 3
Biological basis of FT-IR spectra 3
FT-IR spectroscopic imaging to analyze features not observable through traditional techniques 3
Clinical applications of FT-IR 4
FIGURES 6

CHAPTER 2: METHODS: CHEMICAL IMAGING AND DATA ANALYSIS FOR DIGITAL CANCER DIAGNOSIS 10

ABSTRACT 10
INTRODUCTION 10
IR imaging to address current cancer pathology needs 11
Classification models 13
IMAGE COLLECTION AND PRE-PROCESSING 15
Substrates 15
Signal to noise ratio 16
Spatial and spectral resolution 16
Paraffin removal 17
Preprocessing 18
CLASSIFICATION PROTOCOL 19
Selection of training and validation set 19
Metric definition 20
Identification of classes 20
Evaluating metric distributions 21
Determination of metric order 22
Validation 23
CONCLUSIONS 23
FIGURES 25

CHAPTER 3: QUANTITATIVE CHEMICAL IMAGING AS A TOP-DOWN SYSTEMS PATHOLOGY APPROACH 30

ABSTRACT 30
BACKGROUND 30
MOTIVATION FOR IMPROVING CURRENT PATHOLOGY 32

Inclusion of molecular information *32*
Determining response to therapy *32*
Need of new ideas for prognosis *33*
HOW CAN CHEMICAL IMAGING AID SYSTEMS PATHOLOGY? 33
Chemical imaging for biomolecular characterization at the cellular level: Breast cancer example *34*
Chemical imaging for tissue level characterization: Prostate cancer example *35*
Chemical imaging to characterize the extracellular matrix *37*
Chemical imaging based angiogenesis identification *37*
NEW AND EMERGING CONCEPTS 38
Self-seeding *38*
Metabolism *39*
Use of mathematical methods *39*
CONCLUSIONS 41
FIGURES 43

CHAPTER 4: MICROENVIRONMENT AND TUMOR SPATIAL INTERACTION MODEL USING QUANTITATIVE CHEMICAL IMAGING PREDICTS COLORECTAL CANCER PATIENT OUTCOME... 47

ABSTRACT 47
INTRODUCTION 47
RESULTS 49
Infrared spectroscopic signatures identify tumor stromal components *49*
Biochemically specific spectral machine learning classifier retains high specificity and sensitivity when tested on independent TMAs *50*
The extent of desmoplastic reaction, as well as its proximity to tumor cells, is associated with survival *51*
DISCUSSION 53
CONCLUSIONS 55
METHODS 56
Sample preparation *56*
Imaging *56*
Preprocessing *57*
Feature reduction *57*
Progression analysis *58*
FIGURES 60
TABLES 65

CHAPTER 5: CLINICAL TRANSLATION: AUTOMATION OF BIOPSY ANALYSIS WITH DEEP LEARNING 68

ABSTRACT 68
INTRODUCTION 68
METHODS 69
Data collection and segmentation 69
Tumor grade determination with deep learning neural net transfer 70
RESULTS AND DISCUSSION 70
Identification of spectral regions of importance 70
Differentiation grade classifier achieves high specificity and sensitivity on independent validation set 71
CONCLUSIONS 72
FIGURES 74
TABLES 78

CHAPTER 6 79

CONCLUSIONS 79

SUMMARY 79
FUTURE DIRECTIONS 80
Subtyping stromal cell populations 80
Deep neural networks to analyze infrared spectroscopic imaging data 80
Multi-scale systems pathology 81
Personalized analysis 81

REFERENCES 82

CHAPTER 1: INTRODUCTION

Motivation and impact

Colon and rectal cancer are the second in estimated deaths due to cancer after lung and bronchus cancer[1]. Approximately 4.2 percent of men and women will be diagnosed with this disease at some point during their lifetime, and only about 65% will survive five years after detection[1]. The current clinical needs in colon carcinoma diagnosis and management can be summarized as follows:

(1) Need for objective evaluation: Although histopathology is the current gold standard for colon cancer diagnosis and prognosis, it suffers from numerous drawbacks such as experimental variations, limited information content and inter-observer variability[2,3] resulting in up to 11.8% errors in cancer diagnosis[4]. In addition, several studies have reported a lack of concordance in determining tumor grade[5,6] and interobserver variability in the assessment of dysplasia[2,3]. Therefore, methods that can perform objective evaluation without intensive tissue processing are needed.

(2) Quantification of tumor-microenvironment associated prognosis: Unlike breast cancer where hormone receptor status stratifies outcome and determines therapy options[7], reliable prognostic and response predictive markers are not in clinical use in colon cancer. Carcinoembryonic antigen (CEA) is used to monitor patients post-surgery but is only useful for the early detection of metastasis in stage II and stage III cancers[8,9]. It has been demonstrated that the tumor microenvironment plays a vital role in determining tumor behavior[10]. Specifically, in colon cancer, studies have shown that the desmoplastic reaction around the tumor has prognostic significance[11,12]. Despite the reports, using the desmoplastic response as a prognostic marker is not clinically feasible because the evaluation criteria are subjective, and varies with pathologists. In addition, this model does not take into account the spatial interaction of the tumor with its microenvironment. Therefore, there is a need to develop robust models to quantify tumor-tumor microenvironment interaction and assess their utility in determining prognosis.

(3) Protocols for automation: Automation is possible using deep learning based machine vision applications in the assessment of patient tissue. In a large number of samples, determining the presence or absence of tumor is straightforward but still requires pathologists' time and effort. Thus, there is a need to develop automated tools which can cut down on the workload of pathologists by removing apparent cases.

(4) Improving speed of assessment and in-surgery assistance: At the time of the surgery, if histopathological aid is needed, the tissue is snap frozen, sectioned, stained and a pathologist assesses the sample. There is potential to improve this pipeline by performing rapid tissue assessment right on the surgery bench without the need for tissue processing. Thus, there is a need to develop and evaluate high-speed imaging modalities capable of performing the stainless assessment.

Colorectal cancer prevalence and clinical assessment

Colorectal cancer is the cancer of the colon or rectum. Adenocarcinoma is the most common colorectal cancer subtype, accounting for about 90% of the colorectal cancer cases, although other types of cancers such as lymphoma and squamous cell carcinoma can also originate from the colon. Adenocarcinoma originates from epithelial tissue that has a glandular origin (*adeno*-meaning gland). In colon cancer, the disease arises from the epithelial cells lining the colon or rectum (colon crypts), invades the thin layer of muscle in the gastrointestinal tract known as muscularis mucosae, followed by invasion in the submucosa and eventually muscularis propria (figure 1.1). In cases of colorectal cancer, when submucosal invasion takes place, the tumor is rendered invasive (pT1)[13].

The initial diagnosis of colon cancer is made by colonoscopy, following which surgical excision or biopsy can be performed. Colonoscopy is a versatile method to determine the tumor location. Once a suspicious mass is sampled, pathological diagnosis can be made by examining the tissue after histological stains. The most common stain used for tissue examination is hematoxylin and eosin (H&E). Using the stained tissue, pathologists confirm if a malignant tumor is present, and the depth of invasion. In the case of surgical resection, multiple regional lymph nodes are examined to determine if cancer has spread to the lymph nodes. Based on the structure and organization of the tumor and the nuclei, a tumor grade can also be assigned, which has been shown to be a stage-independent prognostic factor[14] (figure 1.2).

While anatomic pathology utilizes morphometric information to perform diagnosis, it is limited by molecular information content, and often does not provide a functional basis for the abnormality[15] (figure 1.3a). Molecular information can be supplemented by the use of proteomics and genomic tools, which have limited spatial information (figure 1.3b).

Chemical imaging as a tool for colon cancer assessment

Chemical imaging using Fourier transform infrared (FT-IR) spectroscopic imaging offers spatially specific molecular analysis of samples, without the need for stains or dyes (figure 1.3c). Infrared imaging can be used for comprehensive molecular assessment of the tissue and for determining prognosis. This approach is timely to use given the recent advancements in high definition IR spectroscopic imaging coupled with machine learning to perform image analysis and prediction. In the following sections, we review the prior works that have studied colon tissues using chemical imaging.

Biological basis of FT-IR spectra

Prior works have demonstrated that there is a functional difference between a healthy colon and colon cancer that can be measured using chemical imaging. Early studies using FT-IR spectroscopic imaging have shown that the levels of cell metabolites decrease in polyp and colon cancer relative to normal tissue[16]. Further work on the analysis of adenomatous crypts showed that abnormal crypt proliferation could be identified by using FT-IR spectroscopic imaging. The abnormal crypts showed a lower absorbance of glycogens, phosphates and lipids at the bottom and middle portion of the crypt as compared to the top, whereas normal crypts had a higher overall absorbance at the middle[17,18]. In normal crypt, the cells had lower carbohydrate levels at the apex of the crypt, the levels of carbohydrates did not change much between middle and apex in abnormal crypts, showing that the cells in abnormal crypts retained their metabolism activity even at the top of the crypt. Metabolite levels have also been observed by collecting samples from intestinal mucosa as we move away from the tumor and it was found that there is a decrease of lipid and increase of proteins and nucleic acids in the regions close to tumors[19]. A similar increase in protein and nucleic acids has been observed elsewhere[20]. Several studies have attempted to utilize these differences to segment colon tissue using unsupervised clustering approaches (figure 1.4a). The unsupervised classification algorithms perform well on individual samples, and demonstrate the power of infrared spectroscopic imaging in distinguishing colon tissue histological components[21–25]. However, they fail when multiple patient samples are used, given that patient heterogeneity can have strong effects on the signal[26].

FT-IR spectroscopic imaging to analyze features not observable through traditional techniques

Besides conventional FT-IR spectroscopic imaging studies investigating the biochemical signal distribution and attempting to reproduce classical histology[27], FT-IR spectroscopic imaging has

also been employed successfully to identify features that are not detectable with conventional H&E staining. For example, tumor budding and tumor stroma association can be studied using FT-IR spectroscopic imaging; both of these features are either unidentifiable through traditional histological staining or require high power magnification[28].

Colonic carcinogenesis has known variations in mucin-type glycoproteins. MUC1 mucin is increased in colon cancer, and correlates with a worse prognosis, whereas the expression of MUC2 is generally decreased in adenocarcinoma[29]. Multiple studies have attempted to analyze this variation using infrared spectroscopy[30–34]. One study in particular identified that the mucin spectral features did not vary in normal and adenocarcinoma tissues but there was a difference in the surface percentages of mucin which can allow us to differentiate between these two tissue types (figure 1.4b).[34]

Tumor heterogeneity is studied widely in terms of cell surface receptors, proliferation capabilities and angiogenic potential[35,36]. These biological variations are not observable using H&E stain. In work on xenograft colon carcinoma models, IR spectroscopic imaging was shown to be useful in identifying three distinct spectral clusters, one of which was associated with mucin-producing cells[37]. Thus, it is likely that IR imaging is more effective in documenting the tumor heterogeneity as compared to the H&E staining.

Clinical applications of FT-IR

When colon tissue is examined under visible light, specialists look for raised lesions called polyps. These can be either benign or malignant, but this distinction can only be made by looking at the biopsy. Argov et al.[38] attempted to characterize premalignant polyps using IR spectroscopic imaging and compare them with normal and colon cancer cases. The authors used multilayer perception artificial neural networks to classify the tissue and noted that spectral differences between polyp and malignant cases were not significant. Phosphate stretching bands were able to differentiate normal from both polyp and malignant cases but failed to separate pre-malignant polyp from cancerous cells. Instead, it was shown that the glycogen peaks at 1026 cm^{-1} and 1154 cm^{-1} performed better as features to distinguish hyperplasia from dysplasia [39].

Identifying dysplastic polyps through histopathology is a tedious process, involving patient sedation and additional costs. Keeping this in mind, Mackanos et al.[39] developed FT-IR spectroscopy to assist endoscopy using silver halide optical fiber in ATR configuration. The authors used freshly excised specimens to evaluate the potential of infrared spectroscopy to

identify dysplastic mucosa. The samples were blown with cold air for five minutes to remove water interference. Using this model, the authors found subtle differences in the absorption spectra among normal, hyperplasia and dysplasia in the fingerprint region using partial least squares discriminant analysis, reporting a specificity of 92% at 96% sensitivity and an AUC value of 0.953. The authors pointed out that using a classification algorithm that is more efficient regarding calibration transfer between the optical fiber instruments is needed, and can be combined with an endoscope-compatible optical fiber to distinguish premalignant colonic mucosa; producing a significant leap in *in situ* infrared imaging. Other groups have reported a series of experiments starting from in vitro studies to using ATR based fiber optic probe for *in vivo* FT-IR spectroscopy and have reported agreements between *in vivo* and *in vitro* data and the observations being consistent with biopsy results[40]. ATR-FTIR based study, other works have reported identification of colonic inflammation[41] as well as differentiation of colon cancer from colitis using [42]. One such setup is shown in figure 1.4c.

Together, these studies show that FT-IR spectroscopy can produce results equivalent and superior to traditional staining techniques, giving additional biomolecular information and has potential to capture metastasis and prognosis associated features. Clinical implementation of this technique is possible with faster imaging systems such as quantum cascade lasers[43–45] while optimized classification algorithms can produce results at clinically relevant time scales. This is specially needed for colon cancer analysis, which does not have clinically prevalent prognostic markers. In addition, colon tissue is accessible with probe based instruments, and demonstrations that infrared spectroscopic imaging in situ is compatible with endoscope further strengthen the motivation to develop advanced analysis techniques using chemical imaging to probe colon tissue.

In chapter 2, we describe methods to optimize IR data collection and analysis for cancer applications. In chapter 3, we discuss the importance of tumor-microenvironment based analysis in the systems pathology context. Chapters 4 describes our work in probing tumor-tumor microenvironment interactions by utilizing chemical imaging to determine patient prognosis. Finally in chapter 5, we describe approaches to speed up and automate colon cancer tissue imaging and analysis using chemical imaging.

Figures

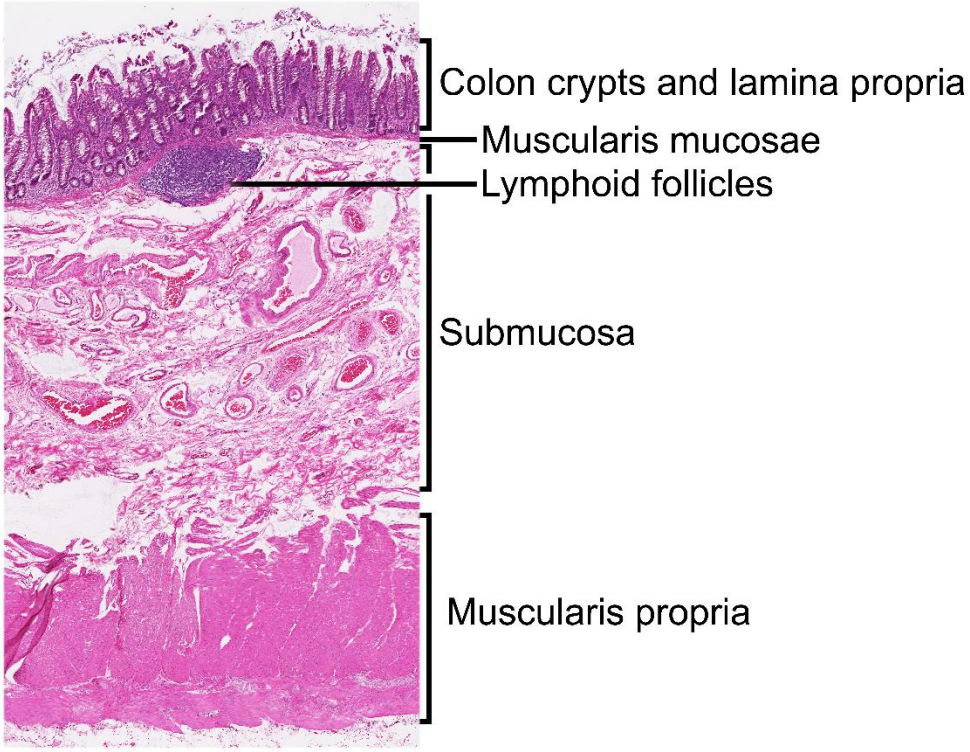

Figure 1.1: A section of colon showing colon histology. The colon crypts consist of mature epithelium that produces mucin, along with stroma surrounding the cells known as lamina propria. A thin muscle layer called as muscularis mucosae is followed by submucosa comprised of large number of blood vessels, lose stroma and neural cells. A thicker muscle layer called as muscularis propria follows submucosa.

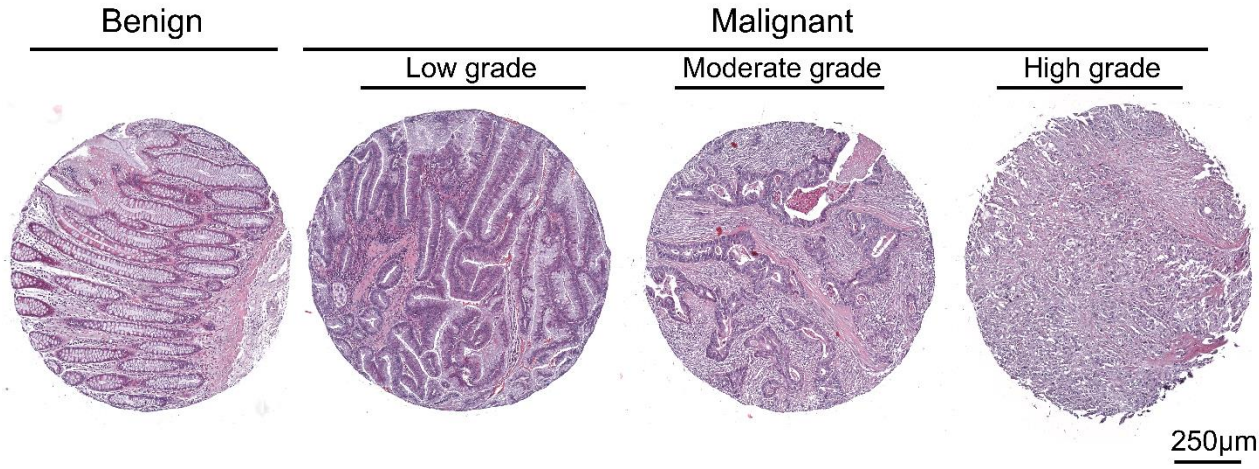

Figure 1.2: Hematoxylin and eosin stained biopsy tissue can be used for diagnosis and determining tumor grade. The figure shows an H&E stained benign colon tissue in comparison to malignant tissues of different tumor grades. The low grade, or "well-differentiated" colon cancer is the closest to normal colon tissue, with well defined glands and polar nuclei. Moderate grade tumors show some degree of gland formation, and the nuclei can be seen as losing polarity. In high grade or "poorly differentiated" carcinomas, the cancer is seen to be growing in sheets with enlarged nuclei that have lost their polarity.

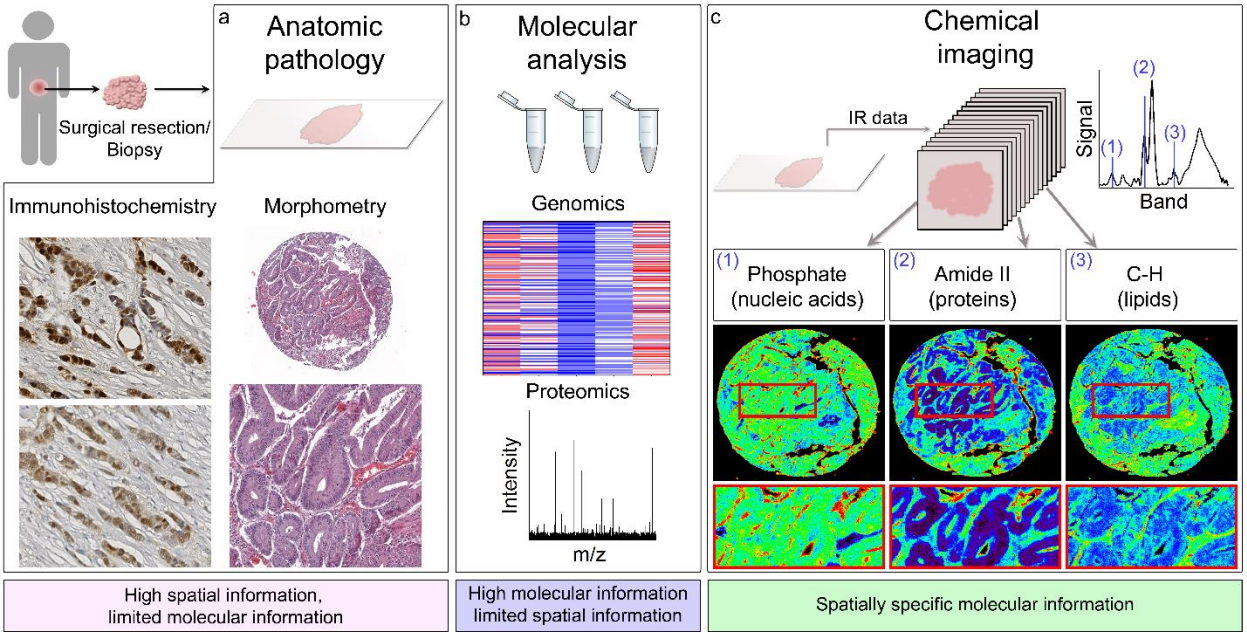

Figure 1.3: Current methods to analyze colon tissue. (a) After surgical resection or biopsy, anatomic pathology can be used to determine the presence of tumor and tumor grade and stage. However, it has limited molecular information. (b) Molecular analysis using tools such as proteomics and genomics provide a wealth of molecular information, but do not provide a spatial context. (c) Chemical imaging using infrared spectroscopic imaging provides higher molecular resolution compared to anatomic pathology in a spatially specific context. Bands in the IR spectrum correspond to specific functional groups, and thus indicate the distribution of macromolecules that contain them.

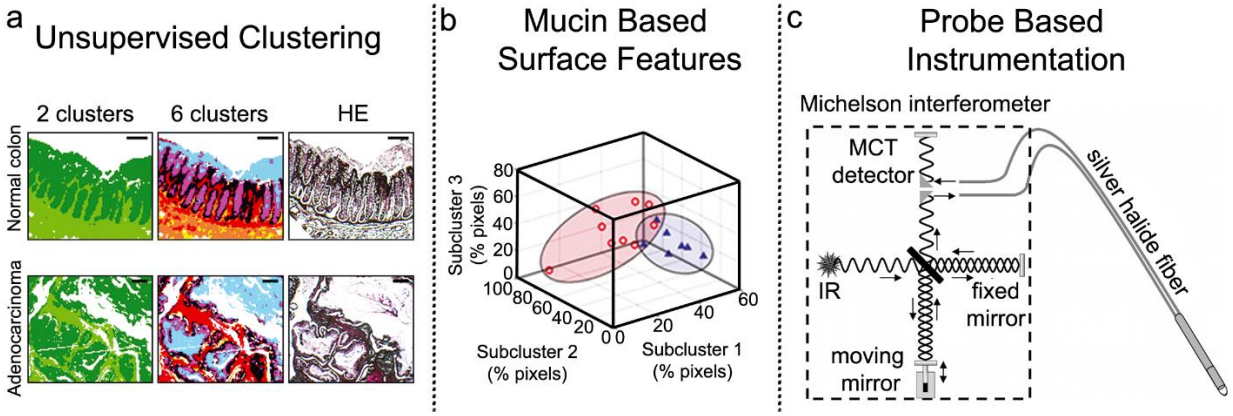

Figure 1.4: Development of computational tools and instrumentation using chemical imaging to diagnose and analyze colon tissue samples. (a)[1] Multiple unsupervised clustering approaches have segmented colon tissues using infrared spectroscopic imaging signals. (b) The surface percentage of spectroscopically distinct mucin can be used as a feature to separate normal colon tissues from adenocarcinoma samples (c) [2]A flexible silver halide fiber can be used to collect infrared absorption spectra from freshly excised tissue, eliminating the need of extensive sample processing.

[1] Parts of figure 1.4 (a) and (b) adapted with permissions from Travo, Adrian, Olivier Piot, Rolf Wolthuis, Cyril Gobinet, Michel Manfait, Jacques Bara, Marie-Elisabeth Forgue-Lafitte, and Pierre Jeannesson. "IR spectral imaging of secreted mucus: a promising new tool for the histopathological recognition of human colonic adenocarcinomas." *Histopathology* 56, no. 7 (2010): 921-931.
[2] Parts of figure 1.4 (c) obtained with permission from Vinay K. Katukuri, John Hargrove, Sharon J. Miller, Kinan Rahal, John Y. Kao, Rolf Wolters, Ellen M. Zimmermann, and Thomas D. Wang, "Detection of colonic inflammation with Fourier transform infrared spectroscopy using a flexible silver halide fiber," Biomed. Opt. Express 1, 1014-1025 (2010).

CHAPTER 2: METHODS: CHEMICAL IMAGING AND DATA ANALYSIS FOR DIGITAL CANCER DIAGNOSIS[3]

Abstract

Fourier transform infrared (FTIR) spectroscopic imaging is an emerging microscopy modality for clinical histopathologic diagnoses as well as for biomedical research. Spectral data recorded in this modality are indicative of the underlying, spatially-resolved biochemical composition but need computerized algorithms to digitally recognize and transform this information to a diagnostic tool to identify cancer or other physiologic conditions. Statistical pattern recognition forms the backbone of these recognition protocols and can be used for highly accurate in results. Aided by biochemical correlations with normal and diseased states and the power of modern computer-aided pattern recognition, this approach is capable of combating many standing questions of traditional histology based diagnosis models. For example, a simple diagnostic test can be developed to determine cell types in tissue. As a more advanced application, IR spectral data can be integrated with patient information to predict risk of cancer, providing a potential road to precision medicine and personalized care in cancer. The IR imaging approach can be implemented to complement conventional diagnoses, as the samples remain unperturbed and are not destroyed. Despite high potential and utility of this approach clinical implementation has not yet been achieved due to practical hurdles like speed of data acquisition and lack of optimized computational procedures for extracting clinically actionable information rapidly. The latter problem has been addressed by developing highly efficient ways to process IR imaging data but remains one that has considerable scope for progress. Here we summarize the major issues and provide practical considerations in implementing a modified Bayesian classification protocol for digital molecular pathology. We hope to familiarize readers with analysis methods in IR imaging data and enable researchers to develop methods that can lead to the use of this promising technique for digital diagnosis of cancer.

Introduction

Infrared (IR) spectroscopic imaging is a promising avenue for computerized disease diagnosis,[46–52] especially for cancer[18,46,47,53–62] and a multitude of other diseases[63]. It is of particular relevance for recognizing features within solid tissues in which a variety of cell types and disease states may be present. Utilizing the tandem spatial and molecular information

[3] Reprinted with permission, from Tiwari, Saumya, and Rohit Bhargava. "Extracting knowledge from chemical imaging data using computational algorithms for digital cancer diagnosis." *The Yale journal of biology and medicine* 88.2 (2015): 131-143.

acquired using a combination of IR spectroscopy and optical microscopy, this technique relies on using the biochemical composition as a means to automate disease identification. In IR imaging, no stains are used. Instead, the chemical composition of the material is recorded via a local spectrum and computer algorithms are used to relate the data to underlying physiologic conditions. Since only light is used to record the necessary data, the technology is entirely non-perturbing to a prepared sample. The overall idea of using IR imaging for biological applications is shown in figure 2.1. This approach is orthogonal to the current practice in histopathology, which requires staining to visualize tissue morphology as well as requires intensive human involvement to recognize and categorize morphological features that are indicative of disease. The IR-based approach strongly relies on sophistication and utility of the numerical methods used. The focus of this article is to describe and highlight the salient features of numerical methods used in IR imaging.

IR imaging to address current cancer pathology needs

At present, the gold standard to identify many types of cancers is to perform a biopsy. The poorly quantitative procedures following the biopsy and staining are semi-automated at best, and still suffer from user introduced variability[64,65]. This not only introduces subjectivity in examination[66], but also increases load on pathologist which they could otherwise devote to more complicated cases. Misclassification of biopsies during screening and diagnosis may lead to overtreatment or undertreatment, posing significant concerns for patients. A recently published report, for example,[67] evaluated the agreement among 115 pathologists who interpreted a total of 240 cases of breast biopsy samples which was compared with the consensus derived reference diagnoses from three expert pathologists. The researchers found out that the overall agreement between the participating pathologists' interpretations with the reference was 75.3%. Alarming underinterpretations were found in Ductal Carcinoma *in situ* (DCIS) cases (13%) and atypia cases (35%). Considering that DCIS accounts for 15% to 25% of the newly diagnosed breast cancer cases currently in the USA[68] and identification of atypical cells often requires further rounds of biopsy to establish aggressiveness of possible tumor, large numbers of patients could be affected every year based on whether or not second opinion is obtained. In another recent study[69], the researchers consulted 252 pathologists to assess the policy of obtaining second opinion on a variety of specimens. Their response indicated that mandatory second opinion was only required in 56% of the laboratories when DCIS was diagnosed and in 36% laboratories when atypical ductal hyperplasia was observed. In many cases, a third opinion was required to resolve the differences between the first and second opinions. Studies like these and others[70–72] clearly

go on to show that there are a lot of cases in breast cancer that are affected by confusions in classification of type and aggressiveness of tumor, and that current pathology practice is in need of better tools to aid diagnoses.

Multiple computer aided detection systems have been used in past to assist the pathologists and help them reduce occurrences of false positives and false negatives[73]. In current practice, the computer aided detection systems that rely on pattern recognition software used by radiologists can be considered semi-automated in that some degree of human interaction is still needed before final decision is given. In that sense, *detection* systems are different from *diagnosis* systems which are capable of rendering a decision based on a consideration of variety of factors like mass of tumor, biochemical data from biopsy and patient characteristics like breast density and age. These systems thus require integration of two major fields; computation and imaging. In terms of imaging for diagnostic cancer pathology, the foremost requirement is the ability to generate contrast between diseased regions and healthy regions. Traditionally, chemical and immunohistochemical stains have been used to produce this contrast that is, in a second step, referred to pathologist for evaluation. The second step is now increasingly involving the use of computers to manage images and assist with decisions using numerical indices or other image analysis techniques. However, there are emerging alternatives to this long standing instrumentation. For example, microscopic contrast can also be produced optically using Raman imaging or IR spectroscopy – two strongly emerging modalities, which also place new requirements and provide new opportunities for the associated computational methods. IR spectroscopic imaging has some distinct advantages over other contrast producing modalities. First, it requires minimal sample preparation. Freshly taken tissue can be snap frozen and imaged without further aids. This greatly reduces variations during experimental stages making the procedure standardized and efficient. It can as easily be applied to archival samples. Second, IR imaging does not require contrast agents but utilizes the inherent biochemical contrast in the tissues for differentiation of diseased state. Third, the chemical changes recorded by infrared spectroscopy across the tissue are capable of giving the same information as achieved by histological stains[74]. In addition to it, since the information is computer generated, they provide greater contrast and statistical confidence, in turn enabling identification of problematic areas easier. A recently published report[27] showed that a single IR spectral image could reproduce staining patterns of multiple stains such as Hematoxylin and Eosin (H&E), Masson's trichrome stain, cytokeratin stain, smooth muscle alpha actin, and vimentin (figure 2.2). This could allow the researchers to analyze the samples through multiple stains, without putting in additional time, effort or resources to develop the stains.

Along with reproducing classical stains with great accuracy, data generated by IR imaging is highly amenable to computational analysis and pattern recognition algorithms are easily integrated for obtaining decisive reports. Currently, a major goal of the typical studies performed using IR imaging on tissue samples is to build classification systems that color code IR images to differentiate between different types of cellular and acellular components, much like H&E and IHC stains. Classes such as epithelium, endothelium, stroma and muscle have been identified[75,76] and more cellular and acellular components are being added through current research. Although this approach provides high contrast images with minimal sample preparation for the use of trained pathologists, in order to truly utilize the potential of IR imaging for cancer diagnosis, further computational prediction needs to be implemented. A recent report,[77] for example, attempted to precisely predict recurrence of prostate cancer using IR imaging data and showed that this approach outperformed both Kattan nomogram and CAPRA-S scores for outcome predictions. Together, emerging studies are opening new avenues for utilization of IR based models for cancer diagnosis and therapy by combining imaging, molecular detection and computational cancer prediction to augment human decision-making. Owing to the practical requirements of speed of imaging and data acquisition and processing, no automated diagnosis systems have been clinically implemented till now; nevertheless, fast progress is being made to achieve this goal and will be discussed briefly in later sections. We first provide an overview of the methods, highlighting special considerations and challenges that use this data and lead to decision-making in cancer research and care.

Classification models

A biological sample characteristically consists of many cell populations and extracellular matrix elements. All of these elements serve a function in the sample, and imbalance in the chemical composition and morphology of these can be a cause or an effect of a disease. Thus, these cellular and acellular components of tissue are carefully scrutinized by pathologists to obtain information about the ailment. We refer to all such functional elements as histological classes or simply classes. The idea underlying the use of IR spectroscopy for disease detection is that each such class will have a different biochemical composition and therefore unique spectral signature in IR absorbance spectra. Since digital spectral data is available for each pixel from the sample, we can employ pattern recognition algorithms to utilize these differences for recognition of classes. Various classification approaches have been used in past to identify classes, termed as classification. Multiple studies have been performed for the analysis of data using various

classification algorithms, and are summarized here. For an in-depth theory on classification methods pertaining to biomedical imaging, the readers are directed to these references[76,78,79]. Typically, all methods can be classified into supervised or unsupervised methods – both of which are described briefly below. Subsequently, we focus here on describing the typical process of obtaining data, computational pipeline and typical results obtained. We illustrate the entire process with representative examples to enable the reader to grasp the essential steps of extracting information from IR images.

(a) Unsupervised Classification

The premise of unsupervised classification is that no prior information (for example, spectral characteristics of the classes) is fed to the method for classification. Hence, distinction between classes is often a problem of finding clusters in which intra-cluster variation is smaller than inter-cluster variation. Unsupervised clustering approach has been applied previously to investigate tissue samples[80–82]. Since nothing is assumed known about the data classes, unsupervised processes can involve data reduction using the variance before applying a classification procedure. Such a methodology has been applied to classify IR imaging data from cervical cancer [83]; Principal Component Analysis (PCA) for data reduction followed by K means clustering was used elsewhere for classification of IR data[57]. Although unsupervised approaches work for exploratory analysis, they have been found to be computationally taxing and unable to differentiate between inter-class and intra-class variations, often necessitating the use of supervised classification algorithms[30,31]. In our opinion, the utility of these methods for IR imaging lies more in discovery rather than consistent knowledge extraction.

(b) Supervised classification

In supervised classification, prior information about the location and spectral properties of the classes is given to the classifier. Supervised algorithms such as discriminant analysis[47,84–86], neural network analysis[30,38,61,87,88] and Bayesian methods-based classification[42,75] have been used to classify tissue into various cellular and disease states. Underlying all these methods is the fundamental property of Bayes' theorem, indicating that known patterns provide a statistical probability for identification of each class. Methods based on this property and its application for biological specimens has been discussed elsewhere[75]. Here we discuss the practical considerations for its implementation; in order to facilitate understanding and ease of use among spectroscopists and medical researchers alike.

Image collection and pre-processing

Collecting a good quality image is the first step of any IR classification experiment. Often, this facet is overlooked. Good quality data reduces complexity of the methods and can provide faster as well as more accurate results. Multiple factors such as choice of substrate signal to noise ratio (SNR), spatial and spectral resolutions, and presence of contaminants like paraffin residue can affect the overall classification accuracy. In this section we will discuss methods employed to collect good quality data and prepare the data for classification.

Substrates

IR spectroscopic imaging data can be collected in both transmission and reflection mode. IR transparent substrates, such as calcium fluoride (CaF_2) and barium fluoride (BaF_2) salt crystals are excellent substrates since they achieve greater than 95% transmission in mid IR region. An overview of properties and uses of CaF_2 and BaF_2 crystals can be found in reference [89]. Specifically for imaging biological samples, BaF_2 is preferable since transmittance of CaF_2 cuts off at about $1000cm^{-1}$ and analysis at lower wavenumber (longer wavelengths) is not possible. BaF_2 is more prone to damage, however, due to higher water solubility compared to that of CaF_2[90], making its handling and maintenance slightly more difficult but not substantially different compared to standard glass slides. Once a sample is placed on these crystals, imaging is rather simple. Using a microscope objective-condenser setup, light simply passes through the substrate and the sample in a “transmission” mode. The major problem with either substrate is cost –which can run from tens to hundreds of dollars. Due to high cost of these substrates and higher maintenance requirements compared to standard glass slides, many IR studies now utilize IR reflective substrates such as gold coated slides and Low-E slides (MirrIR, Kevley Technologies). Low-E slides, in particular have been very useful for IR imaging owing to their ability to transmit visible light and reflect infrared light. Thus, imaging is often conducted in the transflection mode with these substrates. In the transflection mode, light is incident upon the sample, passes through it, is reflected from the sample-substrate interface and re-transmitted through the sample. Due to the sample typically being of a thickness that is the same order as the wavelength of light, passing through the sample twice results in distortions in the spectrum[91,92] compared to the transmission case. However, some pre-processing steps have been reported that can effectively encounter most of the side-effects of transflection mode and are discussed in section 2.5. With emerging methods and more flexibility in terms of cost and maintenance[93] Low-E slides are attractive options to carry forward IR based detection technologies to everyday use in clinics.

Signal to noise ratio

In IR imaging, the spectral signal to noise ratio (SNR) is the primary measure of the quality of data. It has been shown that high levels of noise in data negatively impact the classification accuracy[94]. Hence, SNR should be carefully considered in the design and use of any protocol. Modern infrared imaging instruments have combated the problem of low SNR quite well, and one can routinely obtain an SNR of greater than 200 on commercial instruments. There are multiple factors that can determine the SNR for data collected. For commonly used Focal Plane Array (FPA) detectors in IR imaging instruments, each element in detector records the spectrum from one pixel in the sample. As the number of co-additions is increased, the signal is recorded multiple number of times and averaged. This improves the SNR by the square root of the number of co-additions. However, this also increases the time required for data acquisition almost linearly with the number of co-additions. Another option is to reduce spatial resolution (increase the size of the pixel at the sample plane) which can provide a higher SNR in smaller time due to a larger angle of light collected, but this may compromise identification of small sized cells in biological samples. An additional key factor while image collection is background spectrum. Every IR imaging experiment requires collection of background spectra that are used as a reference to obtain absorbance measurements. The number of co-additions for background spectrum should be much larger than the number of co-additions for the image in order to have minimal introduction of noise in signal from background[95]. Some limits on SNR are also imposed by the interferometer and other hardware, as well as multiple other factors such as spectral and spatial resolution, which is a result of complexities in the acquisition process. Some of the factors that affect SNR have been discussed in previous works[94–96]. Here we want to emphasize that the data quality in IR imaging is a balance between optimum SNR, optical configuration needed and the time required to achieve the desired SNR. One method we have not discussed thus far is the use of post-acquisition numerical processing techniques that can use statistical or other measures of noise reduction and lead to reduced noise in the images. The basic principle underlying these methods is to transform the data into a space that collapses all information into a minimum number of factors, for example, using principal components transform[97]. Fortunately, due to these computational noise reduction techniques (discussed in section 2.5) SNR is not a limiting factor for classification accuracy for many of the common tasks in spectroscopic imaging[94].

Spatial and spectral resolution

The main constituents of biological samples are the different types of cells that comprise the tissue

as well as the extracellular matrix (ECM) that holds tissue structures together. The size of eukaryotic cells can vary from about 5 to 30 microns. Sufficient spatial resolution is necessary to identify each cell type[98] and thus the instrumentation and experimental parameters must be carefully selected. Insufficient spatial resolution leads to the problem of mixed pixels, whereby, if the pixel is too large, it can have contribution from multiple cells, leading to greater confusion and low accuracy of classification[76]. Typically, pixel size used for IR microscopy had been approximately 5 µm x 5 µm. Pixel size in attenuated total reflectance (ATR) mode can be higher due to the use of a solid immersion lens[99–101]. A microscope equipped with transmission optics and ATR lenses can provide higher resolution depending on the solid immersion lens or ATR crystal material. For example, one commercial instrument provides a pixel size of 6.25 µm x 6.25 µm in the transmission mode and 1.56 µm x 1.56 µm sized pixels in ATR mode using a Germanium lens (refractive index ~ 4). High definition IR imaging instruments typically seek to provide 1 µm x 1 µm. It should be noted that the pixel size is not the same as resolution. Resolution is still determined by the Rayleigh Criterion; for example, it is ~5 □m for transmission mode imaging and 1 □m for ATR imaging. A comparison of IR images taken at various pixel sizes for mammalian cells is shown in figure 2.3. As can be seen, high amide absorbance region of nucleus is much better resolved with high spatial resolution as compared to the low resolution transmission image. Effect of varying pixel size on classification is shown in figure 2.4(ii, iii) where 6.25 µm x 6.25 µm pixel size data is compared to 25 µm x 25 µm pixel size data. H&E image with marked classes is shown for comparison (figure 2.4(i)). Higher pixel density via smaller pixel sizes provides IR images that are closer to histologic stain image, whereas more averaging to increase SNR and larger scanning time to acquire more pixels is required. The large pixel sizes result in overlapping of signals from different cell types and the ECM, reducing confidence in classification. A large pixel can reduce the scanning time greatly and provide high SNR. For most biological problems involving complex tissues, however, a high spatial resolution is oftentimes needed. An equally important factor for good classification is spectral resolution. For very coarse spectral resolution, the peaks begin to overlap, causing significant reduction in classification accuracy[102]. Typical IR imaging experiments utilize a spectral resolution of 2 cm^{-1} to 16 cm^{-1}. For biological specimens, spectral resolution of 4 cm^{-1} to 8 cm^{-1} is able to differentiate most of the significant peaks and has been found to give good classification results in our experience.

Paraffin removal

Since most samples are typically paraffin embedded and sectioned before IR imaging, the sections need to be deparaffinised in order to remove spectral contributions from paraffin, typically

occurring as a set of peaks from 2800 cm^{-1} to 3000 cm^{-1} due to C-H stretching vibrational modes and a strong peak at 1462 cm^{-1} due to C-H bending modes[103]. Deparaffinization carried out either in Xylene[85], Hexane washes of 16-24 hours with mild stirring or with octane for 4 hours[104] have all shown to remove paraffin features from spectrum. Figure 2.4 compares classification results from a paraffinized sample (figure 2.4(iv)) and same sample after paraffin removal (figure 2.4(iii)) for same spatial resolution. A spectrum from sample before and after de-paraffinization is shown in figure 2.5. Even though we avoided using parts of the spectrum from paraffin affected regions from 2800 cm^{-1} to 3000 cm^{-1} and around 1462 cm^{-1}, the classification was more accurate for deparaffinized sample than the paraffinized sample for same spatial and spectral resolution. Classification of samples imaged without deparaffinization can also work if appropriate corrections are performed[22]. Nevertheless, if paraffin retention is known or suspected, care should be taken to address any signals arising from paraffin while performing classification.

Preprocessing

Once IR images are acquired, minimal data processing is needed for performing classification. Based on the SNR, computational noise reduction methods such as those based on the Minimum Noise Fraction (MNF)[94] may be needed before classification can begin. This is a modification of principal components analysis whereby the ordering of eigenimages is performed in decreasing order of SNR, and high SNR eigneimages are chosen for analysis. Noise statistics are calculated form the image data. MNF transform creates three files, covariance statistics of the noise file, MNF statistics file and forward MNF transformed file which contains bands with descending eigenvalues. Based on the eigenvalues, the user can determine which bands contain data, and which bands have predominant noise. Typically, top 20-30 bands contain good quality data. Inverse MNF transformation is then applied on the forward MNF transformed file by taking high eigenvalue bands. Most commonly, this type of noise reduction is needed for ATR and high definition imaging data. Baseline correction of data is needed for comparing spectral features attributable to absorbance across classes and gives a good estimate of the differences before training can begin. A variety of baseline correction options are known but all essentially approximate the known non-absorbing regions to zero. In one approach, all points where theoretically zero absorption is expected are first identified. Then, a linear two point correction algorithm across peaks of interest is used. It should be noted that, in imaging, the baseline points are often held to the same for all spectra in the sample. To account for thickness variations in the sample or between samples, normalization with amide I peak (1650 cm^{-1}-1656 cm^{-1} based on

location of peak) is often required. For biological tissues, this is the peak of highest absorbance and introduces the least decrease in SNR after normalization.

Classification protocol

The classification protocol followed here is based on modified Bayesian classification. The complex multistep method is explained through the flowchart shown in figure 2.6. We describe the major steps in the workflow and discuss possible pitfalls while building and deploying a classification protocol.

Selection of training and validation set

The goal of the classification protocol discussed here is to identify different types of cells and ECM elements called histological classes. The ultimate goal is to develop a computational algorithm that provides accurate recognition of classes in an unknown data set that can be encountered in practice. In the first step, the protocol needs to be developed and tested to perform optimally. To initiate this process, two separate data sets are selected – one is used for training and the other for independent validation. In some cases, the validation may come from the calibration data set itself. In such cases, one fraction of the data is selected for validation and the protocol is trained on the remainder. The fraction left off is changed and a number of iterations of the process are averaged to train and validate. This “leave-one-out” procedure can be used when the numbers of samples or diversity of the data set is limited but it is always ideal to have completely independent training and validation sets. It must be ensured that there is sufficient representation of all classes for getting satisfactory classification, and to retain sufficient diversity for assessment of accuracy in validation dataset. In this approach, study design is critical as the method cannot predict conditions it has not been trained on. The measures of success should also be carefully defined. We favor the use of the receiver operating characteristic (ROC) curve which includes an assessment of both sensitivity and specificity of the method. Other approaches may be to maximize detection of any class or disease state (e.g. cancer) at a specified error rate or to evaluate errors in a holistic manner such as with confusion matrices. Finally, a statistically significant number of samples must be used to validate the protocol. While the numbers of samples needed for a diagnostic test is well understood, the sample size needed for satisfactory calibration in the IR is an ongoing subject of study[76,105]. In the absence of other guidance, the standard approach is to calibrate, validate and calculate the ROC curves for the classifier in order to assess the accuracy. The errors in classification must additionally be carefully assessed. Based on these results, the investigator may need more data for accurate classification.

Metric definition

Depending on the size of the sample, an FTIR imaging data set can be very massive, ranging from a few hundred megabytes to hundreds of gigabytes. Each pixel in an IR image carries spectrum, which is usually recorded in the FT configuration across the entire bandwidth of the spectrometer but is usually truncated to reduce the size of the stored data to a smaller range, e.g. 750 cm^{-1} to 4000 cm^{-1}. However, not all spectral elements are useful for classification. For example, a region between 1900 cm^{-1} to 2500 cm^{-1} is biologically inactive and can be further removed if spectral corrections that depend on extensive refractive index measurements are not to be performed[106]. One approach to dealing with imaging data is the emergence of the so-called discrete frequency IR imaging in which, using filters[107,108] or a tunable laser[43,109–113], only a few frequencies of interest are collected. This approach will likely prove useful only after the calibration process. Hence, in general, the entire spectrum is acquired and needs to be handled for the calibration step. Data reduction discussed here simply suggests using data that gives qualitative and quantitative information about the sample and removing redundant data. While it is not necessary for single cell studies which do not require large computational power, biopsy sections and tumor micro arrays (of the order greater than 1 mm X 1mm in size) would need much computing time if raw spectrum is used without data reduction. Further, confounding information may become included unless a careful selection of informative spectral regions is used. We can utilize spectral features such as peak height ratios, peak area to height ratio, peak area to area ratio and peak center of gravity to differentiate among classes. These parameters are known as spectral metrics. Metrics are defined by an expert spectroscopist by observing the spectrum in tissue to identify exact peak locations. Many metrics have biological relevance, for example glycogen to phosphate ratio (1030 cm^{-1}/1080 cm^{-1}), but sometimes the physiological relevance is not intuitive. Even then, at this point all possible metrics that show differentiation among classes based on class spectrum should be considered. For every new imaging experiment, it is necessary to define the metric definitions anew, in order to account for spectral differences among classes and small differences in peak locations.

Identification of classes

Identification of classes is the major factor that can determine accuracy of classification. To feed class characteristics as prior information for supervised classification, one needs an accurate identification of pixels used for training. This is typically performed with the help of an expert pathologist, often guided by H&E stained images or immunohistochemical images of

corresponding sections. Typically, the practitioner marks regions corresponding to different classes by microscopic examination of H&E stained section. Correspondingly, regions in IR image are marked as regions of interest (ROI). H&E stained section can be a serial section or neighboring section to the section utilized for IR spectroscopy. A much preferable approach is to first obtain infrared images from the sample and then perform H&E staining on the same sample so that an exact match can be obtained. Once the classes are marked, non-biological pixels from class layers should be removed by setting an intensity threshold value for biologically active band such as amide I band (~1652cm^{-1}) to a high enough value to remove both tissue-less regions as well as those with excessive distortions due to edge effects[114–117]. Subjectivity is the biggest issue in identification of classes and there have been multiple studies in past that show that the interpretation of H&E stain suffers from inter-observer variability, and can have a role in false positive and false negative results[64,65,118]. In absence of any absolute identification criteria at present, we rely on the opinion of pathologist for identification of classes. This adds a human error to the classification, and care is taken to mark the regions on IR image exactly same as the regions identified by the pathologist on the H&E image (considered “gold standard” [76]). This prevents addition of further error in prior information for classifier training which relies on manual identification and marking of classes in IR data. An alternative is to use immunohistochemical stains to identify cell types and overlay the IHC images with the IR images. However, IHC stains are not known to be reliable all the time and staining intensity may be open to interpretation requiring the use of sophisticated methods[119].

Evaluating metric distributions

The distribution of values of metrics forms the basis on which the classifier identifies and learns the differences among classes. An example of histogram is shown in figure 2.7 that is the type of data to evaluate the use of metrics. Here, the number of pixels versus the value of metric parameter for each class is plotted. For large enough number of pixels for each class, the histograms are expected to follow a Normal distribution unless there are sub-classes within the data. Hence, the first check is to determine whether there may be more than one distribution in the pixels, which may cause an examination of the model used in turn. For N metric parameters, we obtain N histograms. This step is important in identifying metrics which can potentially be useful in differentiating between classes. When comparing between two classes, the overlap between the distributions is the critical parameter to evaluate. A small overlap in distributions implies that the values of metric parameters are sufficiently different and can be used to differentiate between the classes. The actual efficacy of metric parameter depends on the fraction

of overlap that the probability distribution functions of different classes have with each other (figure 2.7). It must be noted that abundance also comes into consideration here. For a given pixel, the overlap in normalized histograms can be considered. However, the probability of the selected pixel belonging to any particular class also needs to be considered. This depends not only on the native distribution of classes in normal and diseased conditions but also on the sampling process (e.g. biopsy). For example, it is well known that there is significantly more epithelium in cancer and in the peripheral zone of the prostate. Hence, simple abundance probability can be augmented significantly by known characteristics of the disease, patients and procedures performed. Caution must be exercised, however, in making models that are too specific. While such models may perform at high accuracy, their robustness is likely to be compromised. The metric distribution, hence, must be evaluated in light of the model, the classification methods and on the desired accuracy. A metric parameter which can differentiate at least between two classes is considered useful for the purpose of classification. Since multiple such parameters can eventually be used in conjugation to separate all classes from each other, the set of metrics to be used and the order of their usage will be evaluated next. Following this step, with appropriate user input in determining histogram limits, a probability distribution file is created that contains the prior information of the classes.

Determination of metric order

After determination of probability distribution for every class in our case, a Bayesian classifier, each metric can be considered as a rule that determines which class the pixel belongs to. Therefore, the classifier goes through a series of rules to come to a decision about the class, assigning a class value to the pixel after each step is executed. In this perspective, it becomes important to determine the most optimum order of metrics so that the end result is closest to the true histology. For this average errors for metrics are calculated and pairwise errors are arranged in increasing order. This order is optimized by classifying with reordered metric, calculating the area under the receiver operating characteristic (ROC) curve, and recalculating pairwise error if there is an increase in area under the ROC curve. It has been shown before that only a fraction of metrics are actually needed to achieve the highest accuracy in classification[75]. Thus, after the optimum metric order has been defined, metrics coming at the bottom of the order can be removed from classifier. Typically, this set of 15-25 metrics is identified based on the metric order and area under the ROC curve but an additional step in optimization can be performed by manually removing one metric at a time and assessing whether any increase in accuracy is achieved[75].

Validation

Validation of the classifier is performed on an independent data set by comparing the classifier with pathologist annotated IR data in the manner similar to calibration. ROC curves and confusion matrices are commonly used to assess the accuracy of classification. The ROC curve leads to two measures – the area under the curve (AUC) of the ROC curve and the [sensitivity, specificity] operating point of the classifier. The AUC is a "global" measure of the how accurate the designed protocol can be on an average. Comparisons of AUCs, statistical limits and ordering of different models based on the AUC are all operations that can be used to refine the classifier and gain further insight[120–122]. The operating point, i.e. [sensitivity, specificity] can be considered to be a local condition that determines a particular operation of a diagnostic test. For any selected protocol there will always be an operating point, which trades-off the specificity and sensitivity, but is implemented for the test. This is often determined by the problem and the tolerable error in the test. Sensitivity of greater than 70% at high specificity (90%) are generally considered satisfactory for biomedical detection systems, although a much higher sensitivity and specificity is often desirable for tasks such as disease diagnoses or recognition of particular cells. For example, in one study, among multiple breast cancer surveillance methods such as MRI, mammography, ultrasound and clinical breast examinations; the sensitivity ranged from 9.1% to 77% and specificity ranged from 95.4% to 99.8%[123]. When using IR based staining for digital cancer diagnosis, it is desirable to have sensitivity and specificity reach close to 100%. This has been shown to be possible by various recent studies[124,125]. While ROC curves determine the specificity and sensitivity of classification, the confusion matrices give the investigator an idea of confusion between classes in classification and both should be used to evaluate the performance of the classifier. In validation studies, these matrices often point to systematic errors in the development of the classification protocol and must be examined carefully.

Conclusions

Automated computational classification is a very powerful technique to utilize IR spectroscopic imaging data. We emphasize that due to multiple steps required in image acquisition and classification protocols, careful considerations throughout are needed to assure successful development of assays. Often, the process of development of a classifier is not linear and careful analysis and examination at each step is needed to ensure that the protocol is both accurate and robust. The theory and practice of Bayesian classification is well developed for infrared imaging data[75,76]. The protocols for image acquisition have also been described in detail in the past[102,126–128]. However, practical considerations while performing classification that can

greatly affect the classification accuracy have not been recorded in infrared imaging literature. Through this chapter, with illustrative examples, we have attempted to provide an introduction and a practical guide to considerations in the development of a specific classification protocol. Many of these considerations can be adapted for similar classification procedures, and we do hope that this article would enable and encourage the readers to familiarize themselves with infrared spectroscopy and utilize the avenues it offers for cancer diagnosis.

Figures

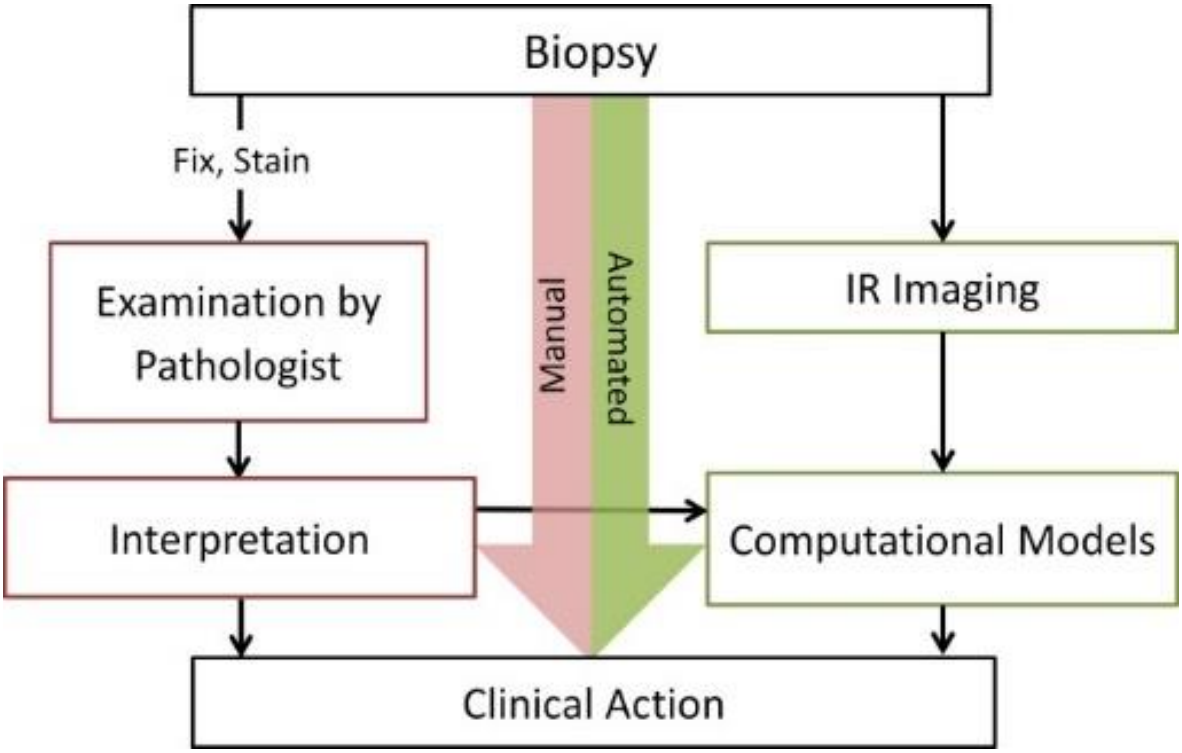

Figure 2.1: Overview of the use of IR imaging for biological analyses.[4]

[4] Adapted with permission from Bhargava R. Towards a practical Fourier transform infrared chemical imaging protocol for cancer histopathology. Anal Bioanal Chem 2007;389:1155–69. doi:10.1007/s00216-007-1511-9.

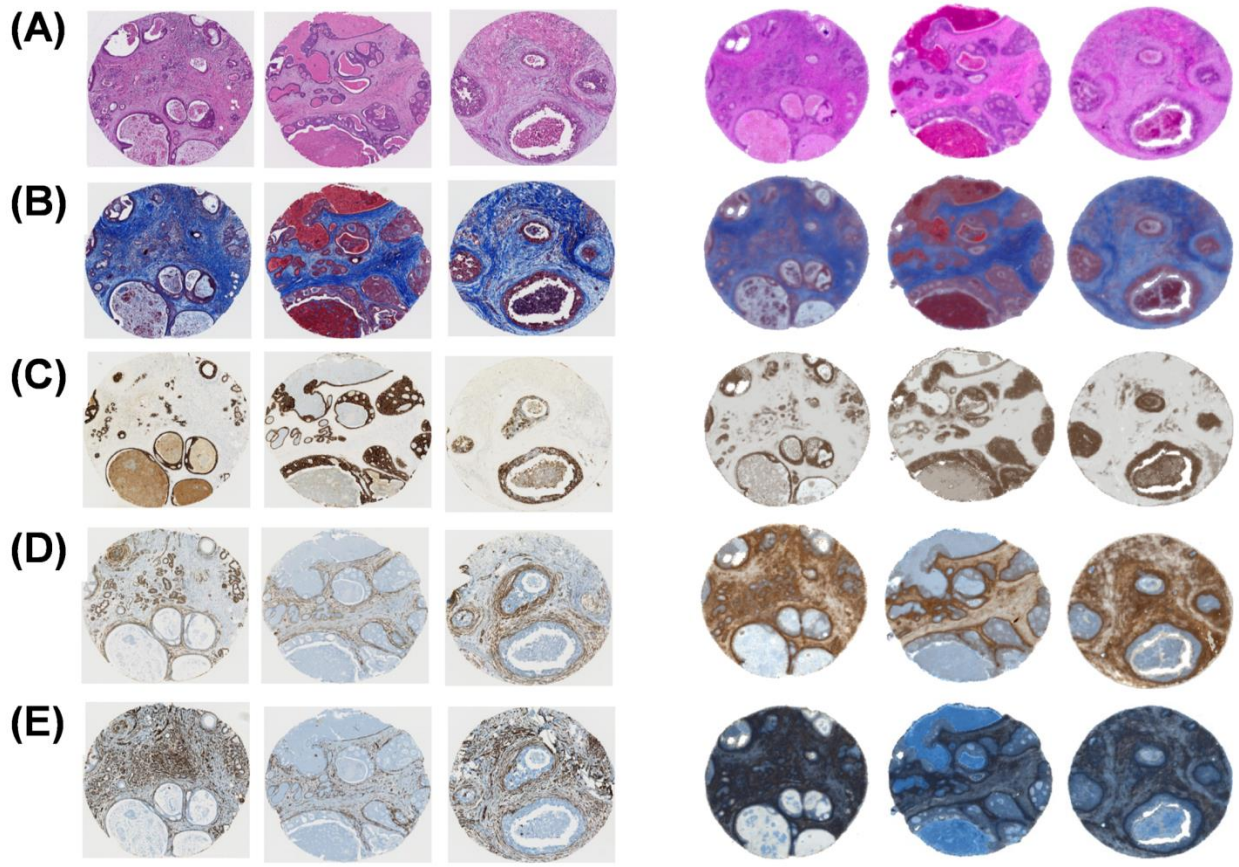

Figure 2.2: Molecular imaging (three sample panel on the left) can be reproduced by chemical imaging (right panel). In addition to H&E stained images (a), we extend the concept of stainless staining to molecularly specific stains, including (b) Masson's trichrome stain (collagen and keratin fibers) (b) high molecular weight (HMW) cytokeratin (epithelial-type cell), (c) smooth muscle alpha actin (myo-like cell) and (d) vimentin (fibroblast-like cell). Each spot is 1.4 mm in diameter.[5]

[5] Adapted with permission from Mayerich D, Walsh MJ, Kadjacsy-Balla A, Ray PS, Hewitt SM, Bhargava R. Stain-less staining for computed histopathology. TECHNOLOGY 2015:1–5. doi:10.1142/S2339547815200010.World Scientific Publishing Co./Imperial College Press

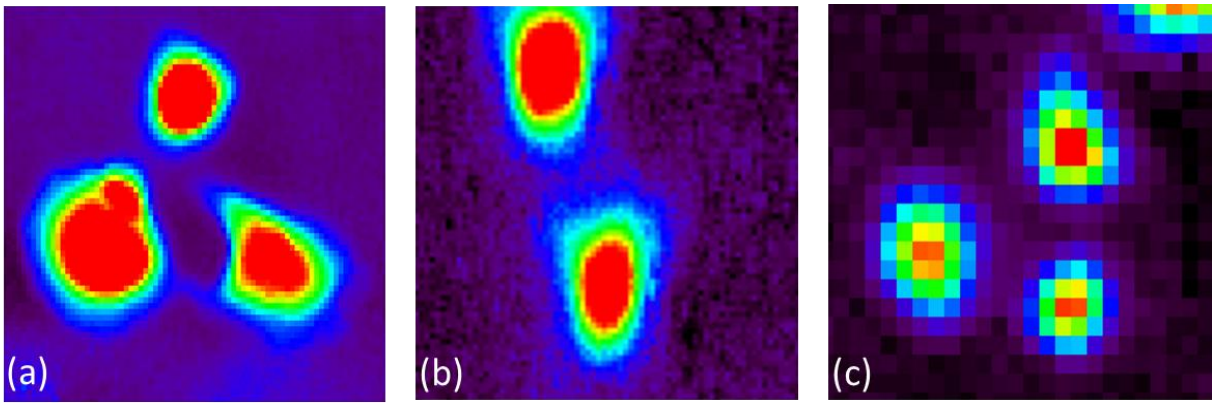

Figure 2.3: Images of eukaryotic cell at varying resolutions; (a) ATR mode, pixel size 1.56µm x 1.56µm; (b) Transflection mode 74X, pixel size 1.1µm x 1.1µm; (c) Transmission mode 14X, pixel size 6.25µm x 6.25µm. All images are at amide I band (1652 cm^{-1})

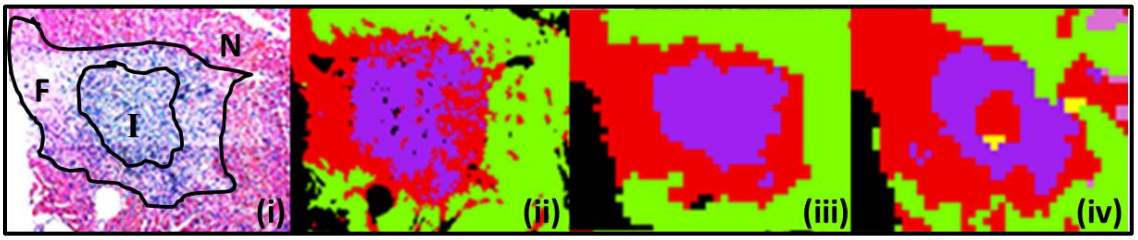

Figure 2.4: Factors affecting classification; (i) H&E image with marked regions, I: Infiltrate, F: Fibrosis, N: Normal tissue; (ii) Classified image pixel size 6.25µm x 6.25µm (deparaffinized); (iii) Classified image pixel size 25µm x 25µm (deparaffinized); (iv) Classified image pixel size 25µm x 25µm (paraffinized)

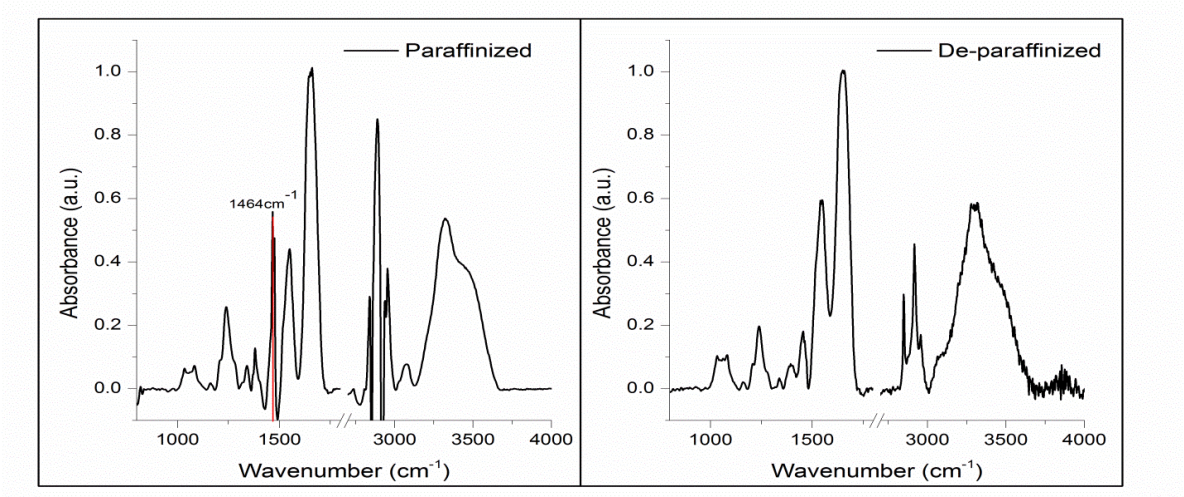

Figure 2.5: Difference in spectrum for tissue with and without paraffin

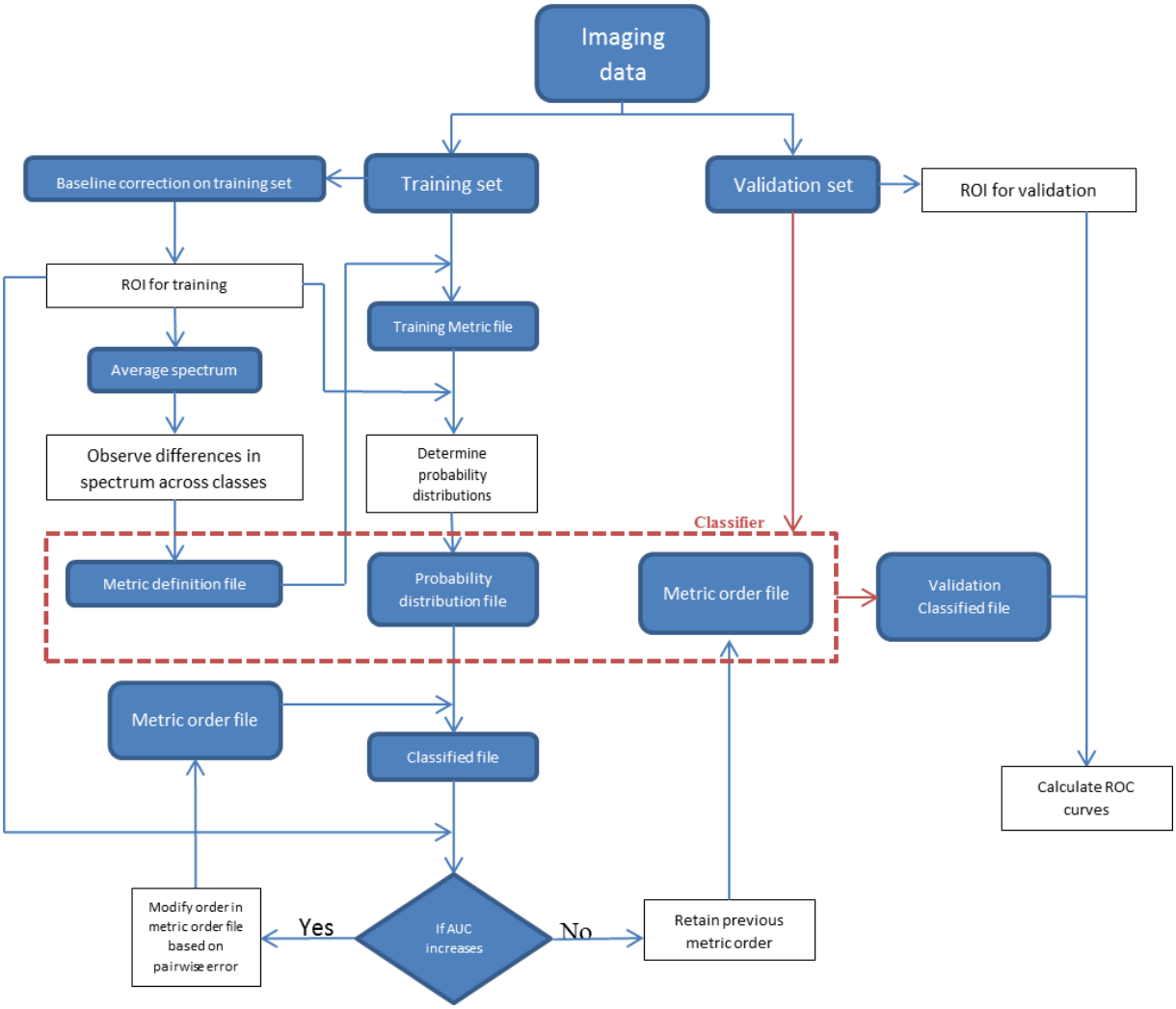

Figure 2.6: Flowchart of building classifier

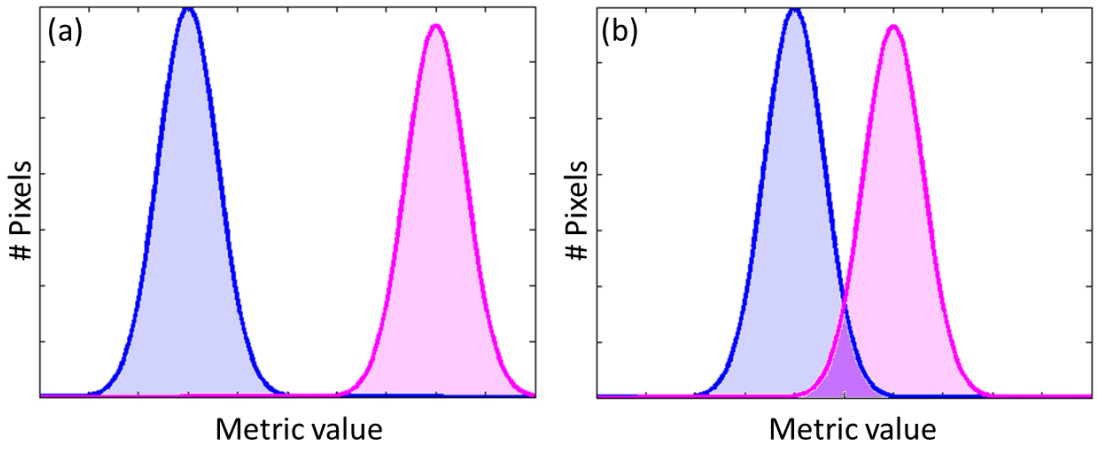

Figure 2.7: Histograms for metric evaluation; (a) An example of good metric (b) An example of metric that will have errors in classification when the metric value lies in the overlapping area of the two curves

CHAPTER 3: QUANTITATIVE CHEMICAL IMAGING AS A TOP-DOWN SYSTEMS PATHOLOGY APPROACH[6]

Abstract

Cancer is a complex set of diseases, presently characterized by the primary site of origin and expression of biomarkers. The diagnostic gold standard, and for much of research, is the tissue structure and organization in microscopy images. Although histopathology of tumors provides necessary information for diagnosis, it is not predictive of therapy response. As a top-down systems pathology approach, the goal of quantitative chemical imaging is to develop computational models to observe, quantify, and validate our understanding of cancer progression. Mathematical models, as well as machine learning approaches, have previously been utilized to predict the tumor response, but comprehensive spatial and biochemical characterization of the tumor is lacking. This gap can be filled by a spatially specific biochemical analysis of tissue using chemical imaging. Here we discuss some fundamental concepts of systems pathology in the context of model developments involving chemical imaging.

Background

Pathology refers to the study of diseases. As an essential element of patient care, pathology is used to diagnose as well as prevent diseases. There are two sub-disciplines within pathology, clinical pathology, which is the analysis of fluid samples such as blood and urine targeting specific analytes and pathogens; and anatomic pathology, pertaining to the microscopic examination of solid samples such as tissue sections for diagnosis of diseases[129]. Histopathology is the gold standard for clinical diagnosis of cancer where morphology based information such as the cell shapes, nuclei shapes, and tissue structure is used to determine the presence of disease and grade (figure 3.1). Few such important morphometry based features have been summarized previously[130].

Cancer is a complex and dynamic disease, and in some cases can quickly proliferate while evading growth suppressors, resisting cell death, developing resistance to drugs and metastasize to different parts of the body[131]. Due to the intricate processes taking place during cancer development and progression, the molecular snapshot of the disease at a specific stage could be descriptive of the future behavior of the tumor. With the developments in precision medicine,

[6] In preparation for publication as Tiwari, Saumya et al. “Quantitative Chemical Imaging as a Top-Down Systems Pathology Approach.”

targeted therapies, imaging, computational and data visualization tools, we have a surge of data, which does not add to our understanding of disease when used in isolation. Therefore, it is timely to develop models that can integrate information obtained at various systems levels. The idea that the response of cancer can be quantified in the form of mathematical or computational models using systems biology has been proposed before[132]. Quantitative chemical imaging (QCI) is a top-down approach of systems pathology that seeks to address the current challenges in predicting response to therapy and outcome of the disease, as well as to develop a mechanistic understanding of disease development and progression, fulfilling the need to quantify tumor-tumor microenvironment interaction at the patient level. By providing quantitative assessment, QCI can play an integral part in evidence-based pathology, which seeks to aid clinical instinct by using evidence derived from large-scale data[133]. Using artificial intelligence models that are capable of combining multi-platform approaches, QCI can be used to place the information in the clinical and biological context, enabling patient specific interpretation.

Biochemical characterization of tissue for developing systems pathology models is a vital component of any tumor prediction model. Conventionally used techniques such as genomics and proteomics provide a wealth of molecular information but are significantly limited in spatial details (figure 3.2). Many changes in tumor environment are spatially specific, for example, extracellular matrix remodeling [134], activation of cancer-associated fibroblasts[135] and angiogenesis[136]. Immunohistochemistry is useful in visualizing molecularly specific changes in tissue but the target needs to be known in advance and multiplexing is often not possible. The limitations of currently used modalities present an informational gap in current systems pathology models that can be filled by chemical imaging such as infrared imaging and Raman imaging (figure 3.2). Specifically, infrared spectroscopic imaging utilizes the interaction of light waves with tissue to measure the biochemical changes occurring in the tissue. Molecular bonds present in a material give it a characteristic chemical spectrum. This spectrum is unique for every chemical and therefore, can be used as a ‘fingerprint’ to identify the molecular content. When there is a change in the biochemistry of the tissue, the chemical constitution changes, causing changes in the chemical spectrum which can be measured using optical spectroscopy[137]. Optical spectroscopic imaging can be used ex vivo in conjugation with histology to bring together tissue biochemical and morphometric profiling (figure 3.3) and to enhance our prediction capabilities for tumor behavior. In this chapter, we will review the recent developments in the field of systems pathology.

Motivation for improving current pathology

Inclusion of molecular information

While morphometry works well for diagnosis, it does not have sufficient features to enable prognosis prediction. Developing an understanding of underlying biological mechanisms of disease development and progression has allowed better prediction of outcome and optimal therapeutic routes. For example, gene expression-based data, in conjugation with clinical data was shown to substantially correlate with survival in lung cancer patients[138]. The inclusion of molecular information has aided the clinical decision-making process[139] and has enabled physicians to assess risk and develop strategies for personalized care. Few such markers are now extensively used in prostate cancer[140], breast cancer[7,139,141], and colon cancer[142]; and a comprehensive review can be found here[143].

In addition to gene-based markers, molecular information is also available through probe-based techniques. Recent advances have enabled multiplexed imaging of antibodies using multiplexed ion beam imaging (MIBI) that utilizes antibodies tagged with isotopically pure elemental reporters, increasing the range of targets analyzed to up to 100[144]. In the case of small biomolecules where traditional antibodies can be too bulky and change functionality of the biomolecule, highly sensitive imaging has been achieved using stimulated Raman scattering (SRS) active vibrational tags[145,146], allowing for real-time imaging of live cells to study molecular dynamics.

Determining response to therapy

The traditional approach towards cancer therapy has been to target specific metabolic pathways active in proliferating cancer cells using drugs. The reductionist approach uses isolated molecules to target a complex disease that often does not work in treating cancer because complete mechanistic understanding is lacking. Many drugs developed by in vitro screening process fail at the clinical stage by failing to account for complex interactions in biological systems[147]. The animal models used as the pre-clinical testers have poor clinical significance. For example, angiogenesis inhibitors such as the antibodies targeting vascular endothelial growth factor failed in phase 3 clinical trials despite an impressive performance in animal models[148]. Anti-angiogenesis medication such as bevacizumab was later shown to work well in a combination therapy regime[149,150]. This case highlights the need to develop the complete understanding of the mechanisms of disease and to account for patient-specific factors while designing a therapy regime. Because cancer can activate alternate pathways to overcome resistance, the trial and

error approaches of testing drug therapies have been shown to have high failure rate[151], in part due to inadequate knowledge of the critical interacting pathways[152].

The advantage of developing a systems pathology model to determine therapy response is twofold. First, the drug interactions can be better understood using a human disease systems model, which can account for biological complexity. Second, this opens up ways to tailor treatment to the patient, known as “personalized medicine”. This approach can enable identification of patients who could potentially have an adverse response to a specific therapy and outcome prediction while combining therapies.

Need of new ideas for prognosis

So far, clinicians use a combination of anatomical, clinical and molecular pathology to determine the best course of action for a patient. Cancer outcome is typically determined by the use of stage and grade information. The American Joint Committee on Cancer’s (AJCC) TNM staging system, coding for the extent of primary tumor (T), regional lymph nodes (N) and distant metastasis (M) is widely used for predicting the survival in cancer. With about 31% of all patients getting laboratory tests[153], an accurate interpretation of diagnostic tests is critical. Far from being negligible, studies have identified that clinically significant diagnostic errors occurred in about 0.26%-1.2% cases when reviewed by a second reviewer[154,155]. In another study, about 12% of all examined cytologic-histologic specimen pairs were found to have errors in cancer diagnosis[4]. There are opportunities to improve diagnostic testing by developing tools and techniques to aid physicians and pathologists. The AJCC’s current edition noted the increasing use of nonanatomic prognostic markers and developments in personalized analytics models for cancer care[156], underlining the application of new concepts to address prognosis as well as determining the disease at an early stage. Chemical imaging-based markers are a good candidate for such an approach since they are independent of anatomy and enhance morphometry based prediction models by adding a biochemical description of the cells and tissues (figure 3.2).

How can chemical imaging aid systems pathology?

Chemical imaging can be used to study cancer-associated biochemical changes in the tissue biopsy. This approach is particularly relevant in developing systems model where both molecular and spatial information is necessary. There are several key pieces of information about a patient’s bio-physiolocial system which can be obtained with previously established methods, such as genomics, and proteomics. While the role of tumor microenvironment in the development and

progression of cancer clear, we do not yet have efficient means to profile microenvironment changes in the native tumor. In this section, we review the effect of tumor microenvironment in disease development and progression and how it has been measured using chemical imaging, starting with two disease-specific examples. Given the strengths and limitations of current technologies, optical spectroscopy proves to be a timely tool to probe the microenvironment that could provide high molecular and spatial detail (figure 3.2).

Chemical imaging for biomolecular characterization at the cellular level: Breast cancer example

Computational modeling at the cellular level is often called as systems biology. This definition includes the use of bioinformatics databases of gene expression, proteomics data and available literature related to metabolic pathways to describe cellular networks[157]. Multiple optical spectroscopy studies have followed this approach by studying tumor cells grown in culture and observing their interactions with other cell types and the extracellular matrix. For example, fibroblast transition when grown in a co-culture with cancerous breast epithelium cell line was characterized using IR spectroscopic imaging[158]. In this paper, the authors correlated α-smooth muscle actin expression with infrared spectra to measure fibroblast transformation in response to the tumor. Fibroblast transformation was induced by either treatment with transforming growth factor-β1 (TGF-β1) or by co-culturing them with tumor cells. The authors found spectral changes in the C-H stretching region (3000-2800cm^{-1}), symmetric phosphate stretching peak (1080 cm^{-1}) and asymmetric phosphate stretching peak (1224 cm^{-1}) using which they were able to differentiate between normal and cancer-activated fibroblasts.

In the follow-up study, infrared spectroscopic imaging was used to characterize the effect of fibroblasts in promoting cancer growth[159]. In this study, the authors developed and applied a 3D cell co-culture system where the tumor cells interacted with fibroblasts in a controlled manner. Different configurations of co-cultures were studied, which altered the means of interaction between the tumor cells and fibroblast. The ‘mixed’ culture allowed direct cell contact between the fibroblasts and tumor cells, while the ‘sandwich’ co-culture allowed interaction via soluble factors. Using gene expression data, the authors established that the fibroblast-tumor cell co-culture altered the estrogen receptor levels and lead to epithelial to mesenchymal transition. Post the molecular analysis; the authors examined the FT-IR spectra of the same 3D culture samples. The decrease in the C-H vibrational spectrum (3000-2800 cm^{-1}), associated with lipids was found with the loss of estrogen receptor signaling. The peak associated with phosphate stretching at 1080 cm^{-1} majorly contributed by nucleic acids, was found to be a marker to assess proliferation

in cells. This peak was shown to reduce in response to the anti-proliferative endocrine drug tamoxifen in hormone-responsive cells but not in hormone therapy-resistant cells. The spectral observations made at the cellular scale were also translatable to human breast tissue samples. Spectroscopic differences between patients with different estrogen receptor status could be observed in the epithelium specifically in the C-H region which showed similar profile to the 3D cultured model[159].

In addition to observing cancer-associated changes, many other studies have sought to study the spectral changes in the cells as they go through various phases of the cell cycle[160–163] which could provide useful cell proliferation markers. These studies show that measuring the chemical response of cancer cells using optical spectroscopy is feasible without the loss of spatial information, and can be used as an in situ alternative to immunohistochemistry for tissues accessible with a probe such as skin, colon and the oral cavity. Using IR spectroscopy also automates the identification of cell types[164], thus enabling cell-type specific spectral analysis.

Chemical imaging for tissue level characterization: Prostate cancer example

Prostate cancer is perhaps the most frequently modeled disease using systems pathology approach. The currently prevalent predictive models for outcome determination in prostate cancer stratify risk of patients based on the biopsy Gleason score, prostate-specific antigen(PSA) levels and clinical stage, and have been reviewed in detail here[165]. The most critical concern while using approaches that heavily rely on the Gleason score is that the Gleason scoring is subjective since it is based on the pathologists' interpretation[165]. In recent years, quantifying the nucleic localization of androgen receptor protein has improved prognosis prediction. The application of systems pathology in determining recurrence based risk groups has been demonstrated with the use of morphological, immunohistochemical and clinicopathologic data[166–168] and an improvement in accuracy of prediction is reported by using multimodal data. In a study to automate classification of cancer versus non-cancer prostate tissue samples, it was shown that conventional histology based diagnosis benefits from multimodal image analysis that integrates IR spectroscopic images with H&E images and improvement is seen in the accuracy of determining cancer within biopsy samples[169]. In this study, the authors first classified the IR spectroscopic images into epithelial, stromal and other components using supervised classification. Next, morphometric information from the H&E images was obtained for segmented epithelial cell regions by fusing classified IR image with the H&E image. Lumen and nuclei related features were then extracted from these images, which were useful in differentiating between

cancerous and non-cancerous samples, much like the procedure a trained pathologist would follow. This automated IR spectroscopic feature based segmentation resulted in AUC value greater than 0.95 on the test dataset when both IR and H&E image data was used which dropped to about 0.92 when only H&E data was used.

In addition to being useful for cell-specific morphometric feature extraction, spectroscopic data has been demonstrated to predict the risk of prostate cancer recurrence more accurately than Kattan nomogram and CAPRA-S score[77]. In this study, the authors first identified a set of IR spectral features that had a discriminating power to differentiate between recurrent and non-recurrent cancer cases using frequent pattern mining. By testing both epithelium IR features and stromal IR features, the authors found that stroma, but not epithelium had predictive capability, and the stromal features were spatially associated with reactive stroma. Using clinical variables of age at prostatectomy, Gleason sum, and pathologic stage, the authors built matched recurrent and non-recurrent patient pair sets. The test sample was compared with training pairs in the dataset to quantify whether the test sample was closer to the recurrent patient or the non-recurrent patient via Ranking support vector machine algorithm. Using the ranks obtained from this algorithm, the authors calculated the predicted probability of recurrence of the test patient, called the IR score. Since the IR score is an independent predictor of recurrence, it can be combined with other clinical variables to fit a logistic regression model given by[77]

$$\log\frac{P(Y=1)}{P(Y=0)} = \beta_0 + \beta_1(I) + \beta_2(A) + \beta_3(G) + \beta_4(S) + \beta_5(P) \quad \text{(eq. 1)}$$

Where Y represents the binary outcome of recurrence (1) and non-recurrence (0), I represents IR score, A represents age at surgery, G represents Gleason grade, S represents pathologic stage and P represents PSA level. β_1-β_5 estimate conditional odds ratios for the corresponding variables. When used as standalone, the IR score achieved an area under the curve (AUC) of the receiver operating characteristic (ROC) curve of 0.73, highlighting the importance of IR spectra based probing of the microenvironment. This is an improvement over the previously proposed CAPRA-N and Kattan classifiers which performed at an AUC of 0.47 and 0.45, nearing almost random classification.

Given that systems pathology models which use the currently prevalent molecular and morphologic markers do not perform better than postoperative biochemical disease recurrence nomogram and Cox regression clinical failure model[170]; these results highlight the importance of using optical spectroscopy based features in the systems pathology models.

Chemical imaging to characterize the extracellular matrix

The extracellular matrix (ECM) is an essential component of an organ or tissue that provides it structure as well as chemical and mechanical signaling cues to maintain healthy structure and function. It has been shown that the changes in ECM are related to carcinogenesis and has been reviewed extensively[134,171–174]. Prolonged inflammation resulting in the activated stroma, changes in extracellular matrix stiffness[175,176], deregulation of specific ECM proteins[177] and extracellular matrix remodeling [178,179] are a few examples of changes that are associated with the development of cancer. Extracellular matrix close to the tumor is modified and represents a potential marker for risk stratification, but it is difficult to recognize changes occurring in the extracellular matrix using conventional histology. Remarkably, IR spectroscopy can differentiate between type I, III, IV, V and VI collagens, making it useful for molecular histology[180]. It has been shown that using infrared spectroscopy, the stromal response to developing tumor has a distinct spectral signature[181]. As an example, in figure 3.4, normal stroma and reactive stroma is identified in colorectal biopsy samples post a supervised learning step described previously[127,164,182]. In a malignant biopsy, the stroma neighboring the cancerous epithelium is identified as reactive whereas, in a normal biopsy section, the stroma neighboring the epithelium is morphometrically and biochemically normal. Degradation of the extracellular matrix via proteolysis can be localized with micrometer resolution[183]. This stromal change is significant in differentiating between normal, benign and malignant breast tissue[184]. Raman spectroscopy[185] can also be used as a tool to probe the extracellular matrix state in situ, achieving distinction between healthy and damaged collagen, and discrete frequency infrared spectroscopic imaging is emerging as a high-speed tool for rapid detection of fibrosis and tissue damage[186,187].

Chemical imaging based angiogenesis identification

Tumor angiogenesis, a hallmark of cancer[131] presents yet another avenue of information that can be useful in predicting the trajectory of the tumor. Tumor sustenance and growth are dependent on the access to blood vessels and often the tumors, and their interaction with other components in the tumor microenvironment create conditions that can induce angiogenic signaling pathway[188–192]. Imaging angiogenesis in-vivo and ex-vivo has been made possible by microcomputed tomography (micro CT)[193], magnetic resonance imaging (MRI), and optoacoustic tomographic imaging[194]. Angiogenesis can also be determined by assaying angiogenic growth factors such as VEGF which is amenable to multiplex molecular profiling

systems, while hypoxia-specific conditions, which are the key regulators of angiogenesis[195–197] can be measured in vivo using near-infrared optical imaging probes[198]. Variations in tissue biochemistry due to hypoxia and low pH conditions can be measured by assaying glucose and lactic acid levels in FT-IR spectroscopy. Glucose content is found to decrease linearly with distance while lactic acid content increases as we move away from the blood vessel[199], making FT-IR a candidate to perform microscale molecular imaging to visualize angiogenesis. In addition to imaging metabolites for assessing angiogenesis, triple helix and β-turn content of the secondary structure of blood vessel proteins has been shown to be a potential FT-IR based marker for imaging angiogenic tumors[200].

New and emerging concepts

In addition to the currently available literature on the mechanism of cancer initiation, growth and spread, new and emerging concepts provide an opportunity to enhance diagnosis and prognosis prediction. With research still underway on the clinical impact of these factors, this section outlines potential areas where developing optical spectroscopy based analysis methods can be useful.

Self-seeding

Metastasis to distant sites requires colonization of circulating tumor cells in unfavorable conditions. In contrast, the primary site of the tumor has more welcoming conditions[201]. Re-infiltration of circulating tumor cells(CTC) to the primary site, known as self-seeding, is facilitated by tumor-derived cytokines that act as CTC attractants[202]. Because self-seeding enriches the tumor with aggressive cells, it is likely that self-seeding can worsen prognosis. A large-scale study[203] published recently reported that the overall survival of patients with metastatic cancer who underwent local therapy was improved as compared to patients that did not receive local therapy. This distinction could be due to reducing tumor burden and interrupting self-seeding when local treatment is given[203]. There is limited clinical evidence with regards to the effects of tumor self-seeding, and it is not possible to directly evaluate self-seeding extent in patients. CTCs, which are vital in the self-seeding process can be monitored with microfluidic devices[204] using blood[205–207] and through other technologies outlined in these reviews[208–210]. With the recent advancements in the CTC capture technologies, it is likely that these devices would soon have clinical applications using patient’s blood or biopsy[211] and potentially impact clinical course of action[212].

Metabolism

Alterations in metabolism can facilitate uncontrolled tumor growth[131]. Otto Warburg first showed that glucose consumption is heightened in tumors when compared to normal tissues[213]. Much research has been done in this field since the first observation, and is reviewed in these articles[214–217]. The altered metabolism in the tumor has been of interest in developing diagnostic techniques as well as in identifying therapeutic targets[218,219]. Positron emission tomography (PET) is a routinely used clinical technique that uses ^{18}F-fluorodeoxyglucose (FDG) to measure glucose metabolism. FDG-PET can, therefore, identify biochemical changes at the molecular level in vivo. Due to low sensitivity and modest specificity, FDG-PET is not a viable diagnosis tool. However, it can be useful in characterizing the disease once a diagnosis has been made[220]. FT-IR spectrometry can assist in studying metabolic changes in tissue, associated with quantification of metabolic molecules such as glucose and lactic acid. In a study to test this approach, the researchers found that FT-IR spectrometry was able to detect nanomolar concentrations of metabolites within biological samples[199]. Interestingly, premalignant spectral changes in cells are detectable much earlier than morphologic changes in the cells[221,222] constituting of significant variations in lipids and proteins and further research in this area could shed light on the changes undergone by the tissue temporally as it changes from normal to a malignant state. A broad spectrum of small biomolecules such as glucose, choline, fatty acids and amino acids can be visualized by using Raman-active probes with high specificity and sensitivity, further enhancing our insights to metabolism in the tumor environment[145,146].

Use of mathematical methods

The current medical diagnosis has been enhanced by the introduction of '-omics' data. The clinicians now consider histopathology based morphometric information in conjugation with molecular information and apply their own experience and knowledge to reach a diagnosis[223,224]. This behavior of pathologist can be replicated using machine learning approaches to develop probabilistic models to determine diagnosis and predict prognosis. One way to do this is to use Bayesian parameter estimation to calculate the weight of various response variables available through experimental data[225]. This approach produces posterior probability distribution that can predict system behavior. A computational approach to translate metabolic networks into mathematical models has also been explored[132]. Briefly, two mathematical models can be used to predict the response of a biochemical system. The first is the Systems Theory (S-system) approach where differential equations are used to model a non-linear system.

The second approach, based on fuzzy logic is based on probabilistic models that output results between 0 and 1, accommodating for imprecision in biological systems. When modeling cancer through systems pathology approach, we need spatial as well as temporal factors[226]. Beginning with the development of the disease due to perturbations in the system: often due to the loss of tumor suppressor gene functions, to the growth and progress of cancer to invasive and metastatic stages; each stage of cancer presents an altered system. In response to therapy, a system can change over time as the disease develops drug resistance. Dynamic modeling or mechanistic modeling used in systems pathology employs previously established mathematical models such as the law of mass action and equations describing enzyme kinetics[227]. These models can be used to predict temporal response[227] albeit at molecular scales. Given the complexity of the system and evolving nature of cancer in response to microenvironmental changes, stochastic modeling of the systems have gained popularity[228–230].

In either of these systems, the input should be quantitative, multiscale and multidimensional, encompassing several levels of the system, and the prognostic model should include the ability to identify and explain factors that were predictive. This requirement makes the development of such models tricky, needing a highly complex and interconnected model. One way to handle the issue of complexity is by assembling small quantifiable pieces to come up with a single predictive model. Imaging provides opportunities to obtain quantifiable chunks of information. One way of integrating imaging data to mathematical models was proposed by Atuegwu et al (2010) and Gore et al (2010) where imaging data from multiple modalities was integrated as initial conditions to determine tumor growth and treatment response. Mathematically, this relationship is written as[231,232]

$$\frac{dN_i}{dt} = \mu_{p,i}N_i(t) - \mu_{d,i}N_i(t) + k_{im}N(t)$$

(eq. 2)

where $N_i(t)$ represents the number of tumor cells in the i^{th} voxel as a function of time, k_{im} term represents the net 'transfer constant' of cells from the i^{th} voxel to the m^{th} voxel obtained using ^{18}F-fluoromisonidazole PET, $\mu_{d,i}$ represents the death rates of tumor cells obtained via 99mTc annexin V imaging, and $\mu_{p,l}$ represents the proliferation rate obtained via fluorodeoxythymidine PET (FLT-PET)[231]. This model could simulate the tumor characteristics in a rat brain as a function of space and time, where the initial parameters were set by imaging data specific to the subject,

potentially leading to patient-specific predictions. This example shows the remarkable prediction capability that can be achieved by integrating imaging data. The prognosis determination example discussed in equation (1) shows that incorporating biomolecular data with clinicopathological data and other predictors renders an informed, quantifiable and accurate prediction. Together, models that can predict tumor growth, drug response, account for temporally and spatially specific microenvironmental changes and patient-specific factors can lead us to precise disease management.

Conclusions

There has been a rapid development of analytical instruments to detect, diagnose and study cancers. CT and MRI can be used to perform anatomic imaging, PET and single photon emission tomography (SPECT) are useful in determining biochemical characteristics, and these techniques are often used in a combination called as multi-modality imaging to collect a broad spectra of information[233,234]. Complementing the conventional tools of biopsies and histopathology, clinicians can now utilize several of these tools to reach a decision. In addition to the macro-level data provided by these imaging modalities that help in determining the existence of tumor and basic biochemistry, a systems pathology approach requires information at the molecular level, such as that provided by proteomics and genomics data. In addition to the ability to probe the tumor microenvironment by delivering spatially specific biochemical data, chemical imaging can provide information independent of histopathology and clinicopathological data which has been shown to improve recurrence prediction[77].

Perhaps the most challenging step in systems pathology approach for disease analysis is the modeling of the system. Many mathematical methods have been developed to explain specific components of the cancer development process such as self-seeding[235], angiogenesis[236–238] and cancer metabolism[239–241]. At the systems pathology level, the model needs to encompass multiscale, multimodality quantitative data (figure 3.5). The availability of data is no more a challenge, rather, identifying useful data and eliminating redundant information is necessary before model implementation. Mathematical models are useful at unimodal stages, where we have an understanding of the process. When many modalities are combined, the effect of such combinations become hard to interpret manually and would require machine learning. Deep learning techniques can be used to consolidate the data and form meaningful conclusions in instances where the bottom up equation driven models fail; through the combination of modalities on space, time and molecular axis in a top-down approach. The next driving

developments in this field should be focused on the precise quantification of the microenvironment using patient biopsies, and a large-scale collaborative effort to realize focused data collection and computational modeling goals.

Figures

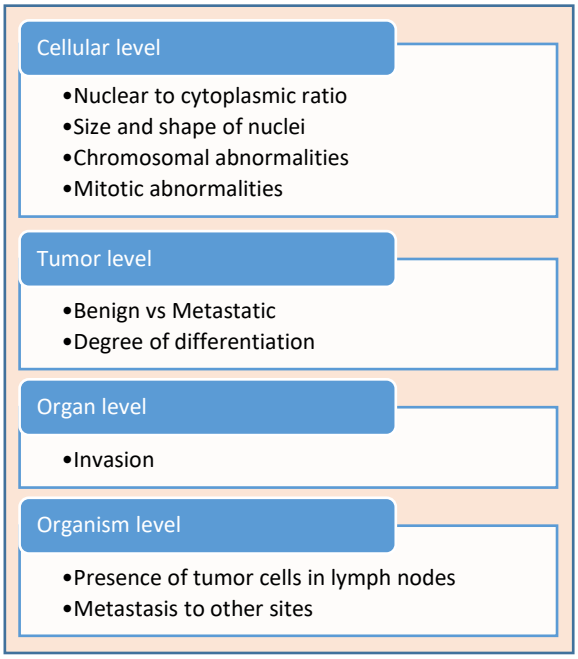

Figure 3.1: Features useful for diagnosis and analysis of cancer

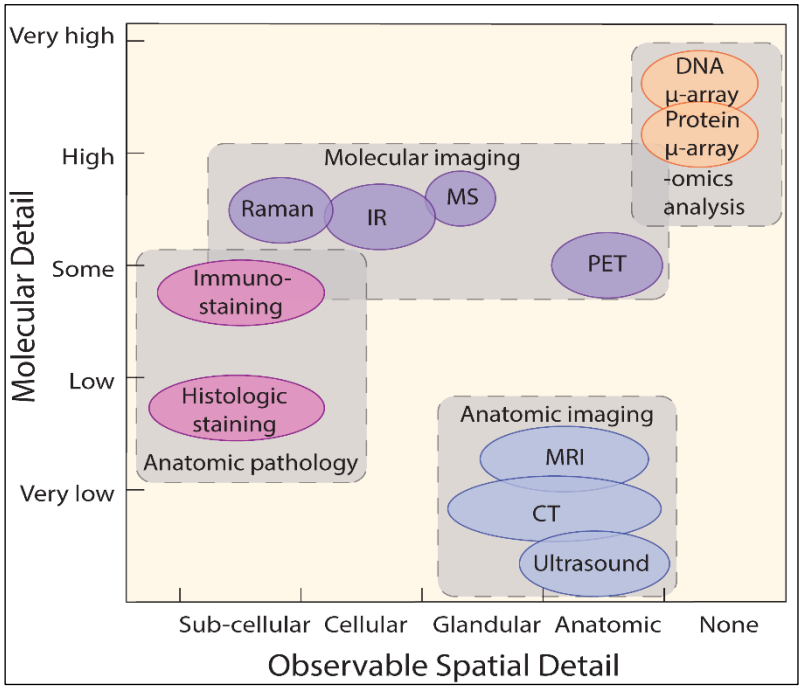

Figure 3.2: Imaging and molecular analysis methods compared against the molecular and spatial details offered by them. Spatial detail is associated with the spatial resolution offered by the techniques in the biological context.

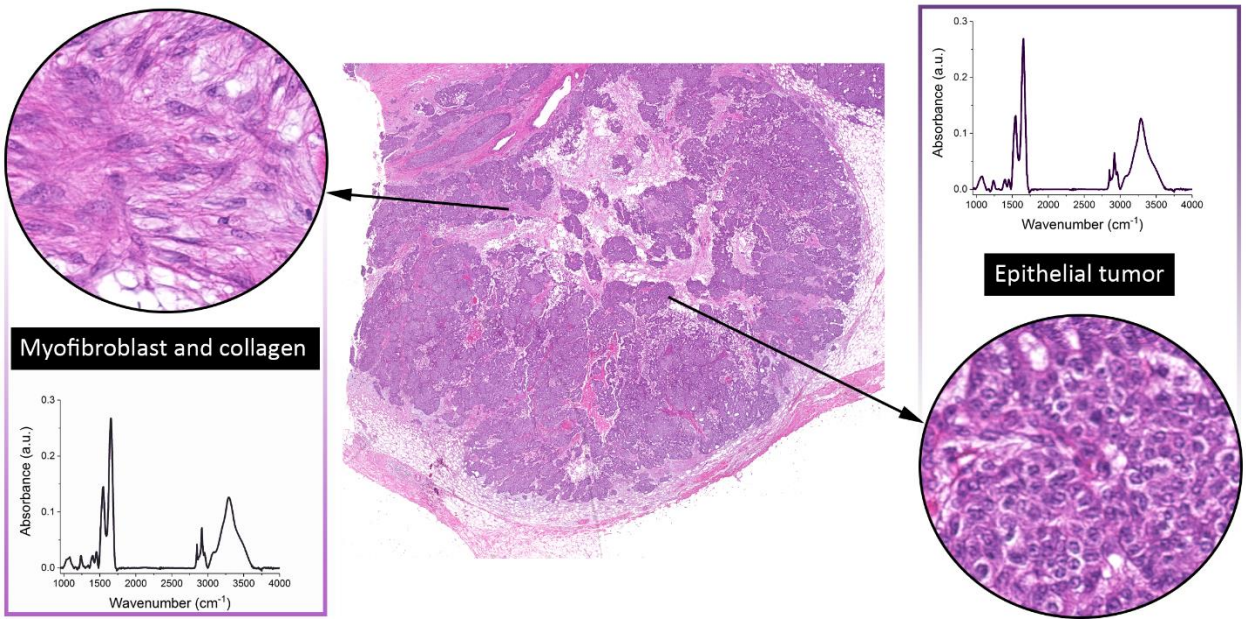

Figure 3.3: IR spectroscopy brings together morphometry and biochemical profiling of the tissue. Each pixel of the image has a spectrum. Different cell types such as myofibroblasts and epithelium have different IR spectra, which are useful in assessing chemical differences and changes undergone by them.

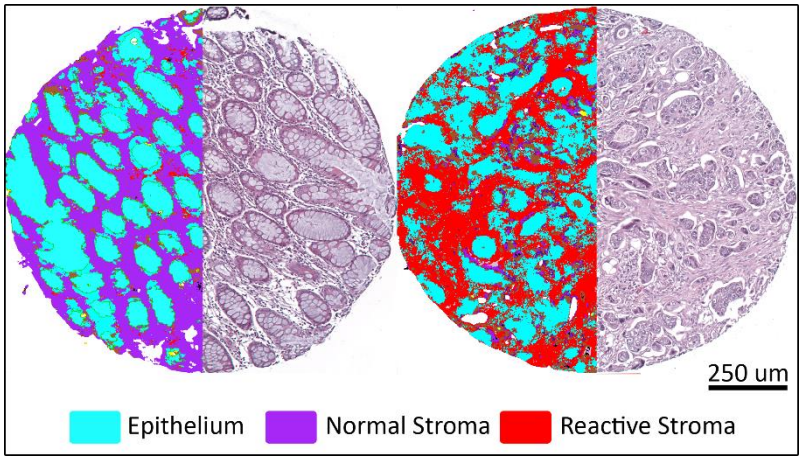

Figure 3.4: Morphometric and biochemical differences exist between normal and cancer-activated (reactive) stroma. These differences can be used to identify normal stroma and reactive stroma in infrared spectroscopic images. In figure, normal stroma is identified in a normal biopsy core (left) and reactive stroma is mapped on a malignant biopsy core (right). Note the morphometric differences between the organization of epithelium in normal and malignant core.

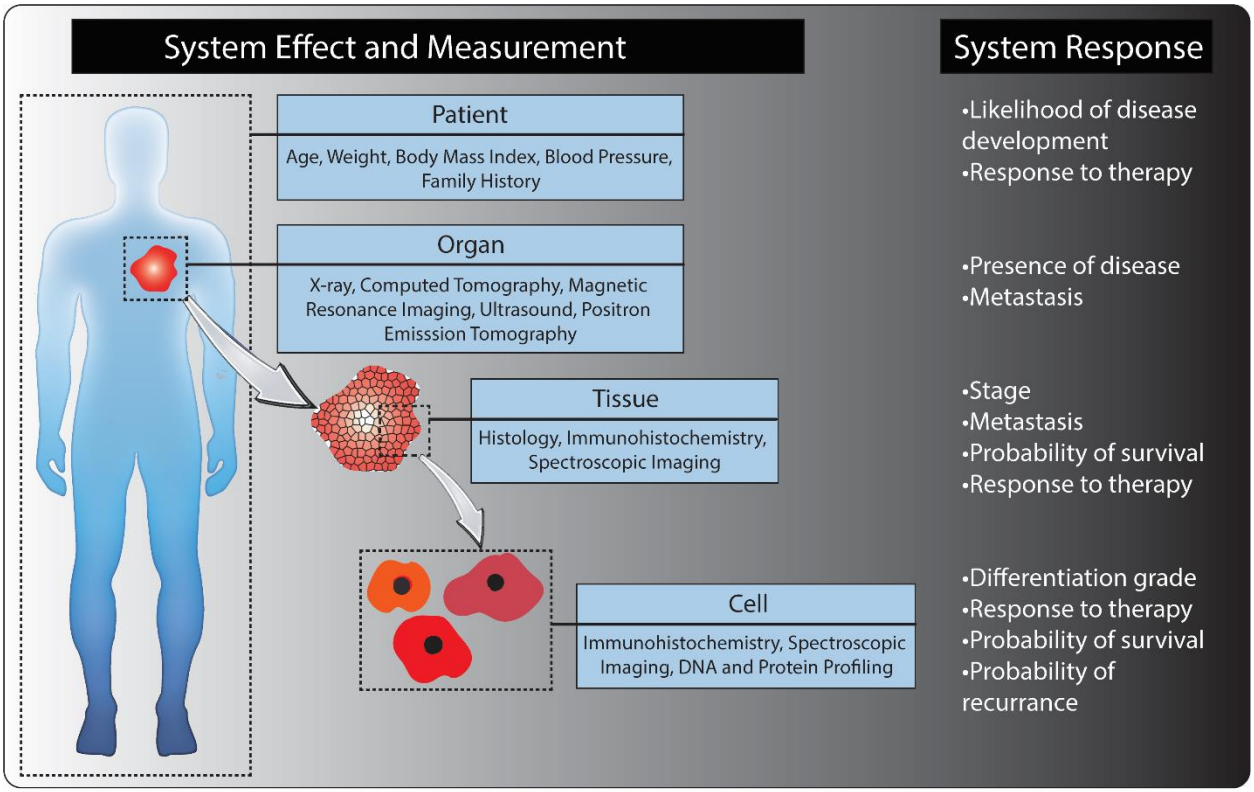

Figure 3.5: Several anatomic and non-anatomic assessment techniques provide useful pieces of response information. When used in isolation, these techniques cannot predict the complete systemic response. Therefore, there is a need to integrate data obtained through various measurement methods into a unified systems pathology model.

CHAPTER 4: MICROENVIRONMENT AND TUMOR SPATIAL INTERACTION MODEL USING QUANTITATIVE CHEMICAL IMAGING PREDICTS COLORECTAL CANCER PATIENT OUTCOME[7]

Abstract

The tumor microenvironment and its interaction with the tumor is indicative of disease progression but has not been clinically applied due to lack of objective assessment criteria. The proximity associated effects of the tumor to its microenvironment which can explain the long-term behavior of tumor remain to be developed. In this work, we utilized the biochemical sensitivity of infrared spectroscopic imaging to segment colon tumor biopsies into major tumor microenvironment components in a 320 patient cohort. A risk score defined by the extent of stromal reaction and its interaction with the tumor stratified overall survival in patients (p-value 0.0003), and disease free survival (p-value 0.0274). The risk score performed independent of stage and grade information of the patient with the hazard ratio of 1.88 at p-value of 0.011, almost doubling the risk of death if the patient had risk score higher than 3.53. Our results objectively quantify and model the spatial interaction of tumor with its microenvironment, which is predictive of the patient outcome.

Introduction

With the developments in precision medicine, targeted therapies, imaging, computational and data visualization tools, we have a surge of clinical data, which is often under-utilized when treated in isolation. Due to the intricate processes taking place during the development and progression of cancer, the tumor microenvironment is continuously interacting with the tumor and changing dynamically[242–244]. Several key changes in the tumor microenvironment, such as cancer-associated fibroblasts, stromal remodeling as well as immune cell infiltration play a role in promoting or resisting tumor growth[131]. Specifically in colon cancer, the fibrotic stromal response known as the desmoplastic reaction has been linked to survival, cancer aggressiveness and degree of invasion [12,245–247]. Although such survival stratification is of high utility in determining the outcome, it is clear that the stromal remodeling in the tumor microenvironment does not act alone in promoting aggressive tumor behavior. The biomolecular snapshot of the tumor in its native microenvironment captured in conjugation with the spatial distribution could be descriptive of the patient outcome but has not been explored to date.

[7] In preparation for publication as Tiwari, Saumya et al. “Microenvironment and Tumor Spatial Interaction Model Using Quantitative Chemical Imaging Predicts Colorectal Cancer Patient Outcome.”

Traditionally, after surgical resection/biopsy and molecular staining, pathological interpretation is used to determine patient outcome in terms of grade and stage (figure 4.1a,b). In contrast, quantitative image analysis seeks to evaluate the tissue biopsy images in the form of quantifiable variables. Such investigations can help us develop an understanding of tumor-microenvironment interaction[248] and give us insights into the spatio-specific tumor progression mechanisms. Previous quantitative image analyses predicted patient survival by merging information from biopsy images with molecular data[249] and demonstrated capturing heterogeneity in cell populations[250]. Despite recent advances, the rich biochemical details present in the tumor cannot be utilized to predict patient outcome without a priori knowledge of molecular targets. Other studies have also identified the link between desmoplastic response in biopsy specimens and the depth of invasion in early colon cancers[12,247]. Although such stratification is of high utility in determining the outcome, the intra- and inter-observer agreement in deciding the desmoplastic reaction is low[251]; varying between 0.30 to 0.71. This lack of concordance found in colon cancer underlines the need to develop objective methods to evaluate the stromal reaction. In addition, current models of quantitative image analysis techniques rely on tissue staining, and suffer from roadblocks such as low contrast, need for annotations by pathologists, as well as multiplexing limitations.

Quantitative chemical imaging (QCI) seeks to address the current challenges in predicting patient outcomes without a priori information about the molecular targets, and fulfill the need to quantify tumor-tumor microenvironment interactions. In particular, chemical imaging using Fourier transform infrared (FT-IR) spectroscopic imaging allows spatially specific multiplexed chemical profiling of samples without the need for stains (figure 4.1c). Cell populations and micro-environmental features show differences in their infrared absorbance spectra[44,74,75,127] owing to the inherent biochemical differences between them. Spectral profiles collected from IR imaging enable sensitive and specific identification of tumor and tumor microenvironment components[164], which can be mapped onto the tissue using artificial intelligence(AI) for robust image quantification (figure 4.1d).

In this work, we hypothesized that by utilizing both molecular as well as morphometric features in patient tumor sections, we will capture the state of the tumor-microenvironment interaction, thus predicting patient outcome. Our work on quantitative chemical imaging provides a robust approach to capture and model the biochemically specific spatial interactions to predict long-term tumor behavior.

Results

Infrared spectroscopic signatures identify tumor stromal components

In this work, we aimed to develop a Fourier transform infrared spectroscopic imaging based machine learning model which allowed for the mapping of several biochemical transformations in the tumor stroma onto the tissue biopsy image. High definition Fourier transform infrared imaging was used to image eight tissue microarrays, collecting the infrared spectrum of every $1\mu m^2$ pixel. The spectral signatures associated with desmoplastic reaction, normal stroma and lymphocytes and seven other tissue components were obtained by matching regions annotated by a pathologist on H&E image to the infrared spectroscopic images (Supplementary figure 4.1a). Figure 4.2a shows the average absorbance spectra of the ten classes that we identified in colon tissue. The most substantial differences between classes were observed in the fingerprint region between 982-1480 cm^{-1}. The most prominent differences were seen in mucin and mature epithelium vs. all other classes in 980-1182 cm^{-1}. This distinction is arising from mucin, which is a glycosylated protein showing strong absorbance at $1038cm^{-1}$[252]. Mature epithelium (goblet cells) containing cytoplasmic mucin also registered glycoprotein associated absorbance. As seen from the spectra, and the images of colon adenocarcinomas in subsequent sections, this functional property of mature epithelium was lost in the malignant or proliferative epithelium. Another major region of difference was found in the CH,CH_2 and CH_3 stretching motion peaks around 2800-3000 cm^{-1} which has been previously noted as well.

While some of the differences shown in figure 4.2a arise due to biochemical differences between histologic classes, we also accounted for other sources of variations in the samples. In our study, we considered patient, array and histological class labels as factors affecting the infrared spectrum and performed ANOVA using the framework described previously[253]. Spectroscopic data collected from three training arrays were utilized for this approach (Supplementary figure 4.1b). From this analysis, using 0.05 as significance level, we removed all spectral metrics where array and patient associated variances were statistically significant. Two hundred and fifty-six spectral metrics were excluded from the ANOVA analysis. Following analysis of variance, we performed an additional step of feature reduction using minimum redundancy maximum relevance (mRMR). Feature reduction was required to (a) Reduce computation time (b) Remove redundant features (c) Prevent overfitting. Briefly, this model used the correlation between variables and outcomes as a means to identify variables that were the most predictive of the class label, and the correlation between variables to identify variables that will cause the least redundancy in the

system[254]. Using mRMR, we were able to reduce the number of variables that ensured better model fit and mitigated overfitting. Post ANOVA and mRMR, we retained 50 spectral metrics that were used for developing histology classifier model. These spectral metrics have been listed in Supplementary table 4.1 with accompanying definitions. From this table, we observed that the retained spectral metrics were most frequently defined from the fingerprint region between 1053 -1593 cm^{-1} and 2939-2987 cm^{-1}; consistent with our observations from fig 4.2a.

Finally, we looked at the differences between the classes in the 50 spectral metrics that were chosen following ANOVA and mRMR (Fig 4.2b). We calculated average spectral metric values across each class in the training set, discretized the values in each of the spectral metrics by equal depth binning and performed hierarchical clustering. Data were first clustered along the classes and then along the metrics using Euclidean distance metric and farthest neighbor distance linkage between the clusters. The heat map in figure 4.2b shows the observed clustering patterns, where each row corresponds to a spectral metric, each column corresponds to the histologic classes, and the intersection indicates the metric discrete value level for the specific metric in that class. As expected, mucin and mature epithelium clustered close together, while blood had the most distinctive features, owing to the absence of nucleic acids. The two most distinct spectral clusters from the hierarchical clustering are labeled C1 and C2 in figure 4.2b. The difference between these clusters can be understood in terms of the spectral regions that were most frequently involved in defining the metrics for these clusters (Supplementary Table 4.1). A similar idea has previously been described as spectral barcoding, where IR spectra are used directly to identify discriminative frequencies by unsupervised analysis[255]. From this analysis, the majority of fingerprint region between ~982-1580 cm^{-1} and CH stretching region between 2800-3000 cm^{-1} clustered together as C1 while OH-NH region between ~3000-3700 cm^{-1} and amide I region clustered together as C2. From the metric expression patterns of the classes in C1 and C2, it is clear that further association of spectral metrics exist. While 50 metrics are used to develop this classifier, it indicates that there is a possibility of trimming down the dataset further to improve the speed of imaging by utilizing discrete frequencies[256].

Biochemically specific spectral machine learning classifier retains high specificity and sensitivity when tested on independent TMAs

We used Random Forest supervised learning algorithm to develop the histology classifier with ten classes, labeled as epithelium (mature), mucin, epithelium (proliferative), necrosis, reactive stroma, blood, inflammatory cells, non-reactive stroma, muscle and loose stroma. The leaf size

and feature size determined for optimal fit were 500 and seven respectively, with 50 total features and an ensemble of 50 decision trees (Supplementary figure 4.1c). We have observed that increasing the number of trees beyond this did not give a proportional increase in accuracy and followed the law of diminishing returns described before[257,258]. This classifier was trained on four arrays (a1,a2,a3,a4) and 126,946 pixels per class, calibrated on two additional arrays (a5,a6) and tested on two independent arrays (a7,a8). For both training and testing area under the curve (AUC) of the receiver operating characteristic (ROC) curve was evaluated. The results from this classifier are shown in figure 4.2c. The performance of the histology classifier was evaluated at pixel level using receiver operating characteristic curves, using pathologist annotated regions as the ground truth. High specificity and sensitivity were obtained, with the training data classified with an average AUC of 0.94, and the validation data classified with an average AUC of 0.93 (figure 4.2c). We also evaluated the importance of metrics in classification by measuring the increase in prediction error in calibration data (a5, a6) when the values of the metric were permuted across all data. Interestingly the most important features identified in this manner (figure 4.2d) were associated with amide I and amide II regions, such as normalized amide II peak height at 1545 cm^{-1}, area to height ratio of amide II peak region between 1591-1757 cm^{-1} and 1645 cm^{-1}, peak centroid position of amide II peak and the normalized intensity of 1645 cm^{-1} band. The cohort used in this study comprised of paraffin-embedded tumor tissue of the surgical specimens, where normal-appearing colorectal mucosa and lymph node metastases were also sampled for some patients. Figure 4.2e shows the comparison of H&E images with corresponding IR histology classified images for normal colorectal mucosa, invasive tumors, and lymph node metastases. The classified images show good correspondence with the H&E images for the three types of tissues. Benign colorectal mucosa is a good example of the diverse tissue components present in the colon, with well-formed mature epithelium glands and normal appearance of (non-reactive) stroma. Mucin can be seen within the glands. In invasive tumors, the glandular structure formed by malignant epithelium is distorted or lost, and the stroma around the tumor is modified due to desmoplastic reaction (reactive stroma)[12]. All of these histologically important features were classified correctly. We were also able to identify the presence of malignant cells in samples from lymph node metastases, indicating superior performance compared to H&E based benchmarks[259].

<u>The extent of desmoplastic reaction, as well as its proximity to tumor cells, is associated with survival</u>

To understand the scope of microenvironment effects on patient survival, we developed the

supervised classification models that performed with high specificity and sensitivity to map stromal changes onto the tissue biopsy images. We classified stroma as reactive, where the desmoplastic reaction was present, non-reactive, where the desmoplastic response was absent and as lymphocytes where lymphocyte specific spectral signatures were observed. The desmoplastic reaction was identified using previously established criteria, namely enrichment of “plump” fibroblast, the organization of stroma and presence of other cell types[260,261]. The pathologist making the ground truth categorization was blind to all accompanying clinicopathological data including the stage. Next, we used the classified images obtained from the supervised classifier to measure quantitative spatial features (Fig 4.3a). Distance feature (d) was defined as the distance to the closest microenvironment component from the tumor pixel, averaged over 500 random tumor pixels in 30% downsampled image. The area feature (N) was defined as the total number of pixels classified as a specific microenvironment component in a radius R from 500 randomly selected tumor pixels as the center. The area was normalized to πR^2 to accommodate for centers close to the biopsy edge. We set the R for our analysis to be 600μm, based on our empirical observation that in comparing invasive and normal cores, any radius above 439μm captured the spatial characteristics between the biopsies. Finally, the interaction feature (M) was defined as the product of d and N averaged over 500 randomly selected tumor pixels as the center. For these tests, we only selected cores with at least 5% malignant epithelium by area. Each of these features was dichotomized by splitting at the median value of 3.53; giving us two patient groups per variable per microenvironment component tested. Next, we performed the univariate log-rank test and multivariate Cox regression analysis to determine if there was a significant difference in the survival of the two groups (Table 4.1). From the two tests, only features measured with reactive stroma as the microenvironment component showed a significant difference in survival. The two features that showed significant differences in the survival were N_{RS} and M_{RS}, with p values of 0.006 and <0.0005. From multivariate Cox regression model of time to death (Table 4.2), the interaction metric variable M_{RS} showed an independent effect on increasing hazard for the patient when modeled with other known covariates such as the stage, grade, age, sex, and source, with a p-value of 0.011. The p-values for three overall tests, the likelihood ratio test, Wald test, and log-rank test were all less than 4e-11, indicating that the model was significant, rejecting the null hypothesis that all of the coefficients(β) are 0. In the multivariate Cox regression analysis, the hazard ratio, evaluated as exp(β) was in the range 1.15-3.07, indicating a strong relationship between the high values of interaction feature M_{RS} and increased risk of death. Thus, higher values of interaction feature M_{RS}, calculated from the patient biopsy images are associated with adverse prognosis. Other features that showed significant association

with risk of death were stage and age, as expected. By contrast, the tumor grade evaluated on whole surgical biopsy images by pathologists did not show significant association with increased risk when modeled with other covariates.

Fig 4.3c shows Kaplan-Meier survival curves for overall survival and disease-free survival for all three features calculated for tumor's interaction with reactive stroma. From univariate log-rank test, both N_{RS} and M_{RS} showed a statistically significant difference in overall survival, while only M_{RS} showed a statistically significant difference in disease-free survival. The role of stromal reaction and its interaction with the tumor in predicting disease-free survival indicates an association with aggressive tumor behavior. By performing two-sample t-test (Table 4.3) on continuous variable M_{RS} grouped by stage, we discovered that the mean value of M_{RS} for reactive stroma was significantly different between Stage 2 and Stage 3 at 0.05 significance level (p-value=0.00142 and power= 0.9) and between Stage 2 and Stage 4 (p-value= 0.00243 and power =0.87). Thus, we can reject the null hypothesis that there is no difference between the means of the above groups. Several other stage grouped combinations were tested, but statistical conclusions could not be drawn due to low power. When stage 1 and stage 2 patients were combined (low stage) and tested against stage 3 and stage 4 patients combined (high stage), we observed a significant difference in the means. Two sample t-test on combining these groups had a p-value of 0.0012 at 0.90 power, confirming the observation. We also tested other histological classes following the same procedure and found that there was no difference between the means of spatial features with respect to the stage. In addition to the two-sample t-test, we performed Mann-Whitney test, which does not assume normal distributions and tests whether the patients are sampled from populations with identical distributions. From this test, we confirmed that the distributions of stage 2 and 3, stage 2 and 4, and low stage vs. high stage were significantly different.

Discussion

The mechanism governing tumor invasion and its interaction with the surrounding stroma and stromal cells is complex and not clearly understood. Dedifferentiation at the invasive front of the tumor is often the beginning of metastasis[262]. Several spatially specific features of solid tumors, such as tumor structure, and proximity related effects cannot be accounted for in traditional molecular assays. Quantitative image analysis using histological stains has previously been proposed for breast cancer but is limited by the molecular information content of the H&E stain, and artifacts introduced at sample preparation, staining and imaging steps[249]. In contrast,

infrared spectroscopic imaging provides molecular information in a spatially specific context[263], without extensive sample processing or staining, enabling us to identify critical biochemical changes in the tissue image. To utilize such a technique for quantitative image analysis, it is crucial to ensure that the biochemical changes associated with activation of stroma are accurate and reproducible. The purpose of our supervised machine learning approach was to ensure that regions of interest in patient biopsy images were identified with high accuracy. Human patient samples are heterogeneous and biochemically complex, with diversity arising due to the inter-patient variations, biological heterogeneity and patient-specific disease development and response[35]. There are also effects introduced by the systems used to probe the samples, such as noise in signal measurement, differences in sample preparation, and several other factors not documented so far[94,264]. When developing a supervised classification model to identify histological classes, it becomes especially imperative to analyze sources of variance to identify spectral regions where histologically irrelevant variations are present and significant. Following ANOVA and mRMR to perform feature reduction, we developed a random forest-based supervised classification model, where we achieved high specificity and sensitivity in classifying ten histological segments in colon biopsy images. At pixel level, this classifier performed at an average AUC of 0.93 when tested on an independent sample set. This is higher and significantly more multiplexed than other proposed digital pathology approaches using H&E images where the benchmark performance is noted for deep learning classifiers at an AUC of 0.93 in identifying metastatic tumor in lymph nodes as the two components[259].

While general tissue organization and structure is typically assessed by the pathologist at the time of examination, this is largely subjective[251,265,266]. Several outcome associated image assessment criteria, such as nuclear to cytoplasmic ratio of molecular markers[267], cellular proportions[268], and measuring immune infiltration[269,270] have been proposed. These procedures often require additional pathologist and laboratory work and do not provide consideration for tumor-stroma interaction. Even established prognostic associated features have not found footing in clinics due to lack of objective assessment criteria. For example, previously, Ueno et al. [260] categorized stroma in colon biopsies into mature, intermediate and immature based on the fibrotic stromal response. Using this stratification, they showed that five-year survival rates were significantly lower for patients with high desmoplastic reaction. Despite the identification of the link between desmoplastic reaction and the depth of invasion in colon cancers[12,247], an objective and reproducible scoring system is undeveloped, largely due to the concerns arising from lack of concordance[251].

Unlike other predominant cancers where molecular markers have established a role in determining the outcome and therapy options[7,271], the criteria to determine the patient outcomes in colon cancers is less direct. The goal of this work was to understand how the changes in the tumor microenvironment and their interaction with the tumor are linked to the patient outcomes by studying the tissue biopsy image. This work draws on the spatially specific molecular assessment provided by infrared spectroscopic imaging combined with machine learning approaches for robust identification of tissue areas as well as statistical methods to determine the underlying mechanisms. We studied multiple tissue-microenvironment components and found a significant association between the extent of stromal reaction and patient outcome. The links were much more pronounced in our interaction model, which intuitively models tumor structure concerning outcome associated microenvironment component. Multivariate Cox regression model showed that the risk of a patient presenting with high M_{RS} biopsy images increased independent of stage. Univariate log-rank test showed a significant difference in overall as well as disease-free survival of patient groups stratified on the basis of the M_{RS} score. From t-test and Wald test, we see an association between the patient's stage and the M_{RS} score, confirming our hypothesis that our model is capturing the switch of tumors to a more aggressive behavior by monitoring its interaction with its microenvironment. Thus, our work provides an objective and fully automated image assessment criteria to assess microenvironment-tumor interaction. We show from our work that there is abundant prognostic information available in a single tumor biopsy snapshot, which currently remains clinically underutilized. Although our spatial interaction model performs very well in stratifying patients, there are many unexplored factors that could potentially stratify patients further. For example, IR spectroscopic imaging is limited by spatial resolution that can be achieved, as well as the level of molecular detail that can be recorded. Finer molecular differences within the reactive stroma as well as cellular heterogeneity in the tumor itself should be probed by combining imaging and molecular assessment modalities. We also anticipate that IR imaging-based quantitative image analysis can also provide key insights into several other cancer types, especially in cases where outcome associated molecular markers are lacking.

Conclusions

The tissue biopsy is a snapshot of the tumor in its native habitat. The complex biochemically specific interaction between tumor and tumor-microenvironment is a key determinant of tumor aggression. In this study, we identified the infrared spectroscopic signatures of ten unique histological segments present in colon biopsies and mapped them onto the tissue image. We stratified the overall patient survival independent of stage, grade and age by modeling the extent

of desmoplastic reaction and its interaction with the tumor cells. This study demonstrates reproducible and objective evaluation of risk-associated features using QCI. This work is especially critical for clinical evaluation of tumors that do not have defined patient outcomes associated with molecular features. By providing quantitative assessment, QCI can play an integral part in evidence-based pathology, which seeks to aid clinical instinct by using evidence derived from large-scale data[133]. Using artificial intelligence models that are capable of combining multi-platform approaches, QCI makes it possible to place the information in the clinical and biological context, which augments the current clinical analysis by harvesting the full potential of big data. With recent developments in the field of chemical imaging that enable stainless tissue characterization at clinically desirable speeds[43,45,187], we anticipate applying quantitative chemical imaging approaches in clinics, allowing automated diagnosis and outcome predictions.

Methods

Sample preparation

The patient cohort used in this study comprised of 320 anonymized patients undergoing elective surgery for colorectal carcinoma. Of these, 158 patients were females, and 162 patients were males. Cores of 1 mm diameter were sampled for each patient from representative invasive areas of paraffin-embedded blocks and were used to construct eight tissue microarrays(TMA). For some patients, normal colon mucosa samples were also included. This cohort has been used previously[272] and described in detail in the cited reference as Cohort II. For IR spectroscopic imaging, a 10 µm thin section of each of the TMAs was obtained on barium fluoride substrate. A consecutive section was collected on a glass slide for hematoxylin and eosin (H&E) staining. Due to the IR absorbance of paraffin at the 1462 cm^{-1}[44], before scanning, paraffin was removed by initially dripping the slide with cold hexane followed by complete submersion in continually stirring hexane for 48 hours at 40ºC where the solvent was renewed every 3 hours. The disappearance of the representative peak over several locations on the slide confirmed the dissolution of the embedding medium. For supervised classification, data was annotated by labeling histologic classes on H&E images by collaborating pathologist. These annotations were manually copied on the infrared spectroscopic images and served as ground truth.

Imaging

High magnification images were taken on Agilent Stingray imaging system in high magnification mode. This microscope was equipped with 128x128 focal plane array MCT detector. Each pixel

of size 1.1 μm was averaged over four scans, and the background spectrum was acquired at 120 scans per pixel on a clean area of the slide. IR spectroscopic images were collected at a spectral resolution of 4 cm^{-1} and step size of 2 cm^{-1} in the spectral range 900-3800 cm^{-1}, providing 1506 bands in the absorbance spectrum.

Preprocessing

After stitching the image tiles, noise reduction was performed using minimum noise fraction (MNF) transform[94]. Savitzky Golay 9 point smoothening, baseline correction, and normalization to amide I peak at 1650 cm^{-1} was done for each core in the TMA. The spectral data were converted to spectral metrics using methods described previously[44,75]. Briefly, we calculated spectral metrics as ratios of peak heights, peak area and heights, peak areas, and centroid wavenumber locations of the peaks. In total, we defined 418 spectral metrics.

Feature reduction

In the first stage of feature reduction, we performed analysis of variance(ANOVA) using a nested, random effect interaction model on three arrays (a1,a3,a4) using ground truth to label classes, patient, TMA and patient core numbers. Since specific patients were only found in particular arrays and each patient had multiple cores, the nesting order was Array, Patient, and Patient-specific core. For this analysis, the classes used were malignant epithelium, necrosis, and reactive stroma since these classes were most commonly observed in cores. From ANOVA, we determined spectral metrics where inter-array, inter-patient and inter-core variations were significant at 0.05 significance level and removed these from the analysis. One hundred and sixty-two metrics were retained after this stage. In the second stage, we used minimum redundancy maximum relevance algorithm (mRMR) in R to further remove redundant and irrelevant features. In this model, the feature with maximum mutual information (MI) is selected first following the equation[273]:

$$x_i = \arg\max_{x_i \in X} I(x_i, y)$$

where x_i represents i^{th} feature in full dataset X, y represents the output variable (class label), and I represents mutual information given by:

$$I(x, y) = -\frac{1}{2}\ln(1 - \rho(x, y)^2)$$

The next feature is added to feature vector S by finding the feature with minimum mutual information with respect to all the prior features in S and maximum mutual information with respect

to the class label. This is represented as:

$$q_j = I(x_i, y) - \frac{1}{|S|}\sum_{x_k \in S} I(x_j, x_k)$$

Applying this using the mRMRe package[273,274] in R, we found a set of 50 features that were relevant to the classification problem while minimizing the redundancy in the data.

Supervised classification: In the model learning step, we defined pixel labels for each cell type by duplicating annotations from H&E stained sections as marked by an expert pathologist onto IR spectroscopic images. Four arrays were used for training (a1, a2, a3, a4). We used a random forest algorithm for supervised classification in Matlab 2016a. To address fitting issues in the classifier such as high bias or high variance, we used two additional arrays (a5, a6) to perform optimization of parameters. The parameters that we optimized in the random forest were (a) Leaf size: size of the group at which decision tree stops splitting further, and (b) Feature size: number of features sampled by the tree randomly for performing the split. The parameters were optimized by calculating the error in classification for both training and calibration sets for multiple leaf sizes and feature sizes given by:

$$\text{e}= \frac{1}{\sum_{j=1}^{n} w_j}\sum_{j=1}^{n} w_j I\left(y_j \neq \hat{y}_j\right)$$

Where e represents error, w represents the weight of the class, n is the number of classes, y is the true class label, ŷ is predicted label, and I is indicator function. Parameters that minimized calibration error and maintained low training error was chosen as optimal. The fully developed supervised model with optimal parameters was validated by two independent arrays (a7, a8).

Progression analysis

Classified images of invasive carcinoma cores from all eight TMAs were used for studying tumor-stroma interaction. A total of 220 patients were analyzed using biopsies containing reactive or nonreactive stroma and at least 5% proliferative epithelium by area. If multiple cores from the same patient were present, means over all available cores were calculated. Three risk-associated features were defined to assess the tumor-stroma interaction. The first risk variable was distance metric (d) and measured as the closest encounter distance of the malignant epithelium pixel to the stromal element being probed. Risk variable area metric (N) was measured as the normalized pixel count of the stromal component being probed in a circle of radius R determined experimentally. Risk variable interaction metric (M) was measured as the interaction of the two features d and N for each pixel. Five hundred random pixels of malignant epithelium were chosen

from each of the 30% downsampled classified IR image to calculate the features. Three stromal elements, the reactive stroma, lymphocytes and normal stroma were evaluated separately for their role in determining outcome. Each risk associated variable was converted to a dichotomous categorical variable by splitting at the median and evaluated for significance by univariate log-rank test and multivariate Cox-regression analysis in R using package ‘survival’[275]. Power analysis was performed in R using the package ‘powerSurvEpi’[276]. Two sample t-test was performed in OriginPro 2017 to test the hypothesis that the means of groups were equal. Mann-Whitney test was performed in OriginPro 2017 as a non-parametric test to test if the distributions were different.

Figures

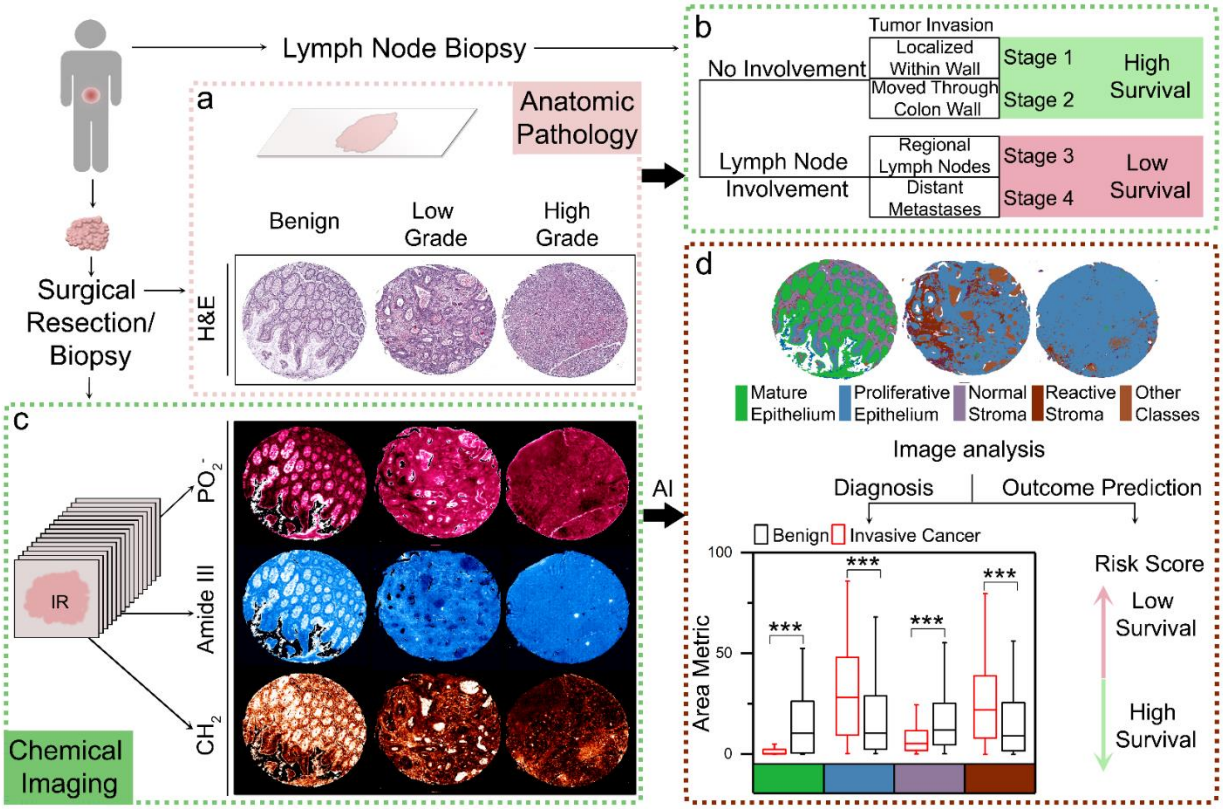

Figure 4.1: Current clinical pipeline and comparison with chemical imaging pipeline. (a) Tissue analysis with anatomic pathology is used for diagnosis but has limited molecular details. (b) Surgical resections are used for staging diagnosed cancers in conjugation with anatomic pathology. (c) Chemical imaging with infrared spectroscopic imaging uses several mid-infrared frequencies of light that capture molecular details in spatially specific context. (d) Data acquired from infrared imaging can enable molecular assessment of the microenvironment, providing a diagnosis as well as predicting the outcome.

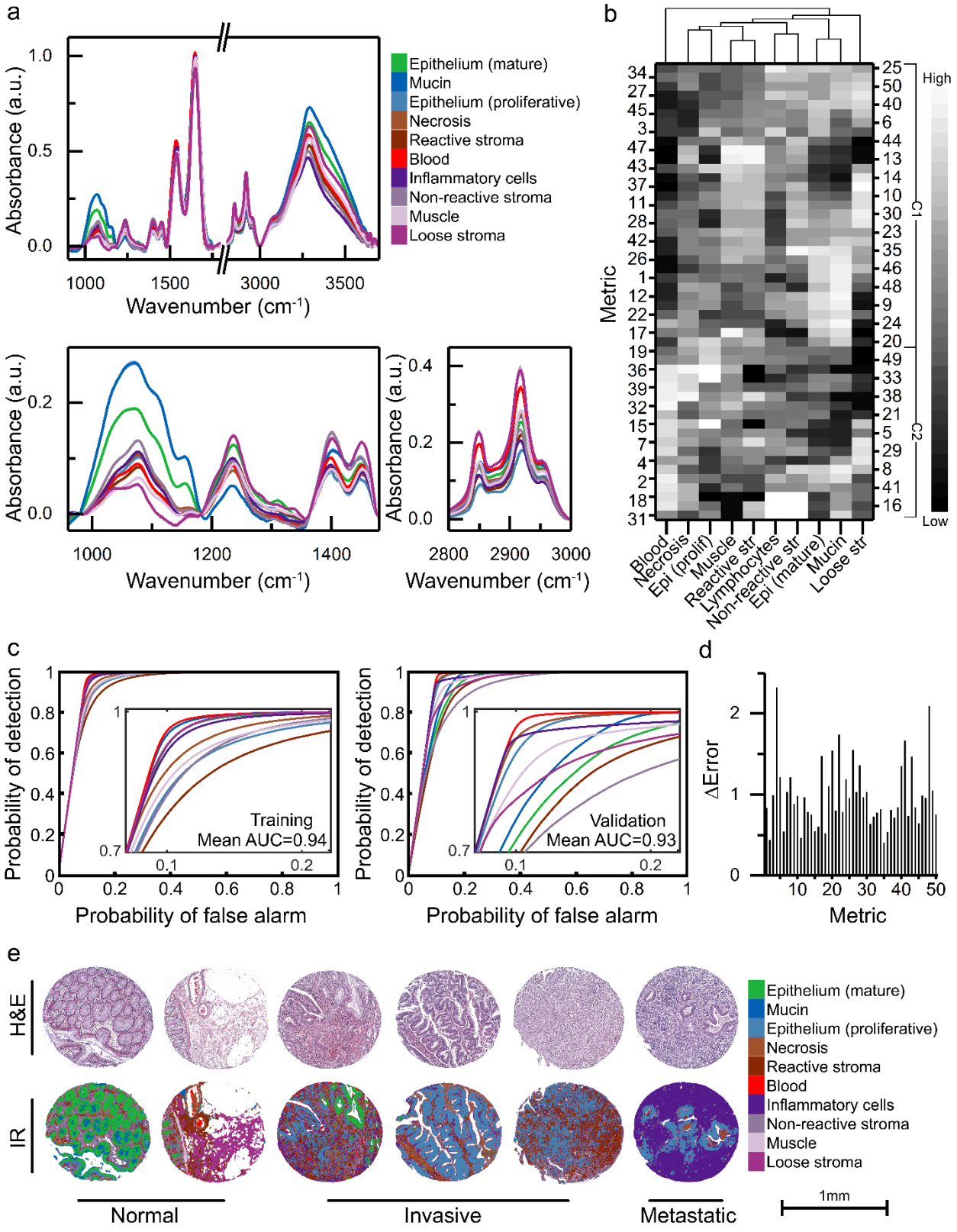

Figure 4.2: Spectral differences between histologic classes in the tissue and the histologic

(Figure 4.2 (cont.) segmentation of colon biopsy sections using supervised classification. (a) Average infrared spectra of the histologic classes. (b) Heat map of cluster analysis based on histologic classes and metrics. (c) Receiver operating characteristics (ROC) curves for training and validation sets show that high sensitivity (probability of detection) and specificity (1-probability of false alarm) for all histological classes. The color key is common for ROC curves and classified images. (d) Increase in error when each metric is permuted shows the importance of individual metrics in classification. (e) IR classified images show good correspondence when compared with H&E images for normal, invasive and lymph node biopsies.

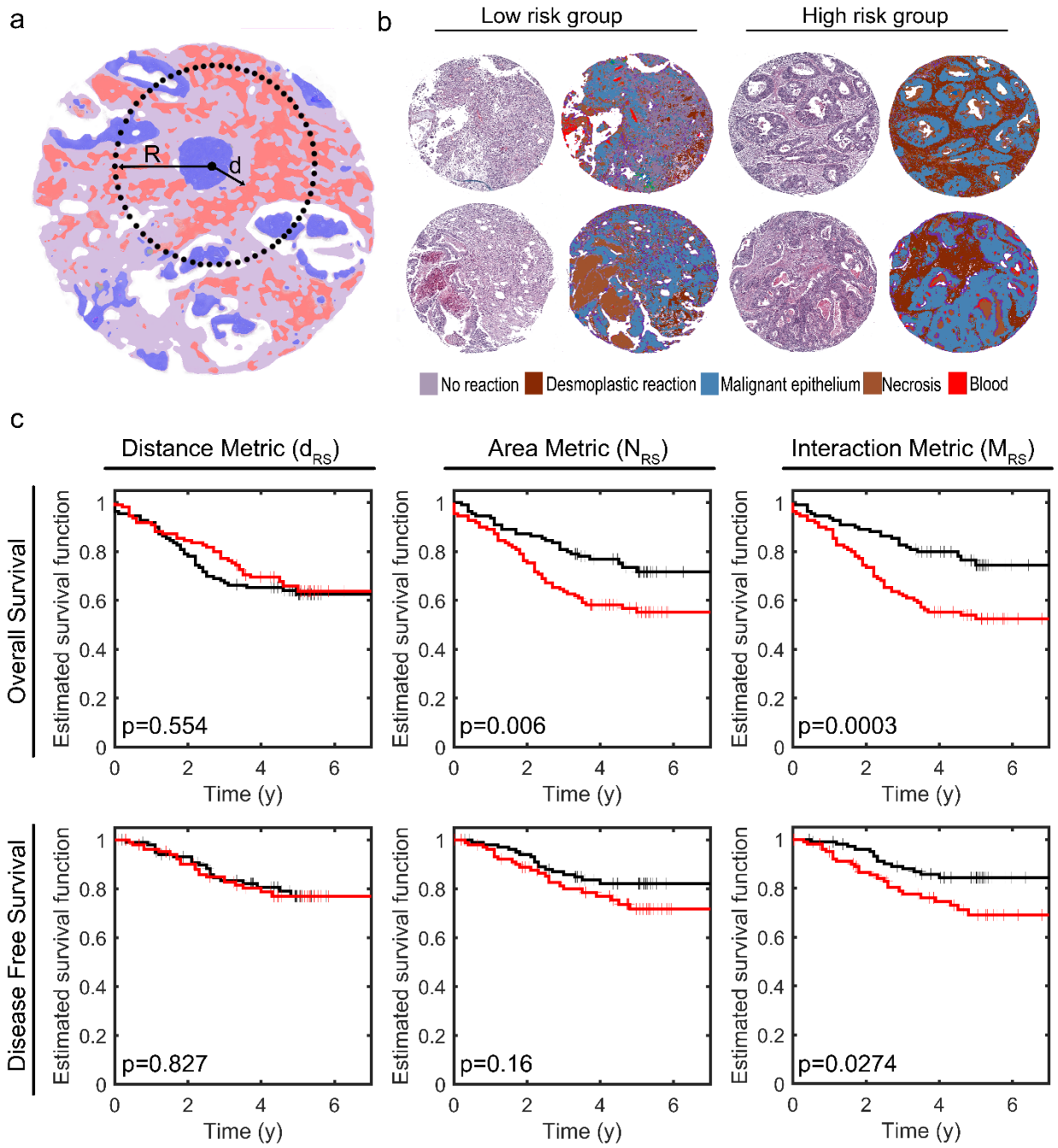

Figure 4.3: Risk associated features and their association with overall and disease free survival. (a) Schematic of feature calculation (b) Montage of high risk and low risk group based on interaction metric feature. (c) Kaplan-Meier survival curves

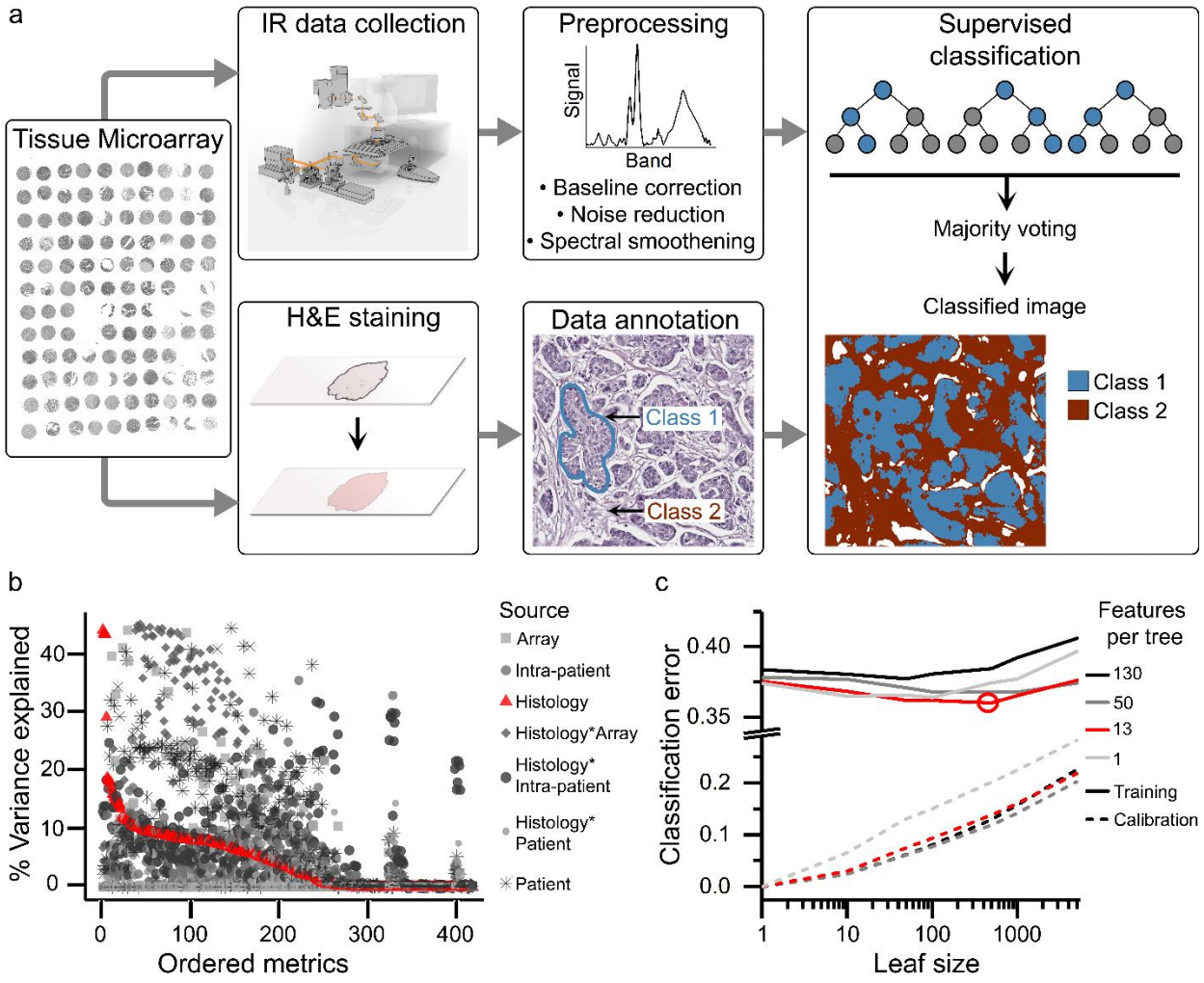

Supplementary figure 4.1: Supervised tissue segmentation of infrared spectroscopic image. (a) Method pipeline. Tissue microarray is imaged with infrared imaging instrument. The data is processed to remove noise, correct baseline and smoothen the spectra. In parallel, another tissue microarray section is stained with H&E. This image is annotated by an expert pathologist to identify distinct areas. Annotations and infrared imaging data is used to train supervised classification algorithm. Here we have used Random forest supervised classification, which takes majority vote of a ensemble of decision trees to determine class label. (b) Results from analysis of variance. This figure demonstrates the percentage contribution of each source in variance of the spectral data, evaluated per metric. The metrics are ordered from highest histology contribution to the lowest. (c) Classifier optimization. In random forest, the two hyperparameters that are optimized are the leaf size and the features fed per tree. The marked circle in the plot shows the most optimal operating point based on a combination of hyperparameters.

Tables

Table 4.1: Univariate and multivariate cox-regression analysis of time to death based on risk features. The p-value corresponds to the test of null hypothesis that the beta coefficient of the risk variable is statistically significantly different from zero

Microenvironment Component	Risk variable	Overall Survival	
		Univariate	Multivariate
Reactive Stroma	d_{RS}	0.554	0.884
	N_{RS}	0.006	0.095
	M_{RS}	0.000	0.011
Normal Stroma	d_{NS}	0.843	0.734
	N_{NS}	0.360	0.474
	M_{NS}	0.247	0.496
Lymphocytes	d_{L}	0.580	0.912
	N_{L}	0.496	0.109
	M_{L}	0.883	0.547

Table 4.2: Multivariate cox-regression analysis of the reactive stroma risk variable M_{RS}

	p	Exp(β)	95.0% CI for Exp(β)	
			Lower	Upper
M_{RS}	0.0113	1.88211	1.1538	3.070
Grade	0.1442	1.46061	0.8784	2.429
Stage	7.78e-10	2.69039	1.9626	3.688
Age	9.02e-07	1.06117	1.0363	1.087
Sex	0.7031	1.09475	0.6874	1.744
Source	0.9418	0.98241	0.6100	1.582

Table 4.3: Results of two sample t-test and Mann-Whitney test to compare values of continuous variable M_{RS} across stages

Group	Two sample t-test		Mann-Whitney test
	p	Power	p
Stage 1 vs Stage 2	0.13	0.32	0.22
Stage 1 vs Stage 3	0.36	0.15	0.27
Stage 1 vs Stage 4	0.23	0.22	0.21
Stage 2 vs Stage 3	0.001	0.9	0.002
Stage 2 vs Stage 4	0.002	0.87	0.005
Stage 3 vs Stage 4	0.51	0.1	0.61
Low Stage vs High Stage	0.001	0.9	9.67E-04

Metric	Metric Definition key	Col1	Col2	Col3	Col4
1	3	3113	3701	1645	0
2	3	1475	1591	1400	0
3	3	1182	1333	1448	0
4	1	1545	0	0	0
5	4	1427	1475	0	0
6	3	1182	1333	3072	0
7	3	1475	1591	1065	1186
8	3	1448	0	1400	0
9	3	1065	1186	3286	0
10	1	1664	0	0	0
11	3	1363	1427	3286	0
12	3	1065	1186	2956	0
13	3	2956	0	1120	0
14	3	1182	1333	980	1065
15	3	2947	2999	1065	1186
16	3	2852	0	1306	0
17	4	1065	1186	0	0
18	3	2947	2999	1306	0
19	3	1065	1186	980	1065
20	3	1363	1427	1448	0
21	1	1306	0	0	0
22	1	1645	0	0	0
23	3	1363	1427	3072	0
24	1	1167	0	0	0
25	3	2999	3113	1475	1591
26	4	1475	1591	0	0
27	3	2999	3113	2956	0
28	1	1448	0	0	0
29	3	1427	1475	1363	1427
30	2	1427	1475	0	0
31	3	1065	1186	1306	0
32	3	1306	0	1043	0
33	2	2947	2999	0	0
34	3	2999	3113	1591	1757
35	3	1363	1427	1545	0
36	3	2947	2999	1182	1333
37	3	1182	1333	1080	0
38	3	2885	2947	1182	1333
39	1	2956	0	0	0
40	1	1240	0	0	0
41	2	2825	2885	0	0
42	3	1363	1427	1645	0
43	3	1080	0	1043	0
44	3	1306	0	1080	0
45	3	1182	1333	1645	0
46	3	3113	3701	2947	2999
47	3	1400	0	1120	0
48	3	1591	1757	1645	0
49	3	1065	1186	1043	0
50	3	3072	0	1645	0

Supplementary table 4.1: Spectral metrics used to develop supervised histology classifier. Definitions: 1: Amide I normalized peak heights, where Col1 represents peak position. 2: Amide I normalized peak area, where Col1 and Col 2 represent peak area bounds. 3: Peak height ratios, where Col1 and Col3 represent numerator and denominator peak heights respectively and Col2 and Col4 are 0. Area to area ratio where Col1 and Col2 represent first area bounds, Col3 and Col 4 represent second area bound. 4: Peak centroid position, where Col1 and Col2 represent area bounds.

CHAPTER 5: CLINICAL TRANSLATION: AUTOMATION OF BIOPSY ANALYSIS WITH DEEP LEARNING[8]

Abstract

Accurate, objective and automated grade diagnosis of cancer biopsies can reduce the burden on pathologists and speed up the clinical cancer detection and diagnosis. Infrared spectroscopic imaging has previously been applied for stain free tissue segmentation, but automated tissue analysis following tissue segmentation remains unexplored. In this study, using 148 patient cohort, we used infrared spectroscopic imaging assisted colon segmentation to determine the tumor grade. We achieved high specificity and sensitivity in tissue segmentation and grade classification, with 0.93 and 0.82 area under the curve (AUC) of the receiver operating characteristic curve (ROC) respectively. This is the first demonstration of infrared spectroscopic imaging based automated tissue assessment.

Introduction

In the United States, approximately 95,520 new colon cancer cases were estimated in 2017[1]. A definitive colon cancer diagnosis requires histopathological evaluation of the biopsy section by a pathologist. If malignancy is identified, tumor grade is determined on the basis of the percentage of malignant epithelium cells forming glands. Well differentiated tumors exhibit glandular structures in more than 95% of the tumor while poorly differentiated tumors form solid mass with less than 5% gland formation[277]. Tumor grade assessed in preoperative biopsies has prognostic value[14,278,279] and is associated with TNM stage[280,281]. Despite shown potential in determining patient prognosis, the clinical application of tumor grade has been limited due to lack of objective evaluation criteria[5,6].

Deep neural networks based tissue segmentation and analysis is gaining traction[282] due to the need of automation and objective evaluation[5,6,283,284]. In colon cancer, this has been applied to segment colon tissue, identify nuclei from stromal and epithelial cell types[285], to characterize polyps[286], and to determine outcome[287]. These approaches typically utilize Hematoxylin and eosin (H&E) stained tissue images and the deep learning algorithms are based on morphometric criteria such as texture, structure and shape. When morphometry is used as a basis for primary tissue segmentation, additional issues are introduced. First, there is a requirement for tissue

[8] In preparation for publication as Tiwari, Saumya et al. “Clinical Translation: Automation of Biopsy Analysis with Deep Learning”

processing and staining. This is time consuming, and is susceptible to staining artifacts, experimental variation and location based variation. Second, the contrast generated by H&E stains is low and many tissue segments can stain identically. Infrared spectroscopic imaging can bypass these issues by utilizing both morphological as well as inherent biochemical differences in the tissue for segmentation and analysis.

The infrared absorbance spectrum of a tissue captures the biochemical profile based on the absorbance of IR light by the functional groups present in the sample. In Fourier transform infrared (FT-IR) spectroscopic imaging, mid-infrared absorbance spectrum of each pixel of the tissue image is collected, thus enabling analysis of biochemical content in spatially specific manner[51]. Applications of FT-IR spectroscopic imaging have demonstrated high accuracy in supervised classification based segmentation of various tissue types, such as prostate[74], breast[288] and heart[186,289] and detailed reviews on the procedure, applications and methods can be found in the references cited herein[28,51,76,79,127,182,290].

Following the tissue segmentation by IR spectroscopic imaging, the potential for automation of tissue analysis exists but has not been demonstrated so far. In this work, we aimed to enable automation in tissue analysis by determining the tumor grade. Using FT-IR spectroscopic imaging, we utilized inherent biochemical differences between tissue segments to accurately and reproducibly identify malignant and benign epithelium. Further, using the labelled tissue image, we achieved high accuracy in determining the grade of the tumor. For this, we extracted features[291,292] from a previously trained deep neural network AlexNet[293] to develop tumor grade classifier on IR histologically segmented images. With this approach, we show that a thin, unstained tissue slice can be imaged using infrared spectroscopic imaging and the resulting images can be processed through a completely automoated manner to render a final tumor grade assessment.

Methods

Data collection and segmentation

The patient cohort used in this study to collect infrared imaging data comprised of 320 anonymous patients undergoing elective surgery for colorectal carcinoma. This cohort has been used previously[272] and described in detail in the cited reference as Cohort II. Sample preparation and infrared imaging of this cohort is described in the methods section in Chapter 4. Briefly, paraffin embedded tissue microarrays were sectioned onto barium fluoride (BaF_2) plates. These

sections were deparaffinized by hexane baths for 48 hours. Infrared images were collected on Agilent Stingray imaging system in high magnification mode with 1.1 µm pixel size at 4cm^{-1} resolution. The noise in data was cleaned and baseline correction and normalization was performed based on previously described protocols[44,127]. The histological segmentation of the images annotated by our pathologist collaborator was performed with random forest supervised classification models and described in details in Chapter 4.

Tumor grade determination with deep learning neural net transfer

For training the tumor grade classifier, 20 poor grade and 50 moderate-well grade patient images were used. These images were stored in .jpg format and rotated 0°, 90°, 180° and 270° , flipped vertically and finally rotated 30° to expand the training set. This resulted in 16-fold expansion of the training set. The number of training examples corresponding to poor grade and moderate-well grade cases were equalized such that 320 randomly chosen moderate-well and 320 poor grade images were used to train the classifier. AlexNet[293], which is a deep convolutional neural network was used for the feature extraction task (figure 5.1a). The architecture of the network is described in the cited literature[293]. Since the network requires 227x227x3 images, full core IR based histology classified images were resized to 227x 227 pixels and saved in .jpg format. Network activations of second fully connected layer were used along with differentiation grade label (figure 5.1b) to develop support vector machine (SVM) classifier (figure 5.1c). Differentiation grade classifier was calibrated on an independent set from 78 patient images of which 18 were poor grade and 60 were moderate-well grade. Calibration dataset was prepared in the same manner as the train set resulting in 288 images of poor and moderate-well categories each. Hyperparameters associated with SVM classifier, namely box constraint and kernel scale were optimized to minimize loss and prevent overfitting. Finally, for independent set, all patient images were used but rotated 45° to generate independent images.

Results and discussion

Identification of spectral regions of importance

In developing a supervised classification model to segment colon tissue, the spectral regions cluster on the basis of functional differences between tissue segments. The difference between these clusters can be understood in terms of the spectral regions that were most frequently involved in defining the metrics for these clusters (figure 5.2). A similar idea has previously been described as spectral barcoading, where IR spectra is used directly to identify discriminative

frequencies by unsupervised analysis[255]. From this analysis, the majority of fingerprint region between ~982-1580 cm^{-1} and CH stretching region between 2800-3000 cm^{-1} clustered together as C1 while OH-NH region between ~3000-3700 cm^{-1} and amide I region clustered together as C2. From the metric expression patterns of the classes in C1 and C2, it is clear that further association of spectral metrics exist. While 50 metrics is a good size of features to develop the classifier, it indicates that there is possibility of trimming down the dataset further. This can be done by identifying the features that are of least importance in supervised classification and retraining the algorithm with trimmed dataset and is demonstrated in the following section.

Differentiation grade classifier achieves high specificity and sensitivity on independent validation set

Following highly specific and sensitive tissue segment identification in infrared spectroscopic images of the colon, we aimed to automate diagnosis of tumor grade (figure 5.3a). For this, we used a machine vision based approach where a set of images is presented to the computer with labels, and training is performed by using specific features extracted from the image. With more than a million images used for training by some networks[293], deep learning based approaches eliminate the need to “hand draw” or manually design the features while improving classifier performance[294]. The features determined by deep convolutional neural networks to be optimum for image classification tasks are oftentimes transferable to image recognition of new objects, known as feature extraction[291,292]. For tumor grade classification, we utilized previously trained deep convolutional neural network known as AlexNet[293]. The architecture of this network is described in detail in the cited reference. Briefly, the deeper end of this network contains three fully connected layers from where features of a 3D image (227x227x3) can be extracted in the shape of 4096x1, 4096x1 and 1000x1 respectively. For developing the tumor grade classifier, we tested all three layers, and found that the second fully connected layer resulted in the least classification loss, leading to a feature vector of size 4096. Using these features, a support vector machine classifier was developed. Hyperparameters were optimized to determine the kernel scale value of 2.5 and box constraint value of 1e-6 (supplementary figure 5.1). With this classifier, we achieved 0.83 training ROC AUC, 0.86 calibration ROC AUC and 0.82 ROC AUC on an independent patient validation set comprising of 148 patient biopsy images (figure 5.3b). It is interesting to note that we have used full tissue microarray core images to perform classification instead of image patching (figure 5.3b). Upon randomizing the labels, the training AUC dropped to 0.43 which indicated that the performance of the classifier was label specific. We note that there are other permutations of classification algorithms and

hyperparameters that can achieve similar results.

Finally, we predicted the tumor grade at the optimum operating point identified from the training ROC curve. The confusion matrices from this prediction are shown in table 5.1. For the validation set, we obtained 69% and 84% accuracy in classifying moderate/well grade and poor grade tumors respectively. There is an opportunity to improve this classification further by using a larger dataset and increasing the diversity of images. To adapt previously developed networks, we also downsampled IR classified images by approximately a factor of 5. It is possible that this suppresses some of the discriminatory features, and this can be tested by using image patch based approaches that do not require downsampling of image, but is much more computationally expensive. We have shown that using previously defined features can give us accurate image classification, and developing deep neural networks with large number of histology images could tailor the features further to identify histologically relevant features.

Conclusions

Histopathology based diagnosis is a gold standard for several diseases including cancer. There is an increasing burden on pathologists to perform histologic assessment, with need to perform time-constrained accurate assessments during surgeries. In one of the earliest work in this area, 2047 sample set cohort was classified by 22 histopathology departments and showed statistically significant differences between observers, possibly arising from systematic differences in the techniques of assessment[5]. A recent study compared both inter and intra observer agreement in tumor grade determination[6]. While intra-observer agreement was substantial with Cohen's κ 0.704, lower inter-observer agreement was found with Fleiss' κ 0.351. Most inter-observer agreement was found in classifying well differentiated cases and least inter-observer agreement was found in classifying moderately differentiated cases. There is a significant interobserver variability in assessing tumor grade. Inter-observer agreement in determining tumor grade can be improved by using two grade system instead of three[6], and by establishing standardized objective evaluation criteria[283,284]. Computational approaches could assist such assessments, and reduce pathologist burden by identifying areas of interest within whole slide images. Additionally, computational approaches can provide a means towards histopathologic assessment in resource-poor settings[295].

In this work, we showed tumor grade assessment of colon biopsy samples using infrared spectroscopic imaging based machine learning models. Using a large patient cohort, we

demonstrated the reproducibility and generalizability of our models. The use of infrared spectroscopic imaging offers three fold advantages in comparison to conventional approaches. First, due to the biochemical sensitivity of infrared spectroscopy, highly accurate tissue segmentation into a large number of classes can be achieved. Second, IR classified images provide an objective and biochemically relevant evaluation criteria for determining tumor grade. Third, using IR spectroscopic imaging to analyze biopsies, we eliminate the need of staining the tissue, staining associated errors, and preserve the tissue sample for further analysis. With the development of discrete frequency infrared imaging instruments[256,289], we are closer to the goal of translating this technology to clinics, enabling rapid imaging and tissue assessment.

Figures

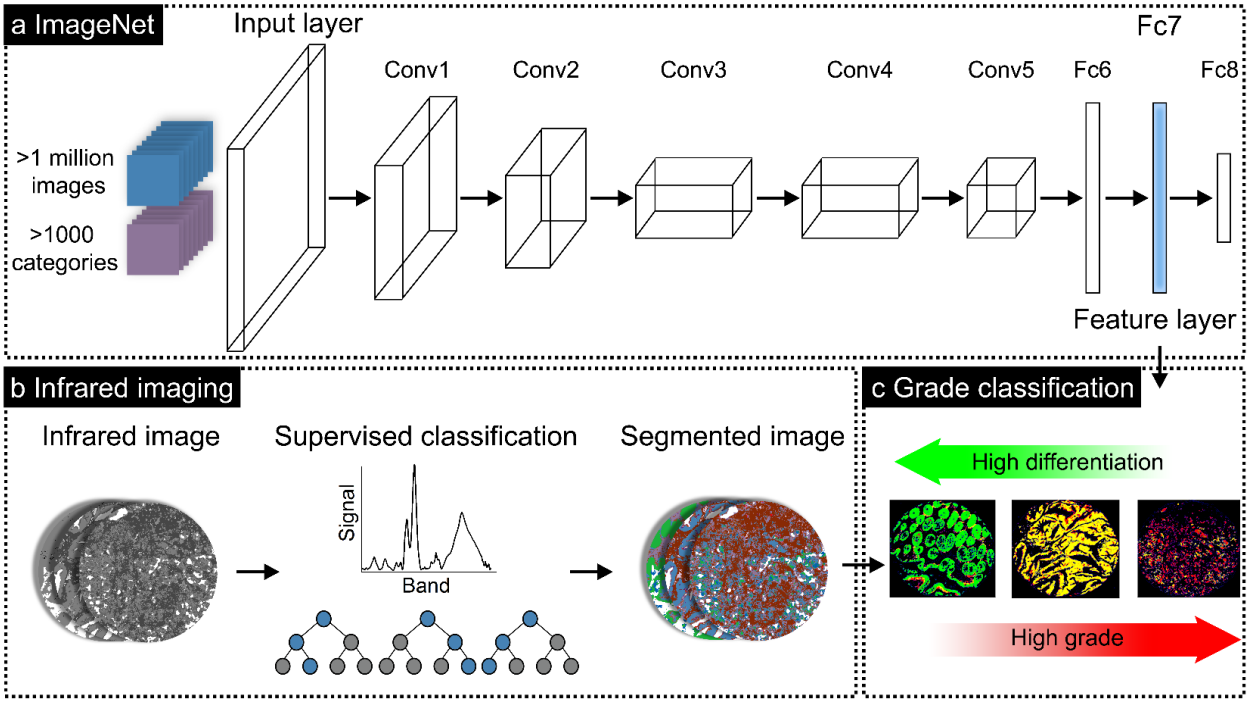

Figure 5.1: Schematic of developing deep learning based tumor grade classifier. (a) A pretrained ImageNet convolutional neural network, which was trained on more than a million images and is able to identify more than a thousand image categories was used for this work. Specifically, the second fully connected layer, Fc7 was used to calculate features from the input images. (b) Input images were obtained from supervised classification of colon infrared spectroscopic images. (c) Tumor grade classifier was developed using IR segmented images and features from ImageNet classifier.

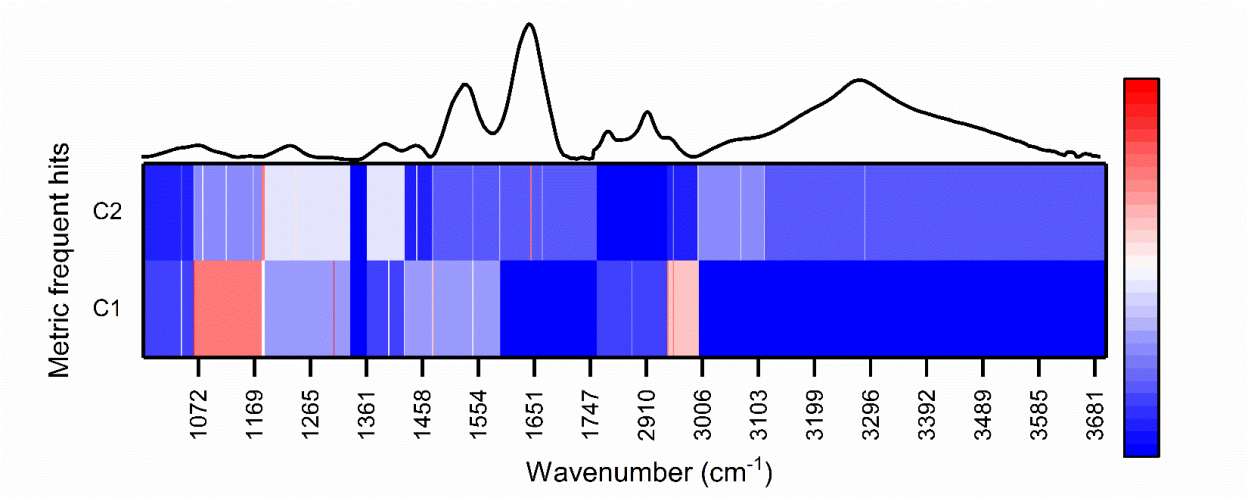

Figure 5.2: Frequently used areas from the IR spectrum for histologic segmentation classifiers.

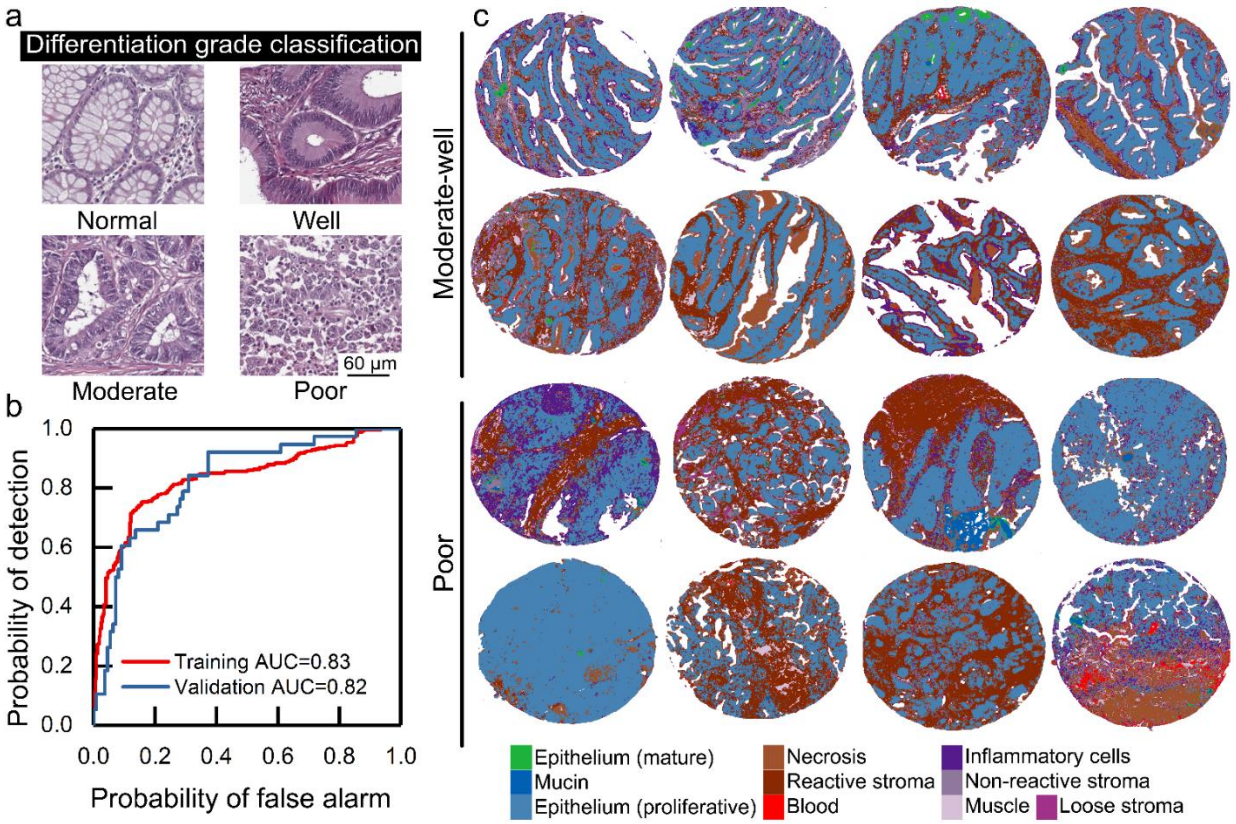

Figure 5.3: Deep learning based tumor grade classification. (a) Examples of normal, well differentiated, moderately differentiated and poorly differentiated cases. The epithelial organization is increasingly disordered in higher grades. (b) Receiver operating characteristic curves of deep learning based tumor grade classifier show high specificity and sensitivity in classification. (c) Examples of IR histology classified images used to develop tumor grade classifier.

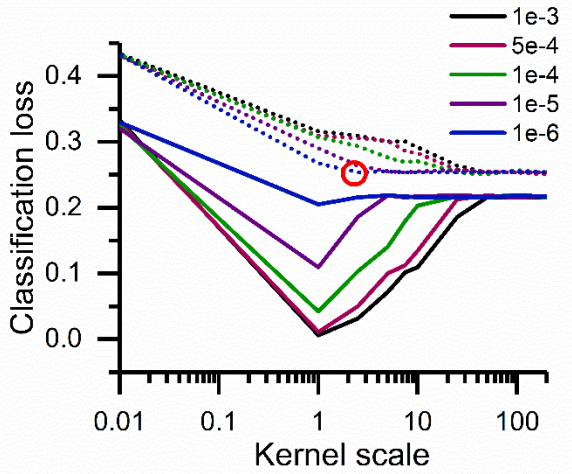

Supplementary Figure 5.1: SVM classifier optimization

Table

Table 5.1: Confusion matrix of differentiation grade classifier. The training set had equal number of Moderate/Well and Poor differentiation grades. The classification decisions were based on the optimum operating point on the receiver operating characteristic curve, considering poor differentiation grade as the positive class.

Training		
Classified →	Moderate/Well	Poor
Ground truth ↓		
Moderate/Well	237/320 (74%)	83/320 (26%)
Poor	61/320 (19%)	259/320 (81%)
Validation		
Classified →	Moderate/Well	Poor
Ground truth ↓		
Moderate/Well	76/110 (69%)	34/110 (31%)
Poor	6/38 (16%)	32/38 (84%)

CHAPTER 6: CONCLUSIONS

Summary

Prognosis specific features are essential in the management of colorectal carcinoma. Morphometry based pathology is used for detection and diagnosis, but performs weakly in terms of prognosis, owing to large interobserver variability and lack of molecular information. In this work, we have developed a quantitative chemical imaging-based approach to determine patient prognosis. Our work presented here has three significant implications:

- First, using infrared chemical staining, we demonstrate that patient-independent colon tissue segmentation can be performed without labels or dyes, providing images rapidly and opening the potential for in situ pathology within a human. The advancement presented in this work is the use of high magnification infrared imaging systems that provide near single cell resolution. This high spatial resolution data is coupled with sophisticated statistical and computational methods that ensure that patient heterogeneity, as well as experimental variations, are not considered while segmenting the tissue image. This approach consistently gave us high specificity and sensitivity when tested on independent samples.
- Second, we have developed a reliable and objective method to evaluate tumor-tumor microenvironment interaction using quantification of infrared spectroscopic images. The innovation in this project is that we have developed computational models to analyze chemical imaging data and provide precise patient prognostic information via simple color-coded maps without the need for human analysis. The morphometric patterns of cellular invasion obtained through digital histology, combined with biochemical characteristics of stroma in the microenvironment gives a robust prognostic marker. While we have focused on colorectal carcinoma in this project, this approach is widely applicable to other types of cancers and has the potential to provide prognostic information in cancers where prognosis markers are not currently available.
- The third implication is that we have developed a novel deep learning based automation of the tumor grade. Using infrared chemical imaging based machine learning eliminates the need for tissue processing and manual examination, thus enabling rapid analysis of a large number of images. This development can allow early translation of infrared spectroscopic imaging as an advanced histopathology tool, opening up avenues for better outcome prediction and personalized tissue analysis.

Future directions

Subtyping stromal cell populations

Immune cells and stromal cells are the major cellular constituents of the tumor microenvironment, and each exerts an effect on the growth of the tumor. The role of lymphocytes, macrophages, dendritic cells, fibroblasts and endothelial cells in the modulation of biochemical and mechanical signals that can initiate, and help in growth and proliferation of tumor has been reviewed and explored before in the noted references and references therein[10,296–303]. While the biological effect of the cells in the tumor microenvironment is well understood, it is challenging to profile the changes undergone by this great variety of cells without the use of multiple probes in tissues. For ex-vivo tissue analysis, such as the excision biopsies, previously established analysis systems using genomics[304–306], proteomics[307,308], microfluidics[211] and spectroscopy[74] are adapted to study the cellular response in the tumor microenvironment. Chemical imaging can fulfill the requirement of technology for obtaining spatially specific biomolecular changes. Infrared spectroscopy can be used to measure early changes in fibroblasts in response to stimulation with cancer mimicking cellular co-culture system[158,309] which are discussed previously in chapter 3. Recently, proliferative and senescent fibroblast subgroups were differentiated using Raman and infrared spectroscopy, with changes majorly associated with degradation and storage of proteins and lipids, and only a small fraction of variation attributed to nucleic acids and carbohydrates[310]. Although many established techniques provide data without spatial information, our work presented here can comprehensively capture molecular changes and could be a critical piece in improving the systems pathology model further.

Deep neural networks to analyze infrared spectroscopic imaging data

Deep neural networks are characterized by a large number of hidden layers that are especially useful to capture complex high-level interactions between the input features[293]. Landmark works in analyzing infrared spectroscopic imaging data towards disease analysis have used simpler supervised classification models[45,74], relying on hand designing features which were then used for classification tasks. Such approaches are limited by spectral interpretation of the differences between classes and often only capture linear relationships in data. With a “large-enough” sample size, deep neural networks could work as “end-to-end,” taking in raw data and learning inherent connections between the variates to perform prediction. We anticipate that with

the surge of high-speed infrared imaging instruments[43,45], end to end deep learning models will be able to take into account complex spatio-spectral features to determine prognosis.

Multi-scale systems pathology

Genomic revolution has provided molecular data, but we are still far from being precise in determining the best therapy and response of the disease. Molecular probing such as fluorescence in situ hybridization (FISH), immunohistochemistry (IHC), polymerase chain reaction (PCR) add vital pieces of information but fail to provide the full picture. Cancer development is a function of genetic and microenvironmental changes. The interaction of tumor cells with its surrounding environment comprising of stromal cells, immune cells and stroma is continually evolving and adapting in response to therapies. While most systems pathology concepts presented in the past have suggested integration of available data at many scales to develop a computational model for modeling diseases, they do not typically include tumor microenvironment factors in the analysis. This omission could be because our understanding of the impact of the tumor microenvironment on cancer progression as well as the technology to probe microenvironment has only developed in the past few years, much after systems pathology models were first explored. From the perspective of systems pathology, it is necessary to identify the sources of perturbations, as well as ways of quantifying these changes to be able to feed the data in computational models. From our work, we demonstrate that infrared spectroscopic imaging accurately profiles tumor microenvironment changes in the biopsies. We anticipate that when integrated with data obtained from genomics and proteomics, we will be able to provide a comprehensive systems pathology analysis of the patient.

Personalized analysis

Our current work enables complete automation of tissue analysis by using IR spectroscopic imaging to determine patient prognosis. The final step is an integration of engineering and medicine, opening up avenues for rapid digital histopathology and personalized tissue analysis. It is likely that each patient is uniquely characterized by their bio-physiological system. Thus, personalized prediction can be enabled by capturing complex interactions between several components of the system, and combining them to perform comprehensive systems pathology. By incorporating patient information with spatially relevant biochemical information, there is potential to enable personalized disease analysis.

References

[1] Howlader N, Noone AM, Krapcho M, Miller D, Bishop K, Kosary CL, Yu M, Ruhl J, Tatalovich Z, Mariotto A, Lewis DR, Chen HS, Feuer EJ CK (eds). SEER Cancer Statistics Review, 1975-2014, based on November 2016 SEER data submission. National Cancer Institute. Bethesda, MD n.d. https://seer.cancer.gov/csr/1975_2014.

[2] Brown LJR, Smeeton NC, Dixon MF. Assessment of dysplasia in colorectal adenomas : an observer variation and morphometric study 1985:174–9.

[3] Jensen P, Ph D, Krogsgaard MR, Christiansen J, Braendstrup O, Johansen A, et al. Observer Variability in the Assessment of Type and Dysplasia of Colorectal Adenomas , Analyzed Using Kappa Statistics n.d.:2–5.

[4] Raab SS, Grzybicki DM, Janosky JE, Zarbo RJ, Meier FA, Jensen C, et al. Clinical impact and frequency of anatomic pathology errors in cancer diagnoses. Cancer 2005;104:2205–13. doi:10.1002/cncr.21431.

[5] Blenkinsopp WK, Stewart-Brown S, Blesovsky L, Kearney G, Fielding LP. Histopathology reporting in large bowel cancer. J Clin Pathol 1981;34:509–13. doi:10.1136/JCP.34.5.509.

[6] Chandler I, Houlston RS. Interobserver agreement in grading of colorectal cancers—findings from a nationwide web-based survey of histopathologists. Histopathology 2008;52:494–9. doi:10.1111/j.1365-2559.2008.02976.x.

[7] Voduc KD, Cheang MCU, Tyldesley S, Gelmon K, Nielsen TO, Kennecke H. Breast cancer subtypes and the risk of local and regional relapse. J Clin Oncol 2010;28:1684–91. doi:10.1200/JCO.2009.24.9284.

[8] Duffy MJ. Carcinoembryonic antigen as a marker for colorectal cancer: is it clinically useful? Clin Chem 2001;47:624–30.

[9] Hostetter RB, Augustus LB, Mankarious R, Chi KF, Fan D, Toth C, et al. Carcinoembryonic antigen as a selective enhancer of colorectal cancer metastasis. J Natl Cancer Inst 1990;82:380–5. doi:10.1093/jnci/82.5.380.

[10] Quail DF, Joyce JA. Microenvironmental regulation of tumor progression and metastasis. Nat Med 2013;19:1423–37. doi:10.1038/nm.3394.

[11] Ueno H, Kanemitsu Y, Sekine S, Ishiguro M, Ito E, Hashiguchi Y, et al. Desmoplastic Pattern at the Tumor Front Defines Poor-prognosis Subtypes of Colorectal Cancer. Am J Surg Pathol 2017;41:1506–12. doi:10.1097/PAS.0000000000000946.

[12] Kimura R, Fujimori T, Ichikawa K, Ajioka Y, Ueno H, Ohkura Y, et al. Desmoplastic reaction in biopsy specimens of early colorectal cancer: A Japanese prospective multicenter study. Pathol Int 2012;62:525–31. doi:10.1111/j.1440-1827.2012.02840.x.

[13] Fleming M, Ravula S, Tatishchev SF, Wang HL. Colorectal carcinoma: Pathologic aspects. J Gastrointest Oncol 2012;3:153–73. doi:10.3978/j.issn.2078-6891.2012.030.

[14] Griffin MR, Bergstralh EJ, Coffey RJ, Beart RW, Melton LJ. Predictors of survival after curative resection of carcinoma of the colon and rectum. Cancer 1987;60:2318–24.

[15] Chowdhury FU, Shah N, Scarsbrook AF, Bradley KM. [18F]FDG PET/CT imaging of colorectal cancer: a pictorial review. Postgrad Med J 2010;86:174–82. doi:10.1136/pgmj.2009.079087.

[16] Ramesh J, Salman A, Mordechai S, Argov S, Goldstein J, Sinelnikov I. FTIR Microscopic Studies on Normal , Polyp , and Malignant Human Colonic Tissues 2001;2:99–117.

[17] Sahu RK, Argov S, Bernshtain E, Salman a, Walfisch S, Goldstein J, et al. Detection of abnormal proliferation in histologically “normal” colonic biopsies using FTIR-microspectroscopy. Scand J Gastroenterol 2004;39:557–66. doi:10.1080/00365520410004695.

[18] Salman a., Sahu RK, Bernshtain E, Zelig U, Goldstein J, Walfisch S, et al. Probing cell proliferation in the human colon using vibrational spectroscopy: a novel use of FTIR-microspectroscopy. Vib Spectrosc 2004;34:301–8. doi:10.1016/j.vibspec.2004.01.009.

[19] Yao H, Shi X, Zhang Y. The Use of FTIR-ATR Spectrometry for Evaluation of Surgical Resection Margin in Colorectal Cancer : A Pilot Study of 56 Samples 2014;2014.

[20] Dong L, Sun X, Chao Z, Zhang S, Zheng J, Gurung R, et al. Evaluation of FTIR spectroscopy as diagnostic tool for colorectal cancer using spectral analysis. Spectrochim Acta A Mol Biomol Spectrosc 2014;122:288–94. doi:10.1016/j.saa.2013.11.031.

[21] Lascha P, Wäsche W, Mccarthy WJ, Muller G, Naumanna D, Berlin D-, et al. Imaging of

human colon carcinoma thin sections by FT-IR microspectrometry n.d.;3257.

[22] Wolthuis R, Travo A, Nicolet C, Neuville A, Gaub M-P, Guenot D, et al. IR spectral imaging for histopathological characterization of xenografted human colon carcinomas. Anal Chem 2008;80:8461–9. doi:10.1021/ac801191x.

[23] Nallala J, Piot O, Diebold M-D, Gobinet C, Bouché O, Manfait M, et al. Infrared imaging as a cancer diagnostic tool: Introducing a new concept of spectral barcodes for identifying molecular changes in colon tumors. Cytom Part A 2013;83A:294–300. doi:10.1002/cyto.a.22249.

[24] Nallala J, Lloyd GR, Shepherd N, Stone N. High-resolution FTIR imaging of colon tissues for elucidation of individual cellular and histopathological features. Analyst 2016;141:630–9. doi:10.1039/c5an01871d.

[25] Nallala J, Piot O, Diebold M-D, Gobinet C, Bouché O, Manfait M, et al. Infrared and Raman Imaging for Characterizing Complex Biological Materials: A Comparative Morpho-Spectroscopic Study of Colon Tissue. Appl Spectrosc 2014;68:57–68. doi:10.1366/13-07170.

[26] Lasch P, Diem M, Hänsch W, Naumann D. Artificial neural networks as supervised techniques for FT-IR microspectroscopic imaging. J Chemom 2006;20:209–20. doi:10.1002/cem.993.

[27] Mayerich D, Walsh MJ, Kadjacsy-Balla A, Ray PS, Hewitt SM, Bhargava R. Stain-less staining for computed histopathology. TECHNOLOGY 2015:1–5. doi:10.1142/S2339547815200010.

[28] Nallala J, Diebold M-D, Gobinet C, Bouché O, Sockalingum GD, Piot O, et al. Infrared spectral histopathology for cancer diagnosis: a novel approach for automated pattern recognition of colon adenocarcinoma. Analyst 2014;139:4005–15. doi:10.1039/c3an01022h.

[29] Byrd JC, Bresalier RS. Mucins and mucin binding proteins in colorectal cancer 2004:77–99.

[30] Naumann D, Lasch P, Diem M, Ha W. Artificial neural networks as supervised techniques

for FT-IR microspectroscopic imaging 2007:209–20. doi:10.1002/cem.

[31] Lasch P, Haensch W, Naumann D, Diem M. Imaging of colorectal adenocarcinoma using FT-IR microspectroscopy and cluster analysis. Biochim Biophys Acta 2004;1688:176–86. doi:10.1016/j.bbadis.2003.12.006.

[32] Lasch P, Haensch WO, Lewis EN, Kidder LH, Ann DN. Characterization of Colorectal Adenocarcinoma Sections by Spatially Resolved FT-IR Microspectroscopy 2002;56:1–9.

[33] Salman A, Argov S, Ramesh J, Goldstein J, Sinelnikov I, Guterman H, et al. FT-IR MICROSCOPIC CHARACTERIZATION OF NORMAL AND MALIGNANT HUMAN COLONIC TISSUES 2001:159–66. doi:10.1170/22.

[34] Travo A, Piot O, Wolthuis R, Gobinet C, Manfait M, Bara J, et al. IR spectral imaging of secreted mucus: a promising new tool for the histopathological recognition of human colonic adenocarcinomas. Histopathology 2010;56:921–31. doi:10.1111/j.1365-2559.2010.03563.x.

[35] Marusyk A, Polyak K. Tumor heterogeneity: causes and consequences. Biochim Biophys Acta 2010;1805:105–17. doi:10.1016/j.bbcan.2009.11.002.

[36] Dieter SM, Ball CR, Hoffmann CM, Nowrouzi A, Herbst F, Zavidij O, et al. Distinct types of tumor-initiating cells form human colon cancer tumors and metastases. Cell Stem Cell 2011;9:357–65. doi:10.1016/j.stem.2011.08.010.

[37] Wolthuis R, Travo A, Guenot D, Ly E, Manfait M, Jeannesson P, et al. IR Spectral Imaging for Histopathological Characterization of Xenografted Human Colon Carcinomas 2008;80:8461–9.

[38] Argov S, Ramesh J, Salman A, Sinelnikov I, Goldstein J, Guterman H, et al. Diagnostic potential of Fourier-transform infrared microspectroscopy and advanced computational methods in colon cancer patients. J Biomed Opt 2002;7:248–54. doi:10.1117/1.1463051.

[39] Mackanos M a, Hargrove J, Wolters R, Du CB, Friedland S, Soetikno RM, et al. Use of an endoscope-compatible probe to detect colonic dysplasia with Fourier transform infrared spectroscopy. J Biomed Opt 2014;14:44006. doi:10.1117/1.3174387.

[40] Li Q-B, Xu Z, Zhang N-W, Zhang L, Wang F, Yang L-M, et al. In vivo and in situ detection

of colorectal cancer using Fourier transform infrared spectroscopy. World J Gastroenterol 2005;11:327–30.

[41] Katukuri VK, Hargrove J, Miller SJ, Rahal K, Kao JY, Wolters R, et al. Detection of colonic inflammation with Fourier transform infrared spectroscopy using a flexible silver halide fiber. Biomed Opt Express 2010;1:1014. doi:10.1364/BOE.1.001014.

[42] Li X, Li Q-B, Zhang G-J, Xu Y-Z, Sun X-J, Shi J-S, et al. Identification of colitis and cancer in colon biopsies by Fourier Transform Infrared spectroscopy and chemometrics. ScientificWorldJournal 2012;2012:936149. doi:10.1100/2012/936149.

[43] Yeh K, Kenkel S, Liu J, Bhargava R. Fast Infrared Chemical Imaging with a Quantum Cascade Laser. Anal Chem 2015.

[44] Tiwari S, Bhargava R. Extracting knowledge from chemical imaging data using computational algorithms for digital cancer diagnosis. Yale J Biol Med 2015;88:131–43.

[45] Mittal S, Yeh K, Leslie LS, Kenkel S, Kajdacsy-Balla A, Bhargava R. Simultaneous cancer and tumor microenvironment subtyping using confocal infrared microscopy for all-digital molecular histopathology. Proc Natl Acad Sci U S A 2018;115:E5651–60. doi:10.1073/pnas.1719551115.

[46] Petibois C, Déléris G. Chemical mapping of tumor progression by FT-IR imaging: towards molecular histopathology. Trends Biotechnol 2006;24:455–62. doi:10.1016/j.tibtech.2006.08.005.

[47] Gazi E, Baker M, Dwyer J, Lockyer NP, Gardner P, Shanks JH, et al. A Correlation of FTIR Spectra Derived from Prostate Cancer Biopsies with Gleason Grade and Tumour Stage. Eur Urol 2006;50:750–61. doi:10.1016/j.eururo.2006.03.031.

[48] Mackanos M a., Contag CH. FTIR microspectroscopy for improved prostate cancer diagnosis. Trends Biotechnol 2009;27:661–3. doi:10.1016/j.tibtech.2009.09.001.

[49] Diem M, Romeo M, Boydston-White S, Miljkovic M, Matthaus C. A decade of vibrational micro-spectroscopy of human cells and tissue (1994-2004). Analyst 2004;129:880–5. doi:10.1039/b408952a.

[50] Naumann D. Ft-Infrared and Ft-Raman Spectroscopy in Biomedical Research. Appl

Spectrosc Rev 2001;36:239–98. doi:10.1081/ASR-100106157.

[51] Levin IW, Bhargava R. Fourier transform infrared vibrational spectroscopic imaging: integrating microscopy and molecular recognition. Annu Rev Phys Chem 2005;56:429–74. doi:10.1146/annurev.physchem.56.092503.141205.

[52] Ellis DI, Goodacre R. Metabolic fingerprinting in disease diagnosis: biomedical applications of infrared and Raman spectroscopy. Analyst 2006;131:875–85. doi:10.1039/b602376m.

[53] Maziak DE, Do MT, Shamji FM, Sundaresan SR, Perkins DG, Wong PTT. Fourier-transform infrared spectroscopic study of characteristic molecular structure in cancer cells of esophagus: An exploratory study. Cancer Detect Prev 2007;31:244–53. doi:10.1016/j.cdp.2007.03.003.

[54] Walsh MJ, German MJ, Singh M, Pollock HM, Hammiche A, Kyrgiou M, et al. IR microspectroscopy: potential applications in cervical cancer screening. Cancer Lett 2007;246:1–11. doi:10.1016/j.canlet.2006.03.019.

[55] Park SC, Lee SJ, Namkung H, Chung H, Han SH, Yoon MY, et al. Feasibility study for diagnosis of stomach adenoma and cancer using IR spectroscopy. Vib Spectrosc 2007;44:279–85. doi:10.1016/j.vibspec.2007.01.001.

[56] Petibois C, Drogat B, Bikfalvi A, Déléris G, Moenner M. Histological mapping of biochemical changes in solid tumors by FT-IR spectral imaging. FEBS Lett 2007;581:5469–74. doi:10.1016/j.febslet.2007.10.052.

[57] Amharref N, Beljebbar A, Dukic S, Venteo L, Schneider L, Pluot M, et al. Brain tissue characterisation by infrared imaging in a rat glioma model. Biochim Biophys Acta 2006;1758:892–9. doi:10.1016/j.bbamem.2006.05.003.

[58] Paluszkiewicz C, Kwiatek WM, Banaś a., Kisiel a., Marcelli a., Piccinini M. SR-FTIR spectroscopic preliminary findings of non-cancerous, cancerous, and hyperplastic human prostate tissues. Vib Spectrosc 2007;43:237–42. doi:10.1016/j.vibspec.2006.08.005.

[59] Gazi E, Dwyer J, Lockyer NP, Miyan J, Gardner P, Hart C a., et al. A study of cytokinetic and motile prostate cancer cells using synchrotron-based FTIR microspectroscopic imaging. Vib Spectrosc 2005;38:193–201. doi:10.1016/j.vibspec.2005.02.026.

[60] Liu C, Zhang Y, Yan X, Zhang X, Li C, Yang W, et al. Infrared absorption of human breast tissues in vitro. J Lumin 2006;119–120:132–6. doi:10.1016/j.jlumin.2005.12.050.

[61] Fabian H, Thi NAN, Eiden M, Lasch P, Schmitt J, Naumann D. Diagnosing benign and malignant lesions in breast tissue sections by using IR-microspectroscopy. Biochim Biophys Acta 2006;1758:874–82. doi:10.1016/j.bbamem.2006.05.015.

[62] Kondepati VR, Keese M, Michael Heise H, Backhaus J. Detection of structural disorders in pancreatic tumour DNA with Fourier-transform infrared spectroscopy. Vib Spectrosc 2006;40:33–9. doi:10.1016/j.vibspec.2005.06.003.

[63] Boskey A, Pleshko Camacho N. FT-IR imaging of native and tissue-engineered bone and cartilage. Biomaterials 2007;28:2465–78. doi:10.1016/j.biomaterials.2006.11.043.

[64] Shanes JG, Ghali J, Billingham ME, Ferrans VJ, Fenoglio JJ, Edwards WD, et al. Interobserver variability in the pathologic interpretation of endomyocardial biopsy results. Circulation 1987;75:401–5. doi:10.1161/01.CIR.75.2.401.

[65] Allsbrook WC, Mangold KA, Johnson MH, Lane RB, Lane CG, Epstein JI. Interobserver reproducibility of Gleason grading of prostatic carcinoma: general pathologist. Hum Pathol 2001;32:81–8. doi:10.1053/hupa.2001.21135.

[66] Edwards WD. Current problems in establishing quantitative histopathologic criteria for the diagnosis of lymphocytic myocarditis by endomyocardial biopsy. Heart Vessels Suppl 1985;1:138–42. doi:10.1007/BF02072381.

[67] Elmore JG, Longton GM, Carney PA, Geller BM, Onega T, Tosteson ANA, et al. Diagnostic Concordance Among Pathologists Interpreting Breast Biopsy Specimens. JAMA 2015;313:1122. doi:10.1001/jama.2015.1405.

[68] Hoffman AW, Ibarra-Drendall C, Espina V, Liotta L, Seewaldt V. Ductal carcinoma in situ: challenges, opportunities, and uncharted waters. Am Soc Clin Oncol Educ Book 2012:40–4. doi:10.14694/EdBook_AM.2012.32.40.

[69] Geller BM, Nelson HD, Carney PA, Weaver DL, Onega T, Allison KH, et al. Second opinion in breast pathology: policy, practice and perception. J Clin Pathol 2014;67:955–60. doi:10.1136/jclinpath-2014-202290.

[70] Allison KH, Reisch LM, Carney PA, Weaver DL, Schnitt SJ, O'Malley FP, et al. Understanding diagnostic variability in breast pathology: lessons learned from an expert consensus review panel. Histopathology 2014;65:240–51. doi:10.1111/his.12387.

[71] Frable WJ. Surgical pathology--second reviews, institutional reviews, audits, and correlations: what's out there? Error or diagnostic variation? Arch Pathol Lab Med 2006;130:620–5. doi:10.1043/1543-2165(2006)130[620:SPRIRA]2.0.CO;2.

[72] Staradub VL, Messenger KA, Hao N, Wiely EL, Morrow M. Changes in breast cancer therapy because of pathology second opinions. Ann Surg Oncol 2002;9:982–7. doi:10.1007/BF02574516.

[73] Castellino RA. Computer aided detection (CAD): an overview. Cancer Imaging 2005;5:17–9. doi:10.1102/1470-7330.2005.0018.

[74] Fernandez DC, Bhargava R, Hewitt SM, Levin IW. Infrared spectroscopic imaging for histopathologic recognition. Nat Biotechnol 2005;23:469–74. doi:10.1038/nbt1080.

[75] Bhargava R, Fernandez DC, Hewitt SM, Levin IW. High throughput assessment of cells and tissues: Bayesian classification of spectral metrics from infrared vibrational spectroscopic imaging data. Biochim Biophys Acta 2006;1758:830–45. doi:10.1016/j.bbamem.2006.05.007.

[76] Bhargava R. Towards a practical Fourier transform infrared chemical imaging protocol for cancer histopathology. Anal Bioanal Chem 2007;389:1155–69. doi:10.1007/s00216-007-1511-9.

[77] Kwak JT, Kajdacsy-Balla A, Macias V, Walsh M, Sinha S, Bhargava R. Improving Prediction of Prostate Cancer Recurrence using Chemical Imaging. Sci Rep 2015;5:8758. doi:10.1038/srep08758.

[78] Reddy RK, Bhargava R. Chemometric Methods for Biomedical Raman Spectroscopy and Imaging. Emerg. Raman Appl. Tech. Biomed. Pharm. Fields, Berlin Heidelberg: Springer; 2010, p. 179–213.

[79] Krafft C, Steiner G, Beleites C, Salzer R. Disease recognition by infrared and Raman spectroscopy. J Biophotonics 2009;2:13–28. doi:10.1002/jbio.200810024.

[80] Wood BR, Chiriboga L, Yee H, Quinn M a., McNaughton D, Diem M. Fourier transform infrared (FTIR) spectral mapping of the cervical transformation zone, and dysplastic squamous epithelium. Gynecol Oncol 2004;93:59–68. doi:10.1016/j.ygyno.2003.12.028.

[81] Tfayli A, Piot O, Durlach A, Bernard P, Manfait M. Discriminating nevus and melanoma on paraffin-embedded skin biopsies using FTIR microspectroscopy. Biochim Biophys Acta - Gen Subj 2005;1724:262–9. doi:10.1016/j.bbagen.2005.04.020.

[82] Mazur AI, Monahan JL, Miljković M, Laver N, Diem M, Bird B. Vibrational spectroscopic changes of B-lymphocytes upon activation. J Biophotonics 2013;6:101–9. doi:10.1002/jbio.201200136.

[83] Walsh MJ, Singh MN, Pollock HM, Cooper LJ, German MJ, Stringfellow HF, et al. ATR microspectroscopy with multivariate analysis segregates grades of exfoliative cervical cytology. Biochem Biophys Res Commun 2007;352:213–9. doi:10.1016/j.bbrc.2006.11.005.

[84] Fujioka N, Morimoto Y, Arai T, Kikuchi M. Discrimination between normal and malignant human gastric tissues by Fourier transform infrared spectroscopy. Cancer Detect Prev 2004;28:32–6. doi:10.1016/j.cdp.2003.11.004.

[85] Patel II, Trevisan J, Singh PB, Nicholson CM, Krishnan RKG, Matanhelia SS, et al. Segregation of human prostate tissues classified high-risk (UK) versus low-risk (India) for adenocarcinoma using Fourier-transform infrared or Raman microspectroscopy coupled with discriminant analysis. Anal Bioanal Chem 2011;401:969–82. doi:10.1007/s00216-011-5123-z.

[86] Krafft C, Shapoval L, Sobottka SB, Schackert G, Salzer R. Identification of primary tumors of brain metastases by infrared spectroscopic imaging and linear discriminant analysis. Technol Cancer Res Treat 2006;5:291–8.

[87] Lascha P, Schmittb J, Naumanna D, Institut RK, Berlin D-. Colorectal Adenocarcinoma Diagnosis by FT-IR Microspectrometry 2000;3918:45–56.

[88] Lasch P, Haensch W, Lewis EN, Kidder LH, Naumann D. Characterization of Colorectal Adenocarcinoma Sections by Spatially Resolved FT-IR Microspectroscopy. Appl Spectrosc 2002;56:1–9.

[89] Hahn D. Calcium Fluoride and Barium Fluoride Crystals in Optics. Opt Photonik 2014;9:45–8.

[90] Weber MJ. Handbook of optical materials. vol. 19. CRC press; 2002.

[91] Bassan P, Lee J, Sachdeva A, Pissardini J, Dorling KM, Fletcher JS, et al. The inherent problem of transflection-mode infrared spectroscopic microscopy and the ramifications for biomedical single point and imaging applications. Analyst 2013:144–57. doi:10.1039/c2an36090j.

[92] Filik J, Frogley MD, Pijanka JK, Wehbe K, Cinque G. Electric field standing wave artefacts in FTIR micro-spectroscopy of biological materials. Analyst 2012;137:853. doi:10.1039/c2an15995c.

[93] Bird B, Miljkovic M, Romeo MJ, Smith J, Stone N, George MW, et al. Infrared micro-spectral imaging: distinction of tissue types in axillary lymph node histology. BMC Clin Pathol 2008;8:8. doi:10.1186/1472-6890-8-8.

[94] Reddy RK, Bhargava R. Accurate histopathology from low signal-to-noise ratio spectroscopic imaging data. Analyst 2010;135:2818–25. doi:10.1039/c0an00350f.

[95] Griffiths PR, De Haseth JA. Fourier transform infrared spectrometry. vol. 171. John Wiley & Sons; 2007.

[96] Bhargava R, Levin IW. Fourier transform infrared imaging: theory and practice. Anal Chem 2001;73:5157–67.

[97] Bhargava R, Wang S-Q, Koenig JL. Processing FT-IR Imaging Data for Morphology Visualization. Appl Spectrosc 2000;54:1690–706.

[98] Lasch P, Naumann D. Spatial resolution in infrared microspectroscopic imaging of tissues. Biochim Biophys Acta 2006;1758:814–29. doi:10.1016/j.bbamem.2006.06.008.

[99] Sommer AJ, Tisinger LG, Marcott C, Story GM. Attenuated Total Internal Reflection Infrared Mapping Microspectroscopy Using an Imaging Microscope. Appl Spectrosc 2001;55:252–6.

[100] Patterson BM, Havrilla GJ, Marcott C, Story GM. Infrared microspectroscopic imaging

using a large radius germanium internal reflection element and a focal plane array detector. Appl Spectrosc 2007;61:1147–52. doi:10.1366/000370207782596969.

[101] Ippolito SB, Goldberg BB, Ünlü MS. High spatial resolution subsurface microscopy. Appl Phys Lett 2001;78:4071. doi:10.1063/1.1381574.

[102] Keith FN, Reddy RK, Bhargava R. Practical protocols for fast histopathology by Fourier transform infrared spectroscopic imaging 2008;6853:1–10. doi:10.1117/12.762468.

[103] Snyder RG, Schachtschneider JH. Vibrational analysis of the n-paraffins—I. Spectrochim Acta 1963;19:85–116. doi:10.1016/0371-1951(63)80095-8.

[104] Pallua JD, Pezzei C, Zelger B, Schaefer G, Bittner LK, Huck-Pezzei V a., et al. Fourier transform infrared imaging analysis in discrimination studies of squamous cell carcinoma. Analyst 2012;137:3965–74. doi:10.1039/c2an35483g.

[105] Beleites C, Neugebauer U, Bocklitz T, Krafft C, Popp J. Sample size planning for classification models. Anal Chim Acta 2013;760:25–33. doi:10.1016/j.aca.2012.11.007.

[106] van Dijk T, Mayerich D, Carney PS, Bhargava R. Recovery of Absorption Spectra from Fourier Transform Infrared (FT-IR) Microspectroscopic Measurements of Intact Spheres. Appl Spectrosc 2013;67:546–52.

[107] Kodali AK, Schulmerich M, Ip J, Yen G, Cunningham BT, Bhargava R. Narrowband Midinfrared Reflectance Filters Using Guided Mode Resonance. Anal Chem 2010;82:5697–706. doi:10.1021/ac1007128.

[108] Liu J-N, Schulmerich M V, Bhargava R, Cunningham BT. Optimally designed narrowband guided-mode resonance reflectance filters for mid-infrared spectroscopy. Opt Express 2011;19:24182–97. doi:10.1364/OE.19.024182.

[109] Kole MR, Reddy RK, Schulmerich M V, Gelber MK, Bhargava R. Discrete frequency infrared microspectroscopy and imaging with a tunable quantum cascade laser. Anal Chem 2012;84:10366–72. doi:10.1021/ac302513f.

[110] Bassan P, Weida MJ, Rowlette J, Gardner P. Large scale infrared imaging of tissue micro arrays (TMAs) using a tunable Quantum Cascade Laser (QCL) based microscope. Analyst 2014;139:3856–9. doi:10.1039/c4an00638k.

[111] Kölhed M, Haberkorn M, Pustogov V, Mizaikoff B, Frank J, Karlberg B, et al. Assessment of quantum cascade lasers as mid infrared light sources for measurements of aqueous solutions. Vib Spectrosc 2002;29:283–9.

[112] Brandstetter M, Koch C, Genner A, Lendl B. Measures for optimizing pulsed EC-QC laser spectroscopy of liquids and application to multi-analyte blood analysis. In: Razeghi M, Tournié E, Brown GJ, editors. SPIE OPTO, International Society for Optics and Photonics; 2013, p. 89931U. doi:10.1117/12.2038585.

[113] Kröger N, Egl A, Engel M, Gretz N, Haase K, Herpich I, et al. Quantum cascade laser-based hyperspectral imaging of biological tissue. J Biomed Opt 2014;19:111607. doi:10.1117/1.JBO.19.11.111607.

[114] Diem M, Miljković M, Bird B, Chernenko T, Schubert J, Marcsisin E, et al. Applications of Infrared and Raman Microspectroscopy of Cells and Tissue in Medical Diagnostics: Present Status and Future Promises. Spectrosc An Int J 2012;27:463–96. doi:10.1155/2012/848360.

[115] Bassan P, Kohler A, Martens H, Lee J, Byrne HJ, Dumas P, et al. Resonant Mie scattering (RMieS) correction of infrared spectra from highly scattering biological samples. Analyst 2010;135:268–77. doi:10.1039/b921056c.

[116] Mohlenhoff B, Romeo M, Diem M, Wood BR. Mie-type scattering and non-Beer-Lambert absorption behavior of human cells in infrared microspectroscopy. Biophys J 2005;88:3635–40. doi:10.1529/biophysj.104.057950.

[117] Bird B, Miljković M, Diem M. Two step resonant Mie scattering correction of infrared micro-spectral data: Human lymph node tissue. J Biophotonics 2010;3:597–608. doi:10.1002/jbio.201000024.

[118] Cserni G, Bianchi S, Boecker W, Decker T, Lacerda M, Rank F, et al. Improving the reproducibility of diagnosing micrometastases and isolated tumor cells. Cancer 2005;103:358–67. doi:10.1002/cncr.20760.

[119] Camp RL, Chung GG, Rimm DL. Automated subcellular localization and quantification of protein expression in tissue microarrays. Nat Med 2002;8:1323–7. doi:10.1038/nm791.

[120] Bradley AP. The use of the area under the ROC curve in the evaluation of machine learning algorithms. Pattern Recognit 1997;30:1145–59. doi:10.1016/S0031-3203(96)00142-2.

[121] Beck JR, Shultz EK. The use of relative operating characteristic (ROC) curves in test performance evaluation. Arch Pathol Lab Med 1986;110:13–20.

[122] Zweig M, Campbell G. Receiver-operating characteristic (ROC) plots: a fundamental evaluation tool in clinical medicine [published erratum appears in Clin Chem 1993 Aug;39(8):1589]. Clin Chem 1993;39:561–77.

[123] Warner E, Plewes DB, Hill KA, Causer PA, Zubovits JT, Jong RA, et al. Surveillance of BRCA1 and BRCA2 mutation carriers with magnetic resonance imaging, ultrasound, mammography, and clinical breast examination. JAMA 2004;292:1317–25. doi:10.1001/jama.292.11.1317.

[124] Bassan P, Sachdeva A, Shanks JH, Brown MD, Clarke NW, Gardner P. Automated high-throughput assessment of prostate biopsy tissue using infrared spectroscopic chemical imaging. In: Gurcan MN, Madabhushi A, editors. SPIE Med. Imaging, International Society for Optics and Photonics; 2014, p. 90410D. doi:10.1117/12.2043290.

[125] Khanmohammadi M, Bagheri Garmarudi A, Samani S, Ghasemi K, Ashuri A. Application of linear discriminant analysis and Attenuated Total Reflectance Fourier Transform Infrared microspectroscopy for diagnosis of colon cancer. Pathol Oncol Res 2011;17:435–41. doi:10.1007/s12253-010-9326-y.

[126] Petter CH, Heigl N, Rainer M, Bakry R, Pallua J, Bonn GK, et al. Development and application of Fourier-transform infrared chemical imaging of tumour in human tissue. Curr Med Chem 2009;16:318–26. doi:10.2174/092986709787002664.

[127] Baker MJ, Trevisan J, Bassan P, Bhargava R, Butler HJ, Dorling KM, et al. Using Fourier transform IR spectroscopy to analyze biological materials. Nat Protoc 2014;9:1771–91. doi:10.1038/nprot.2014.110.

[128] Martin FL, Kelly JG, Llabjani V, Martin-Hirsch PL, Patel II, Trevisan J, et al. Distinguishing cell types or populations based on the computational analysis of their infrared spectra. Nat Protoc 2010;5:1748–60. doi:10.1038/nprot.2010.133.

[129] National Academies of Sciences, Engineering and M and others. Improving diagnosis in health care. National Academies Press; 2016.

[130] He L, Long LR, Antani S, Thoma GR. Histology image analysis for carcinoma detection and grading. Comput Methods Programs Biomed 2012;107:538–56. doi:10.1016/j.cmpb.2011.12.007.

[131] Hanahan D, Weinberg R a. Hallmarks of cancer: the next generation. Cell 2011;144:646–74. doi:10.1016/j.cell.2011.02.013.

[132] Faratian D, Harrison DJ, Simbios), Clyde RG, Crawford JW, Faratian D, et al. Systems pathology—taking molecular pathology into a new dimension. Nat Publ Gr 2009;6:455–64. doi:10.1038/nrclinonc.2009.102.

[133] Costa J. Reflections About Evidence-Based Pathology. Int J Surg Pathol 2007;15:230–2. doi:10.1177/1066896907303207.

[134] Lu P, Weaver VM, Werb Z. The extracellular matrix: A dynamic niche in cancer progression. J Cell Biol 2012;196.

[135] Erez N, Truitt M, Olson P, Hanahan D. Cancer-Associated Fibroblasts Are Activated in Incipient Neoplasia to Orchestrate Tumor-Promoting Inflammation in an NF-κB-Dependent Manner. Cancer Cell 2010;17:135–47. doi:10.1016/j.ccr.2009.12.041.

[136] Sherwood LM, Parris EE, Folkman J. Tumor Angiogenesis: Therapeutic Implications. N Engl J Med 1971;285:1182–6. doi:10.1056/NEJM197111182852108.

[137] Bhargava R. What is chemical imaging ? 2009:1–12.

[138] Director's Challenge Consortium for the Molecular Classification of Lung Adenocarcinoma K, Shedden K, Taylor JMG, Enkemann SA, Tsao M-S, Yeatman TJ, et al. Gene expression-based survival prediction in lung adenocarcinoma: a multi-site, blinded validation study. Nat Med 2008;14:822–7. doi:10.1038/nm.1790.

[139] Esteva FJ, Hortobagyi GN. Prognostic molecular markers in early breast cancer. Breast Cancer Res 2004;6:109. doi:10.1186/bcr777.

[140] Quinn DI, Henshall SM, Sutherland RL. Molecular markers of prostate cancer outcome.

Eur J Cancer 2005;41:858–87. doi:10.1016/j.ejca.2004.12.035.

[141] Sotiriou C, Wirapati P, Loi S, Harris A, Fox S, Smeds J, et al. Gene expression profiling in breast cancer: understanding the molecular basis of histologic grade to improve prognosis. J Natl Cancer Inst 2006;98:262–72. doi:10.1093/jnci/djj052.

[142] Marzouk O, Schofield J. Review of Histopathological and Molecular Prognostic Features in Colorectal Cancer. Cancers (Basel) 2011;3:2767–810. doi:10.3390/cancers3022767.

[143] Harris TJR, McCormick F. The molecular pathology of cancer. Nat Rev Clin Oncol 2010;7:251–65. doi:10.1038/nrclinonc.2010.41.

[144] Angelo M, Bendall SC, Finck R, Hale MB, Hitzman C, Borowsky AD, et al. Multiplexed ion beam imaging of human breast tumors. Nat Med 2014;20:436–42. doi:10.1038/nm.3488.

[145] Wei L, Hu F, Shen Y, Chen Z, Yu Y, Lin C-C, et al. Live-cell imaging of alkyne- tagged small biomolecules by stimulated raman scattering n.d. doi:10.1038/nmeth.2878.

[146] Wei L, Hu F, Chen Z, Shen Y, Zhang L, Min W. Live-Cell Bioorthogonal Chemical Imaging: Stimulated Raman Scattering Microscopy of Vibrational Probes n.d. doi:10.1021/acs.accounts.6b00210.

[147] Zhao S, Iyengar R. Systems Pharmacology: Network Analysis to Identify Multiscale Mechanisms of Drug Action. Annu Rev Pharmacol Toxicol 2012;52:505–21. doi:10.1146/annurev-pharmtox-010611-134520.

[148] Garber K. Angiogenesis inhibitors suffer new setback. Nat Biotechnol 2002;20:1067–8. doi:10.1038/nbt1102-1067.

[149] Ferrara N. Commentary on “Humanization of an Anti-VEGF Monoclonal Antibody for the Therapy of Solid Tumors and Other Disorders.” Cancer Res 2016;76.

[150] Hurwitz H, Fehrenbacher L, Novotny W, Cartwright T, Hainsworth J, Heim W, et al. Bevacizumab plus Irinotecan, Fluorouracil, and Leucovorin for Metastatic Colorectal Cancer. N Engl J Med 2004;350:2335–42. doi:10.1056/NEJMoa032691.

[151] Jardim DL, Groves ES, Breitfeld PP, Kurzrock R. Factors associated with failure of oncology drugs in late-stage clinical development: A systematic review. Cancer Treat Rev

2017;52:12–21. doi:10.1016/j.ctrv.2016.10.009.

[152] Azmi AS, Wang Z, Philip PA, Mohammad RM, Sarkar FH. Proof of Concept: Network and Systems Biology Approaches Aid in the Discovery of Potent Anticancer Drug Combinations n.d. doi:10.1158/1535-7163.MCT-10-0642.

[153] Hickner J, Thompson PJ, Wilkinson T, Epner P, Sheehan M, Pollock AM, et al. Primary care physicians' challenges in ordering clinical laboratory tests and interpreting results. J Am Board Fam Med 2014;27:268–74. doi:10.3122/jabfm.2014.02.130104.

[154] Safrin RE, Bark CJ. Surgical pathology sign-out. Routine review of every case by a second pathologist. Am J Surg Pathol 1993;17:1190–2.

[155] Lind AC, Bewtra C, Healy JC, Sims KL. Prospective peer review in surgical pathology. Am J Clin Pathol 1995;104:560–6.

[156] Edge SB, Compton CC. The American Joint Committee on Cancer: the 7th Edition of the AJCC Cancer Staging Manual and the Future of TNM. Ann Surg Oncol 2010;17:1471–4. doi:10.1245/s10434-010-0985-4.

[157] Demin O, Goryanin I. Kinetic modelling in systems biology. CRC Press; 2008.

[158] Holton SE, Walsh MJ, Bhargava R. Subcellular localization of early biochemical transformations in cancer-activated fibroblasts using infrared spectroscopic imaging. Analyst 2011;136:2953–8. doi:10.1039/c1an15112f.

[159] Holton SE, Bergamaschi A, Katzenellenbogen BS, Bhargava R. Integration of molecular profiling and chemical imaging to elucidate fibroblast-microenvironment impact on cancer cell phenotype and endocrine resistance in breast cancer. PLoS One 2014;9:e96878. doi:10.1371/journal.pone.0096878.

[160] Tiwari S, Zong X, Holton SE, Prasanth K V., Bhargava R. Fourier transform infrared (FT-IR) spectroscopy and imaging of the nucleus to characterize DNA contributions in different phases of the cell cycle. In: Gimi B, Molthen RC, editors. SPIE Med. Imaging, International Society for Optics and Photonics; 2015, p. 941720. doi:10.1117/12.2082347.

[161] Whelan DR, Bambery KR, Puskar L, McNaughton D, Wood BR. Synchrotron Fourier transform infrared (FTIR) analysis of single living cells progressing through the cell cycle.

Analyst 2013;138:3891–9. doi:10.1039/c3an00316g.

[162] Boydston-White S, Gopen T, Houser S, Bargonetti J, Diem M. Infrared spectroscopy of human tissue. V. Infrared spectroscopic studies of myeloid leukemia (ML-1) cells at different phases of the cell cycle. Biospectroscopy 1999;5:219–27. doi:10.1002/(SICI)1520-6343(1999)5:4<219::AID-BSPY2>3.0.CO;2-O.

[163] Jimenez-Hernandez M, Hughes C, Bassan P, Ball F, Brown MD, Clarke NW, et al. Exploring the spectroscopic differences of Caki-2 cells progressing through the cell cycle while proliferating in vitro. Analyst 2013;138:3957–66. doi:10.1039/c3an00507k.

[164] Fernandez DC, Bhargava R, Hewitt SM, Levin IW. Infrared spectroscopic imaging for histopathologic recognition. Nat Biotechnol 2005;23:469–74. doi:10.1038/nbt1080.

[165] Lowrance WT, Scardino PT. Predictive models for newly diagnosed prostate cancer patients. Rev Urol 2009;11:117–26.

[166] Cordon-Cardo C, Kotsianti A, Verbel DA, Teverovskiy M, Capodieci P, Hamann S, et al. Improved prediction of prostate cancer recurrence through systems pathology. J Clin Invest 2007;117:1876–83. doi:10.1172/JCI31399.

[167] Donovan MJ, Hamann S, Clayton M, Khan FM, Sapir M, Bayer-Zubek V, et al. Systems pathology approach for the prediction of prostate cancer progression after radical prostatectomy. J Clin Oncol 2008;26:3923–9. doi:10.1200/JCO.2007.15.3155.

[168] Donovan MJ, Costa J, Cordon-Cardo C. Systems pathology. Cancer 2009;115:3078–84. doi:10.1002/cncr.24353.

[169] Kwak JT, Hewitt SM, Sinha S, Bhargava R. Multimodal microscopy for automated histologic analysis of prostate cancer. BMC Cancer 2011;11:62. doi:10.1186/1471-2407-11-62.

[170] Eggener SE, Vickers AJ, Serio AM, Donovan MJ, Khan FM, Bayer-Zubek V, et al. Comparison of models to predict clinical failure after radical prostatectomy. Cancer 2009;115:303–10. doi:10.1002/cncr.24016.

[171] Lu P, Takai K, Weaver VM, Werb Z. Extracellular matrix degradation and remodeling in development and disease. Cold Spring Harb Perspect Biol 2011;3. doi:10.1101/cshperspect.a005058.

[172] Gattazzo F, Urciuolo A, Bonaldo P. Extracellular matrix: A dynamic microenvironment for stem cell niche. Biochim Biophys Acta - Gen Subj 2014;1840:2506–19. doi:10.1016/j.bbagen.2014.01.010.

[173] Pickup MW, Mouw JK, Weaver VM. The extracellular matrix modulates the hallmarks of cancer. EMBO Rep 2014;15:1243–53. doi:10.15252/embr.201439246.

[174] Bissell MJ, Radisky D. Putting tumours in context. Nat Rev Cancer 2001;1:46–54. doi:10.1038/35094059.

[175] Baker EL, Bonnecaze RT, Zaman MH. Extracellular matrix stiffness and architecture govern intracellular rheology in cancer. Biophys J 2009;97:1013–21. doi:10.1016/j.bpj.2009.05.054.

[176] Levental KR, Yu H, Kass L, Lakins JN, Egeblad M, Erler JT, et al. Matrix crosslinking forces tumor progression by enhancing integrin signaling. Cell 2009;139:891–906. doi:10.1016/j.cell.2009.10.027.

[177] Oskarsson T. Extracellular matrix components in breast cancer progression and metastasis. The Breast 2013;22:S66–72. doi:10.1016/j.breast.2013.07.012.

[178] Karsdal MA, Nielsen MJ, Sand JM, Henriksen K, Genovese F, Bay-Jensen A-C, et al. Extracellular matrix remodeling: the common denominator in connective tissue diseases. Possibilities for evaluation and current understanding of the matrix as more than a passive architecture, but a key player in tissue failure. Assay Drug Dev Technol 2013;11:70–92. doi:10.1089/adt.2012.474.

[179] Cox TR, Erler JT. Remodeling and homeostasis of the extracellular matrix: implications for fibrotic diseases and cancer. Dis Model Mech 2011;4:165–78. doi:10.1242/dmm.004077.

[180] Belbachir K, Noreen R, Gouspillou G, Petibois C. Collagen types analysis and differentiation by FTIR spectroscopy. Anal Bioanal Chem 2009;395:829–37. doi:10.1007/s00216-009-3019-y.

[181] Benard A, Desmedt C, Smolina M, Szternfeld P, Verdonck M, Rouas G, et al. Infrared imaging in breast cancer: automated tissue component recognition and spectral characterization of breast cancer cells as well as the tumor microenvironment. Analyst

2014;139:1044–56. doi:10.1039/c3an01454a.

[182] Tiwari S, Bhargava R. Extracting knowledge from chemical imaging data using computational algorithms for digital cancer diagnosis. Yale J Biol Med 2015;88:131–43.

[183] Federman S, Miller LM, Sagi I. Following matrix metalloproteinases activity near the cell boundary by infrared micro-spectroscopy. Matrix Biol 2002;21:567–77. doi:10.1016/S0945-053X(02)00089-6.

[184] Feng J, Gao TY, Ci YX, Guo ZQ. Fourier Transform Infrared Spectroscopic Characterization of Human Breast Tissue: Implications for Breast Cancer Diagnosis. Appl Spectrosc Vol 53, Issue 3, Pp 312-315 1999;53:312–5.

[185] Votteler M, Carvajal Berrio DA, Pudlas M, Walles H, Stock UA, Schenke-Layland K. Raman spectroscopy for the non-contact and non-destructive monitoring of collagen damage within tissues. J Biophotonics 2012;5:47–56. doi:10.1002/jbio.201100068.

[186] Tiwari S, Reddy VB, Bhargava R, Raman J. Computational chemical imaging for cardiovascular pathology: chemical microscopic imaging accurately determines cardiac transplant rejection. PLoS One 2015;10:e0125183. doi:10.1371/journal.pone.0125183.

[187] Tiwari S, Raman J, Reddy V, Ghetler A, Tella RP, Han Y, et al. Towards Translation of Discrete Frequency Infrared Spectroscopic Imaging for Digital Histopathology of Clinical Biopsy Samples. Anal Chem 2016;88:10183–90. doi:10.1021/acs.analchem.6b02754.

[188] Weis SM, Cheresh DA. Tumor angiogenesis: molecular pathways and therapeutic targets. Nat Med 2011;17:1359–70. doi:10.1038/nm.2537.

[189] Nishida N, Yano H, Nishida T, Kamura T, Kojiro M. Angiogenesis in cancer. Vasc Health Risk Manag 2006;2:213–9.

[190] Nyberg P, Salo T, Kalluri R. Tumor microenvironment and angiogenesis. Front Biosci 2008;13:6537–53.

[191] Watnick RS. The Role of the Tumor Microenvironment in Regulating Angiogenesis. Cold Spring Harb Perspect Med 2012;2:a006676–a006676. doi:10.1101/cshperspect.a006676.

[192] Mittal K, Ebos J, Rini B. Angiogenesis and the Tumor Microenvironment: Vascular

Endothelial Growth Factor and Beyond. Semin Oncol 2014;41:235–51. doi:10.1053/j.seminoncol.2014.02.007.

[193] Savai R, Langheinrich AC, Schermuly RT, Pullamsetti SS, Dumitrascu R, Traupe H, et al. Evaluation of angiogenesis using micro-computed tomography in a xenograft mouse model of lung cancer. Neoplasia 2009;11:48–56.

[194] Kiessling F, Razansky D, Alves F. Anatomical and microstructural imaging of angiogenesis. Eur J Nucl Med Mol Imaging 2010;37:4–19. doi:10.1007/s00259-010-1450-0.

[195] Pugh CW, Ratcliffe PJ. Regulation of angiogenesis by hypoxia: role of the HIF system. Nat Med 2003;9:677–84. doi:10.1038/nm0603-677.

[196] Krock BL, Skuli N, Simon MC. Hypoxia-induced angiogenesis: good and evil. Genes Cancer 2011;2:1117–33. doi:10.1177/1947601911423654.

[197] Liao D, Johnson RS. Hypoxia: A key regulator of angiogenesis in cancer. Cancer Metastasis Rev 2007;26:281–90. doi:10.1007/s10555-007-9066-y.

[198] Zheng X, Wang X, Mao H, Wu W, Liu B, Jiang X. Hypoxia-specific ultrasensitive detection of tumours and cancer cells in vivo. Nat Commun 2015;6:5834. doi:10.1038/ncomms6834.

[199] Petibois C, Gionnet K, Gonçalves M, Perromat A, Moenner M, Déléris G, et al. Analytical performances of FT-IR spectrometry and imaging for concentration measurements within biological fluids, cells, and tissues. Analyst 2006;131:640–7. doi:10.1039/B518076G.

[200] Wehbe K, Pinneau R, Moenner M, Déléris G, Petibois C. FT-IR spectral imaging of blood vessels reveals protein secondary structure deviations induced by tumor growth. Anal Bioanal Chem 2008;392:129–35. doi:10.1007/s00216-008-2230-6.

[201] Norton L, Massagué J. Is cancer a disease of self-seeding? Nat Med 2006;12:875–8. doi:10.1038/nm0806-875.

[202] Kim M-Y, Oskarsson T, Acharyya S, Nguyen DX, H-F Zhang X, Norton L, et al. Tumor Self-Seeding by Circulating Cancer Cells. Cell n.d.;139:1315–26. doi:10.1016/j.cell.2009.11.025.

[203] Parikh RR, Byun J, Goyal S, Kim IY. Local Therapy Improves Overall Survival in Patients

With Newly Diagnosed Metastatic Prostate Cancer. Prostate 2017. doi:10.1002/pros.23294.

[204] Miyamoto DT, Sequist L V., Lee RJ. Circulating tumour cells—monitoring treatment response in prostate cancer. Nat Rev Clin Oncol 2014;11:401–12. doi:10.1038/nrclinonc.2014.82.

[205] Karabacak NM, Spuhler PS, Fachin F, Lim EJ, Pai V, Ozkumur E, et al. Microfluidic, marker-free isolation of circulating tumor cells from blood samples. Nat Protoc 2014;9:694–710. doi:10.1038/nprot.2014.044.

[206] Sarioglu AF, Aceto N, Kojic N, Donaldson MC, Zeinali M, Hamza B, et al. A microfluidic device for label-free, physical capture of circulating tumor cell clusters. Nat Methods 2015;12:685–91. doi:10.1038/nmeth.3404.

[207] Sheng W, Ogunwobi OO, Chen T, Zhang J, George TJ, Liu C, et al. Capture, release and culture of circulating tumor cells from pancreatic cancer patients using an enhanced mixing chip. Lab Chip 2014;14:89–98. doi:10.1039/C3LC51017D.

[208] Alix-Panabières C, Pantel K. Circulating Tumor Cells: Liquid Biopsy of Cancer. Clin Chem 2013;59.

[209] Joosse SA, Gorges TM, Pantel K. Biology, detection, and clinical implications of circulating tumor cells. EMBO Mol Med 2014;7:1–11. doi:10.15252/emmm.201303698.

[210] Haber DA, Velculescu VE. Blood-Based Analyses of Cancer: Circulating Tumor Cells and Circulating Tumor DNA. Cancer Discov 2014;4.

[211] Holton AB, Sinatra FL, Kreahling J, Conway AJ, Landis DA, Altiok S. Microfluidic Biopsy Trapping Device for the Real-Time Monitoring of Tumor Microenvironment. PLoS One 2017;12:e0169797. doi:10.1371/journal.pone.0169797.

[212] Khoo BL, Chaudhuri PK, Lim CT, Warkiani ME. Advancing Techniques and Insights in Circulating Tumor Cell (CTC) Research, Springer International Publishing; 2017, p. 71–94. doi:10.1007/978-3-319-45397-2_5.

[213] Warburg O, Wind F, Negelein E. THE METABOLISM OF TUMORS IN THE BODY. J Gen Physiol 1927;8.

[214] Pavlova NN, Thompson CB. The Emerging Hallmarks of Cancer Metabolism. Cell Metab 2016;23:27–47. doi:10.1016/j.cmet.2015.12.006.

[215] Dang C V. Links between metabolism and cancer. Genes Dev 2012;26:877–90. doi:10.1101/gad.189365.112.

[216] Vander Heiden MG, DeBerardinis RJ. Understanding the Intersections between Metabolism and Cancer Biology. Cell 2017;168:657–69. doi:10.1016/j.cell.2016.12.039.

[217] DeBerardinis RJ, Chandel NS. Fundamentals of cancer metabolism. Sci Adv 2016;2:e1600200. doi:10.1126/sciadv.1600200.

[218] Schwartz L, Seyfried T, Alfarouk KO, Da Veiga Moreira J, Fais S. Out of Warburg effect: An effective cancer treatment targeting the tumor specific metabolism and dysregulated pH. Semin Cancer Biol 2017. doi:10.1016/j.semcancer.2017.01.005.

[219] Halbrook CJ, Lyssiotis CA. Employing Metabolism to Improve the Diagnosis and Treatment of Pancreatic Cancer. Cancer Cell 2017;31:5–19. doi:10.1016/j.ccell.2016.12.006.

[220] Farwell MD, Pryma DA, Mankoff DA. PET/CT imaging in cancer: Current applications and future directions. Cancer 2014;120:3433–45. doi:10.1002/cncr.28860.

[221] Bogomolny E, Huleihel M, Salman A, Zwielly A, Moreh R, Mordechai S. Attenuated total reflectance spectroscopy: a promising technique for early detection of premalignancy. Analyst 2010;135:1934. doi:10.1039/b920591h.

[222] Bogomolny E, Huleihel M, Suproun Y, Sahu RK, Mordechai S. Early spectral changes of cellular malignant transformation using Fourier transform infrared microspectroscopy. J Biomed Opt 2007;12:24003. doi:10.1117/1.2717186.

[223] Costa J. Systems Approach to the Practice of Pathology A New Role for the Pathologist. Arch Pathol Lab Med—Vol 2009;133.

[224] Saidi O, Cordon-Cardo C, Costa J. Technology Insight: will systems pathology replace the pathologist? Nat Clin Pract Urol 2007;4:39–45. doi:10.1038/ncpuro0669.

[225] Liebermeister W, Klipp E. Bringing metabolic networks to life: integration of kinetic, metabolic, and proteomic data. Theor Biol Med Model 2006;3:42. doi:10.1186/1742-4682-

3-42.

[226] Faratian D, Langdon SP, Harrison DJ. How can systems pathology help us personalize cancer therapy? Discov Med 2009;8:81–6.

[227] Zou J, Zheng M-W, Li G, Su Z-G. Advanced systems biology methods in drug discovery and translational biomedicine. Biomed Res Int 2013;2013:742835. doi:10.1155/2013/742835.

[228] Baar M, Coquille L, Mayer H, Hölzel M, Rogava M, Tüting T, et al. A stochastic model for immunotherapy of cancer. Sci Rep 2016;6:24169. doi:10.1038/srep24169.

[229] Stocks T, Hillen T, Gong J, Burger M. A Stochastic Model for the Normal Tissue Complication Probability (NTCP) and Applications n.d.

[230] Tonekaboni SAM, Dhawan A, Kohandel M. Mathematical modelling of plasticity and phenotype switching in cancer cell populations. Math Biosci 2017;283:30–7. doi:10.1016/j.mbs.2016.11.008.

[231] Atuegwu NC, Gore JC, Yankeelov TE. The integration of quantitative multi-modality imaging data into mathematical models of tumors. Phys Med Biol 2010;55:2429–49. doi:10.1088/0031-9155/55/9/001.

[232] Yankeelov TE, Atuegwu NC, Deane NG, Gore JC. Modeling tumor growth and treatment response based on quantitative imaging data. Integr Biol 2010;2:338. doi:10.1039/b921497f.

[233] Histed SN, Lindenberg ML, Mena E, Turkbey B, Choyke PL, Kurdziel KA. Review of functional/anatomical imaging in oncology. Nucl Med Commun 2012;33:349–61. doi:10.1097/MNM.0b013e32834ec8a5.

[234] Frangioni J V. New technologies for human cancer imaging. J Clin Oncol 2008;26:4012–21. doi:10.1200/JCO.2007.14.3065.

[235] Scott JG, Basanta D, Anderson ARA, Gerlee P. A mathematical model of tumor self-seeding reveals secondary metastatic deposits as drivers of primary tumor growth 2012. doi:10.1098/rsif.2013.0011.

[236] Xu J, Vilanova G, Gomez H. A Mathematical Model Coupling Tumor Growth and Angiogenesis. PLoS One 2016;11:e0149422. doi:10.1371/journal.pone.0149422.

[237] Travasso RDM, Corvera Poiré E, Castro M, Rodrguez-Manzaneque JC, Hernández-Machado A. Tumor Angiogenesis and Vascular Patterning: A Mathematical Model. PLoS One 2011;6:e19989. doi:10.1371/journal.pone.0019989.

[238] Peirce SM. Computational and mathematical modeling of angiogenesis. Microcirculation 2008;15:739–51. doi:10.1080/10739680802220331.

[239] Resendis-Antonio O, González-Torres C, Jaime-Muñoz G, Hernandez-Patiño CE, Salgado-Muñoz CF. Modeling metabolism: A window toward a comprehensive interpretation of networks in cancer. Semin Cancer Biol 2015;30:79–87. doi:10.1016/j.semcancer.2014.04.003.

[240] Resendis-Antonio O, Checa A, Encarnación S. Modeling Core Metabolism in Cancer Cells: Surveying the Topology Underlying the Warburg Effect. PLoS One 2010;5:e12383. doi:10.1371/journal.pone.0012383.

[241] Markert EK, Vazquez A. Mathematical models of cancer metabolism. Cancer Metab 2015;3:14. doi:10.1186/s40170-015-0140-6.

[242] Colangelo T, Polcaro G, Muccillo L, D'Agostino G, Rosato V, Ziccardi P, et al. Friend or foe?: The tumour microenvironment dilemma in colorectal cancer. Biochim Biophys Acta - Rev Cancer 2017;1867:1–18. doi:10.1016/J.BBCAN.2016.11.001.

[243] Peddareddigari VG, Wang D, Dubois RN. The tumor microenvironment in colorectal carcinogenesis. Cancer Microenviron 2010;3:149–66. doi:10.1007/s12307-010-0038-3.

[244] Lin W-W, Karin M. A cytokine-mediated link between innate immunity, inflammation, and cancer. J Clin Invest 2007;117:1175–83. doi:10.1172/JCI31537.

[245] Halvorsen TB, Seim E. Association between invasiveness, inflammatory reaction, desmoplasia and survival in colorectal cancer. J Clin Pathol 1989;42:162–6. doi:10.1136/JCP.42.2.162.

[246] Ueno H, Shinto E, Shimazaki H, Kajiwara Y, Sueyama T, Yamamoto J, et al. Histologic Categorization of Desmoplastic Reaction: Its Relevance to the Colorectal Cancer

Microenvironment and Prognosis. Ann Surg Oncol 2015;22:1504–12. doi:10.1245/s10434-014-4149-9.

[247] Hirose M, Fukui H, Igarashi Y, Fujimori Y, Katake Y, Sekikawa A, et al. Detection of desmoplastic reaction in biopsy specimens is useful for predicting the depth of invasion of early colorectal cancer: a Japanese collaborative study. J Gastroenterol 2010;45:1212–8. doi:10.1007/s00535-010-0288-3.

[248] Heindl A, Nawaz S, Yuan Y. Mapping spatial heterogeneity in the tumor microenvironment: a new era for digital pathology. Lab Investig 2015;95:377–84. doi:10.1038/labinvest.2014.155.

[249] Yuan Y, Failmezger H, Rueda OM, Ali HR, Graf S, Chin S-F, et al. Quantitative Image Analysis of Cellular Heterogeneity in Breast Tumors Complements Genomic Profiling. Sci Transl Med 2012;4:157ra143-157ra143. doi:10.1126/scitranslmed.3004330.

[250] Carstens JL, Correa de Sampaio P, Yang D, Barua S, Wang H, Rao A, et al. Spatial computation of intratumoral T cells correlates with survival of patients with pancreatic cancer. Nat Commun 2017;8:15095. doi:10.1038/ncomms15095.

[251] Okamoto Y, Fujimori T, Ohkura Y, Sugai T, Arai T, Watanabe G, et al. Histological assessment of intra- and inter-institutional reliabilities in detection of desmoplastic reaction in biopsy specimens of early colorectal carcinomas. Pathol Int 2013;63:539–45. doi:10.1111/pin.12110.

[252] Patel MM, Smart JD, Nevell TG, Ewen RJ, Eaton PJ, Tsibouklis J. Mucin/Poly(acrylic acid) Interactions: A Spectroscopic Investigation of Mucoadhesion n.d. doi:10.1021/bm034028p.

[253] Kwak JT, Reddy R, Sinha S, Bhargava R. Analysis of variance in spectroscopic imaging data from human tissues. Anal Chem 2012;84:1063–9. doi:10.1021/ac2026496.

[254] DING C, PENG H. MINIMUM REDUNDANCY FEATURE SELECTION FROM MICROARRAY GENE EXPRESSION DATA. J Bioinform Comput Biol 2005;3:185–205. doi:10.1142/S0219720005001004.

[255] Nallala J, Piot O, Diebold M-D, Gobinet C, Bouché O, Manfait M, et al. Infrared imaging as a cancer diagnostic tool: introducing a new concept of spectral barcodes for identifying

molecular changes in colon tumors. Cytometry A 2013;83:294–300. doi:10.1002/cyto.a.22249.

[256] Yeh K, Bhargava R. Discrete frequency infrared imaging using quantum cascade lasers for biological tissue analysis. In: Mahadevan-Jansen A, Petrich W, editors. vol. 9704, International Society for Optics and Photonics; 2016, p. 970406. doi:10.1117/12.2230003.

[257] Oshiro TM, Perez PS, Baranauskas JA. How Many Trees in a Random Forest?, Springer, Berlin, Heidelberg; 2012, p. 154–68. doi:10.1007/978-3-642-31537-4_13.

[258] Latinne P, Debeir O, Decaestecker C. Limiting the Number of Trees in Random Forests, Springer, Berlin, Heidelberg; 2001, p. 178–87. doi:10.1007/3-540-48219-9_18.

[259] Wang D, Khosla A, Gargeya R, Irshad H, Beck AH. Deep Learning for Identifying Metastatic Breast Cancer 2016.

[260] Ueno H, Jones AM, Wilkinson KH, Jass JR, Talbot IC. Histological categorisation of fibrotic cancer stroma in advanced rectal cancer. Gut 2004;53:581–6. doi:10.1136/GUT.2003.028365.

[261] Ueno H, Jones A, Jass JR, Talbot IC. Clinicopathological significance of the “keloid-like” collagen and myxoid stroma in advanced rectal cancer. Histopathology 2002;40:327–34.

[262] Thiery JP, Acloque H, Huang RYJ, Nieto MA. Epithelial-Mesenchymal Transitions in Development and Disease. Cell 2009;139:871–90. doi:10.1016/j.cell.2009.11.007.

[263] Bhargava R. Infrared spectroscopic imaging: the next generation. Appl Spectrosc 2012;66:1091–120. doi:10.1366/12-06801.

[264] Mattson EC, Unger M, Clède S, Lambert F, Policar C, Imtiaz A, et al. Toward optimal spatial and spectral quality in widefield infrared spectromicroscopy of IR labelled single cells. Analyst 2013;1:19–22. doi:10.1039/c3an00383c.

[265] Santana MF, Carlos Ferreira LL. Diagnostic errors in surgical pathology Erros diagnósticos em patologia cirúrgica. J Bras Patol Med Lab 2017;53:124–9. doi:10.5935/1676-2444.20170021.

[266] Gomes DS, Porto SS, Balabram D, Gobbi H. Inter-observer variability between general

pathologists and a specialist in breast pathology in the diagnosis of lobular neoplasia, columnar cell lesions, atypical ductal hyperplasia and ductal carcinoma in situ of the breast. Diagn Pathol 2014;9:121. doi:10.1186/1746-1596-9-121.

[267] Sung W-W, Lin Y-M, Wu P-R, Yen H-H, Lai H-W, Su T-C, et al. High nuclear/cytoplasmic ratio of Cdk1 expression predicts poor prognosis in colorectal cancer patients. BMC Cancer 2014;14:951. doi:10.1186/1471-2407-14-951.

[268] West NP, Dattani M, McShane P, Hutchins G, Grabsch J, Mueller W, et al. The proportion of tumour cells is an independent predictor for survival in colorectal cancer patients. Br J Cancer 2010;102:1519–23. doi:10.1038/sj.bjc.6605674.

[269] Fridman WH, Pagès F, Sautès-Fridman C, Galon J. The immune contexture in human tumours: impact on clinical outcome. Nat Rev Cancer 2012;12:298–306. doi:10.1038/nrc3245.

[270] Galon J, Costes A, Sanchez-Cabo F, Kirilovsky A, Mlecnik B, Lagorce-Pagès C, et al. Type, density, and location of immune cells within human colorectal tumors predict clinical outcome. Science 2006;313:1960–4. doi:10.1126/science.1129139.

[271] Partin AW, Kattan MW, Subong ENP, Walsh PC, Wojno KJ, Oesterling JE, et al. Combination of Prostate-Specific Antigen, Clinical Stage, and Gleason Score to Predict Pathological Stage of Localized Prostate Cancer. JAMA 1997;277:1445. doi:10.1001/jama.1997.03540420041027.

[272] Gaber A, Johansson M, Stenman U-H, Hotakainen K, Pontén F, Glimelius B, et al. High expression of tumour-associated trypsin inhibitor correlates with liver metastasis and poor prognosis in colorectal cancer. Br J Cancer 2009;100:1540–8. doi:10.1038/sj.bjc.6605047.

[273] De Jay N, Papillon-Cavanagh S, Olsen C, El-Hachem N, Bontempi G, Haibe-Kains B. mRMRe: an R package for parallelized mRMR ensemble feature selection. Bioinformatics 2013;29:2365–8. doi:10.1093/bioinformatics/btt383.

[274] De Jay N, Papillon-Cavanagh S, Olsen C, Bontempi G, Haibe-Kains B. mRMRe: an R package for parallelized mRMR ensemble feature selection 2014.

[275] Terry M Therneau TL. Package “survival” 2018.

[276] Qiu W. Package “powerSurvEpi” 2018.

[277] Hamilton SR, Aaltonen LA. Pathology and Genetics of Tumours of the Digestive System 2006;16:110–1.

[278] Wiggers T, Arends JW, Volovics A. Regression analysis of prognostic factors in colorectal cancer after curative resections. Dis Colon Rectum 1988;31:33–41.

[279] Chapuis PH, Dent OF, Fisher R, Newland RC, Pheils MT, Smyth E, et al. A multivariate analysis of clinical and pathological variables in prognosis after resection of large bowel cancer. Br J Surg 1985;72:698–702.

[280] Barresi V, Bonetti LR, Ieni A, Branca G, Baron L, Tuccari G. Histologic grading based on counting poorly differentiated clusters in preoperative biopsy predicts nodal involvement and pTNM stage in colorectal cancer patients. Hum Pathol 2014;45:268–75. doi:10.1016/j.humpath.2013.07.046.

[281] Derwinger K, Kodeda K, Bexe-Lindskog E, Taflin H. Tumour differentiation grade is associated with TNM staging and the risk of node metastasis in colorectal cancer. Acta Oncol (Madr) 2010;49:57–62. doi:10.3109/02841860903334411.

[282] Esteva A, Kuprel B, Novoa RA, Ko J, Swetter SM, Blau HM, et al. Dermatologist-level classification of skin cancer with deep neural networks. Nature 2017;542:115–8. doi:10.1038/nature21056.

[283] Ueno H, Kajiwara Y, Shimazaki H, Shinto E, Hashiguchi Y, Nakanishi K, et al. New Criteria for Histologic Grading of Colorectal Cancer. Am J Surg Pathol 2012;36:193–201. doi:10.1097/PAS.0b013e318235edee.

[284] Ueno H, Hase K, Hashiguchi Y, Shimazaki H, Tanaka M, Miyake O, et al. Site-specific Tumor Grading System in Colorectal Cancer. Am J Surg Pathol 2014;38:197–204. doi:10.1097/PAS.0000000000000113.

[285] Sirinukunwattana K, Raza SEA, Tsang Y-W, Snead DRJ, Cree IA, Rajpoot NM. Locality Sensitive Deep Learning for Detection and Classification of Nuclei in Routine Colon Cancer Histology Images. IEEE Trans Med Imaging 2016;35:1196–206. doi:10.1109/TMI.2016.2525803.

[286] Korbar B, Olofson AM, Miraflor AP, Nicka CM, Suriawinata MA, Torresani L, et al. Deep-Learning for Classification of Colorectal Polyps on Whole-Slide Images 2017. doi:10.11.1/Figures/Figure1.png.

[287] Bychkov D, Linder N, Turkki R, Nordling S, Kovanen PE, Verrill C, et al. Deep learning based tissue analysis predicts outcome in colorectal cancer. Sci Rep 2018;8:3395. doi:10.1038/s41598-018-21758-3.

[288] Mayerich DM, Walsh M, Kadjacsy-Balla A, Mittal S, Bhargava R. Breast histopathology using random decision forests-based classification of infrared spectroscopic imaging data. In: Gurcan MN, Madabhushi A, editors., SPIE; 2014, p. 904107. doi:10.1117/12.2043783.

[289] Tiwari S, Raman J, Reddy V, Ghetler A, Tella RP, Han Y, et al. Towards Translation of Discrete Frequency Infrared Spectroscopic Imaging for Digital Histopathology of Clinical Biopsy Samples. Anal Chem 2016;88:10183–90. doi:10.1021/acs.analchem.6b02754.

[290] Hirschmugl CJ, Gough KM. Fourier Transform Infrared Spectrochemical Imaging: Review of Design and Applications with a Focal Plane Array and Multiple Beam Synchrotron Radiation Source. Appl Spectrosc 2012;66:475–91.

[291] Razavian AS, Azizpour H, Sullivan J, Carlsson S. CNN Features off-the-shelf: an Astounding Baseline for Recognition 2014.

[292] Donahue J, Jia Y, Vinyals O, Hoffman J, Zhang N, Tzeng E, et al. DeCAF: A Deep Convolutional Activation Feature for Generic Visual Recognition 2013.

[293] Krizhevsky A, Sutskever I, Hinton GE. ImageNet Classification with Deep Convolutional Neural Networks n.d.

[294] Ahmad J, Muhammad K, Baik SW. Data augmentation-assisted deep learning of hand-drawn partially colored sketches for visual search. PLoS One 2017;12:e0183838. doi:10.1371/journal.pone.0183838.

[295] Roberts DJ. Pathology Functionality in Resource-Poor Settings n.d. doi:10.5858/arpa.2011-0559-ED.

[296] Balkwill FR, Capasso M, Hagemann T. The tumor microenvironment at a glance. J Cell Sci 2013;125.

[297] Whiteside TL. The tumor microenvironment and its role in promoting tumor growth. Oncogene 2008;27:5904–12. doi:10.1038/onc.2008.271.

[298] Gajewski TF, Schreiber H, Fu Y-X. Innate and adaptive immune cells in the tumor microenvironment. Nat Immunol 2013;14:1014–22. doi:10.1038/ni.2703.

[299] Whiteside TL. The role of immune cells in the tumor microenvironment. Cancer Treat Res 2006;130:103–24.

[300] Hanahan D, Coussens LM. Accessories to the Crime: Functions of Cells Recruited to the Tumor Microenvironment. Cancer Cell 2012;21:309–22. doi:10.1016/j.ccr.2012.02.022.

[301] Joyce JA, Fearon DT. T cell exclusion, immune privilege, and the tumor microenvironment. Science (80-) 2015;348.

[302] Li H, Fan X, Houghton J. Tumor Microenvironment: The Role of the Tumor Stroma in Cancer. J Cell Biochem J Cell Biochem 2007;101:805–15. doi:10.1002/jcb.21159.

[303] Kalluri R, Zeisberg M. Fibroblasts in cancer. Nat Rev Cancer 2006;6:392–401. doi:10.1038/nrc1877.

[304] Navin NE. The first five years of single-cell cancer genomics and beyond. Genome Res 2015;25:1499–507. doi:10.1101/gr.191098.115.

[305] Troester MA, Hoadley KA, D'Arcy M, Cherniack AD, Stewart C, Koboldt DC, et al. DNA defects, epigenetics, and gene expression in cancer-adjacent breast: a study from The Cancer Genome Atlas. Npj Breast Cancer 2016;2:16007. doi:10.1038/npjbcancer.2016.7.

[306] Palumbo A, Da Costa N de OM, Bonamino MH, Pinto LFR, Nasciutti LE, Nasciutti LE. Genetic instability in the tumor microenvironment: a new look at an old neighbor. Mol Cancer 2015;14:145. doi:10.1186/s12943-015-0409-y.

[307] Hanash S, Schliekelman M. Proteomic profiling of the tumor microenvironment: recent insights and the search for biomarkers. Genome Med 2014;6:12. doi:10.1186/gm529.

[308] Pitteri SJ, Kelly-Spratt KS, Gurley KE, Kennedy J, Buson TB, Chin A, et al. Tumor microenvironment-derived proteins dominate the plasma proteome response during breast cancer induction and progression. Cancer Res 2011;71:5090–100. doi:10.1158/0008-

5472.CAN-11-0568.

[309] Holton SE, Walsh MJ, Kajdacsy-Balla a, Bhargava R. Label-free characterization of cancer-activated fibroblasts using infrared spectroscopic imaging. Biophys J 2011;101:1513–21. doi:10.1016/j.bpj.2011.07.055.

[310] Eberhardt K, Beleites C, Marthandan S, Matthä Us C, Diekmann S, Rgen Popp J. Raman and Infrared Spectroscopy Distinguishing Replicative Senescent from Proliferating Primary Human Fibroblast Cells by Detecting Spectral Differences Mainly Due to Biomolecular Alterations n.d. doi:10.1021/acs.analchem.6b04264.